

(U) 17/9/86
BAL

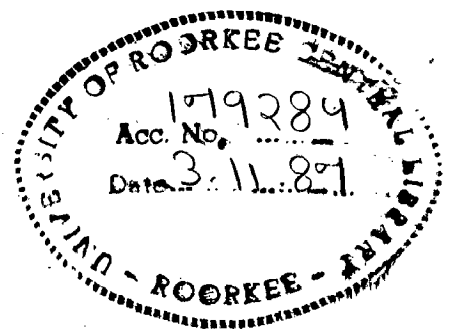
BONDING IN PURE SOLIDS— A DENSITY FUNCTIONAL APPROACH

A THESIS

Submitted in fulfilment of the
requirements for the award of the degree
of
DOCTOR OF PHILOSOPHY
in
METALLURGICAL ENGINEERING

By

V. BALASUBRAMANIAN



DEPARTMENT OF METALLURGICAL ENGINEERING
UNIVERSITY OF ROORKEE
ROORKEE-247 667 (INDIA)


MARCH, 1986

CANDIDATE'S DECLARATION


I hereby certify that the work which is being presented in the thesis entitled 'BONDING IN PURE SOLIDS - A DENSITY FUNCTIONAL APPROACH' in fulfilment of the requirement for the award of the Degree of Doctor of Philosophy, submitted in the Department of METALLURGICAL ENGINEERING of the University is an authentic record of my own work carried out during a period from August 1979 to March 1986 under the supervision of Dr. S.Ray.

The matter embodied in this thesis has not been submitted by me for the award of any other degree.

31, MARCH 1986


(V. BALASUBRAMANIAN)

This is to certify that the above statement made by the candidate is correct to the best of my knowledge.


(S. RAY)
Reader
Department of Met. Engineering,
University of Roorkee,
ROORKEE - 247667 (INDIA)

Bonding in pure solids - A Density
Functional approach

Synopsis

The understanding of the mode of bonding in different elements have begun in 1916 with the pioneering contribution of G.N.Lewis [1] . He propounded the electronic theory of chemical bond by assuming that a single bond forms due to sharing of two electrons participating in the bond by two atoms. It was thus possible to distinguish between various modes of bonding - ionic bond, covalent bond co-ordinative bond etc. However, these concepts faced formidable difficulties with the advent of quantum mechanics. A molecule consists of an ensemble of nuclei exerting mutually repulsive forces. Their dispersion is prevented by the attractive forces brought to bear by the electrons. Any two nuclei are always interacting with the entire electron cloud and it is not permitted to associate two particular electrons with a bond since the principle of indistinguishability leads to an antisymmetric wave function and imposes on all electrons the duty to play, on the average, the same role. However, it is possible to translate some of the classical concepts of bonding in terms of electron density which has characteristic forms for different types of bonding.

The quantum mechanical calculations on molecules have been performed and the electron distribution has been determined in order to understand its characteristic forms. But the calculation becomes more involved as the number of participating atoms increases. The application of Density Functional Formalism proposed by Hohenberg and Kohn [2] to the problem of bonding has been done in this investigation for evolving a suitable frame work for the study of bonding. The conventional approach of having different types of theories for different bonding poses the problem of describing the intermediate types. The Born- Meyer theory of ionic bonding cannot incorporate naturally the mixed ionic-covalent bonding. The Density Functional Theory has the potential to incorporate all types of bonding along with their intermixing in terms of characteristic electron distributions.

In the present investigation the attempt has been limited to the metallic and covalent bonding as observed in pure elements. The systematics of the bonding behaviour and the competition of these two possible types of bonding have been investigated by varying the potential for a given valency. Since the efforts have been primarily limited to testing the workability of the framework rigour has been sacrificed many a times for simplicity.

Chapter 1 describes the preliminaries of the Density Functional Theory and the current approaches to the under-

standing of the phenomenon of bonding. The parametric pseudopotential theory has also been discussed as it has been used for ionic potential in the present investigation.

Chapter 2 is devoted to Metallic bonding. Since the metallic bond is volume dependent and lacks directionality, the electrons are assumed to form a homogeneous electron gas in the simplest approach. The local density functional equation has been used to determine the total energy of the system by using Ashcroft's empty core pseudopotential. The electron distribution has one parameter and the energy has been expressed as a parametric function. The elements are characterised by the valency and the core-radius in the pseudopotential. The Davidson Fletcher and Powell method has been carried out in all the cases of optimization required in this investigation. The variation in the minimum of energy and the corresponding atomic radius has been found out as a function of the core radius for different valencies. By direct minimisation an analytical relation between the core radius and the atomic radius has been determined. The total energy obtained in this model for various elements has been found to be lower than the experimental values. Further, the pseudo-potential for a given element as obtained from the observed value of atomic radii has been compared with that used by previous workers.

The stability in the uniform gas model has been analysed with respect to a flow of charge out of the atomic cell lowering its energy. The uniform gas model has been found to be stable in the above sense for elements with $r_s > 2.4127$ a.u, when r_s is the radius of the spherical volume containing one electron. The Univalent elements have r_s greater than this limiting value and so, uniform gas model works quite well for these elements. There are a large number of elements in metallic and covalent solids having $r_s < 2.4127$ a.u, where an inhomogeneity in electron density is expected. A weak inhomogeneity in electron density has been introduced earlier within the frame work of second order perturbation theory. In the present investigation a step model has been introduced where the atomic cell has been split into two segments having different electron densities. The segment immediately around the ion core has been termed as the inner cell and it is surrounded by a outer spherical shell. The electrons in the inner cell and the outer shell are distributed homogeneously with different densities. Thus, the inhomogeneity in electron density in the atomic cell has been created. The energy functional has been worked out with this density profile in the atomic cell and it has been expressed as a function of three parameters namely, the inner cell radius, the amount of charge in the outer shell and the radius of the atomic cell.

The variation in the total energy has been observed with the accumulation of charge in the outer shell for a particular valency and core radius. It is observed that the inner cell energy reduces from large negative value to zero whereas the outer shell energy increases from zero to higher negative value. However, the total energy of an atomic cell passes through a minimum for a specific amount of charge in the outer shell and thus, corresponds to the stable electron distribution. For small amount of charge in the outer shell the decrease in kinetic energy of the inner cell and the exchange and correlation energy of the outer shell favour a further transfer of charge to the outer shell. But this tendency is soon overcome by the adverse potential energy contribution from the inner cell and a minimum in energy is observed. The ground state energy for every element has been evaluated for various valencies. It has been observed that at lower core radii the difference in electron densities between the inner cell and the outer shell is large and the corresponding total energy is also large and negative as compared to that obtained from uniform gas model. The difference in total energy obtained from the step model and the uniform gas model starts reducing for higher core radii and at a particular core radius termed the crossover core radius, the difference vanishes. Since the metallic bond is prevalent upto a valency of $Z = 4$ the ground state energy has been obtained by optimization of the energy

function for various elements characterised by core radius and valency and are observed to be more negative as compared to the values determined experimentally. The neglect of the gradient energy in the density functional equation has been responsible for this anomaly.

To overcome the deficiencies due to the neglect of the gradient term a similar inhomogeneity in electron density has been introduced in a continuous manner across the segment through a tangent hyperbolic function in continuous density model. The results of this phase of investigation is given in chapter 3. The electron density in this model has four parameters characterising the level of electron density in the two segments, the boundary position of the segments and the rate of change in the charge density at the boundary. One of these parameters can be found out from charge neutrality of the atomic cell. The Hohenberg-Kohn equation has been used along with its gradient terms to find out the energy function in terms of the four floating parameters - three from the electron density and the atomic radius. This model shows the presence of a substantial inhomogeneity in electron density at lower core radii inspite of the gradient energy term. For the same core radius the extent of inhomogeneity comes down as compared to that in the step model. At higher core radius the extent of inhomogeneity reduces in the continuous density model as it has been observed for the step model. The cross-over core radius at which the electron gas inhomogeneity

almost vanishes, remains the same as these obtained from the step model. The quantitative features and trends of variation in both the step model and the continuous model are similar. The total energy for various elements obtained from this model has been found to agree with the experimental results to within $\pm 10\%$ in extreme cases.

The difference in total energy for a given core radius and valency with that obtained in the step model shows a linearity with the density difference within the atomic cell of the step model. Due to this linear relationship, it has been possible to correct the total energies obtained in the step model and use it further for a discussion on bonding behaviour.

The model for covalent bonding has been presented in chapter 4, to describe the inhomogeneous electron distribution characteristic of covalently bonded elements. Since the covalent bond is directional, the space of the element has been subdivided into a charged cell around the ion core and electron cells representing the bonding charges. The ion core cell and electron cells outside have uniform gas of different densities. The number of electron cells per atom has been found out by the number of bonds given by octet rule. The charge in the cell around the ion core and those in the electron cells should be together equal to valency. Thus, these cells together is equivalent to neutral atomic cell as it is present in the covalent.

solids. While using the Density Functional Equation the gradient energy has been neglected because these two cells are assumed to have very little physical contact in the covalent elements. However, the electrostatic energy between the charged cell around the ion core and the electron cell has been considered through a Madelung type of energy term in the energy functional. With the electron density as described the energy functional is now reduced to a parametric function with three parameters namely, the radius of the cell around the ion core, the radius of the electron cells and the amount of charge present in the electron cell. The energy has been optimised with respect to these three parameters and the atomic radius of the system is calculated from the volume of the inner cell and the electron cells. With the increasing charge in the electron cell the energy of the cell around the ion core reduces from large negative value to zero and the electron cell energy increases from zero to higher negative value for an element with a given valency and core radius. The total energy of the atomic cell shows a minimum at a specific amount of charge in the electron cell thereby leading to a stable electron distribution. For small amount of charge in the electron cell, the positive terms like kinetic energy and electron-electron repulsion energy of the cell around the ion core reduces and the negative energy terms like the potential, the exchange and the correlation energy also reduces in the cell around the ion core. But the exchange and correlation energy more than

balances the kinetic energy and electron-electron repulsion energy in the electron cell because the electron density is small. The electron density in the cell around the ion core has increased upto a charge flow into the electron cell and then it decreases. Whereas the density in electron cell increases steadily. The increase in density in the cell around the ion core is attributed towards the recovery of some potential energy by an appropriate redistribution of electrons since the cost in the kinetic and electron-electron repulsion energies are less. The electrostatic Madelung energy is small initially but reinforces the tendency to increase electron density because a reduction in the sizes of the cells leads to a gain in Madelung energy. But at higher charge transfer it is no longer possible to reduce the size of the ion core cell because the gain in energy is more than balanced by the enhanced kinetic and electron-electron repulsion energies. On the contrary, the electron gas cells remain more compressible and the gain in electrostatic energy causes a reduction in its size resulting in a continuous rise in the electron density. The cell around the ion core has a lower energy compared to that of the neutral atomic cell. This is due to large reduction in kinetic and electron-electron repulsion energies compared to the increase in potential and exchanges and correlation energies. In addition to negative energy of the electron cell, Madelung energy helps a continued

flow of charge to the electron cell. When the Madelung energy becomes dominating at higher charge in the electron cell these cells are so much compressed so as to lead to a positive energy of the electron cell. Under these circumstances the only energy term favouring electron flow is the Madelung energy.

The ground state energy obtained from this model are large and negative with more charge in the electron cell at lower core radius. As the core radius increases the ground state energy increases to a less negative value. However, beyond a particular core radius the charge in the electron cells become zero and the model evolves naturally to the uniform gas model. The ground state energies have been obtained in this model for different core radii and valencies. The core radius at which the electron cell charge vanishes, increases with valency. Covalency is observed to be prevalent at higher valencies within the framework of this model. The total energy for elements in the model for covalent bonding are studied by taking the most favourable observed Madelung constant, $\alpha = 1.76$ corresponding to an assumed spatial arrangement of electron cells and charged atomic cells. Since the exact Madelung constant will depend on the number of electron cells and the precise arrangements varying from element to element the impact of this assumption has been assessed by comparing the energies with those obtained from the most unfavourable values of the Madelung

constant. The optimum total energy for various elements are compared with the experimental values and the agreement is quite encouraging.

In chapter 5 the relative stability of the models characterising the types of bonding have been discussed. The results of the model for covalent bonding are compared with the gradient corrected step model to find the region of stability of covalent bonding over the metallic bonding with inhomogeneous electron gas. The inhomogeneity of the electron gas reduces with the increase in the core radius finally leading to uniform electron gas metallic bonding. For the elements with valency, $Z = 1$, the energy obtained from the model for covalent bond is higher than the uniform gas model and the gradient corrected step model in the range of total energies observed in elements. Also, the gradient corrected model yields a higher energy for lower core radii in comparison with uniform gas model. Thus, uniform gas model is eminently suitable for elements with valency, $Z = 1$. For the elements with valency, $Z \geq 5$, the model for covalent bonding gives the lowest energies as compared to the energies observed in the other two models in the range of energies observed in elements. The region of stability of the uniform gas model, gradient corrected step model and the model for covalent bonding for valencies, $Z = 2, 3$ and 4 , have also been studied. The stability for the model for covalent bonding has been overestimated due to the use of the most favourable

value of the Madelung constant, $\alpha = 1.76$. These results have been supplemented with a calculation taking the most unfavourable Madelung constant which shows the possible limits of stability of covalent bonds. In general, the uniform gas model is stable at low negative values of total energy, then the corrected step model takes over and at still higher values of negative energy the covalent bonds are stable. With an increase in valency the limit of stability of each model shifts to higher negative energies.

The core radius for various elements have been obtained by comparing the observed energies of those elements with the calculated curves for the most stable model at that energy. These core radii are quite comparable with but lower than the core radii reported by earlier workers. The total energies have been compared to find the core radii because the atomic radii have been observed to be a relatively insensitive variable for the variation in energy especially in the model for covalent bonding and the gradient corrected step model. However, the present investigation has established the possibility of using the Density Functional Formalism for the study of chemical bonding. The systematic results as obtained in the present investigation are in conformity with the general trends of bonding as observed for the elements in the periodic table.

I express my sincere gratitude and thanks to my teacher Dr. Ratna Gosh who has encouraged and appreciated my interest in this field. She introduced me to Dr. S.Ray in a fateful moment to initiate me to the world of research. It was a turning point in my carrier. The guidance, help and co-operation of Dr. S.Ray is gratefully acknowledged. My association with him far excels the scope of this study. His co-operation and understanding has helped me to get over the moments of frustations and crisis generally inevitable during any research work.

My sincere thanks are due to Dr. S.Basu, who helped me in computer programming. His strong but constructive criticisms and suggestions have provided the incentive to improve my results.

I would also like to take this opportunity to thank my friends, Mr. S.Chakravarthi, Mr. and Mrs. R.C.Agarwala, Mr. and Mrs. R.Shankar, Mr. R.Sadasivam and Mr. C.Mohan Ram, who shared my joys and sorrows with me. My grateful thanks are due to my parents who inspired me to go in for higher studies and research. It will be unjust on my part if I fail to make a special mention of the patience and co-operation of my wife during this investigation.

The financial assistance provided by CSIR for carrying out this investigation is acknowledged. Special thanks are due to Dean of Research and Industrial Laison who provided me adhoc U.G.C. Senior fellowship in the final phase of this work.

I thank Mr. Ram Gopal for neatly typing the thesis.

Behind every study there stands a myraid of people whose help and contribution make it successful. Since such a list will be prohibitively long, I may be excused for important omissions.

LIST OF FIGURES

<u>Fig.No.</u>	<u>Title</u>	<u>Page</u>
1.1	Magnitudes of the reciprocal lattice vectors, g with structural weights, $W(g)$ for the fcc, hcp and bcc structures, relative to $2k_F$ for various electron-per-atom ratios, Z .	43
1.2	The coupling of atomic orbitals in Lithium-Row Diatomic molecules and the resultant bond designations.	54
1.3	Various contributions to the total energy per bond.	58
2.1	The variation in total energy, E_n in a.u. with atomic cell radius, R_a in a.u. for elements in group I of the periodic table.	94
2.2	The variation in total energy, E_n in a.u. with atomic cell radius, R_a in a.u. for elements in group II of the periodic table.	95
2.3	The pseudopotential of a bare Sodium ion, shown in real space used in the calculation of Ashcroft [43], Weaire [71] and the present investigation.	96

<u>Fig.No.</u>	<u>Title</u>	<u>Page</u>
2.4	The change of core radii, r_c in a.u. with r_s in a.u. for various elements with valencies, $Z = 1$ to 7. The uniform gas model stable after $r_s \geq 2.4127$ a.u.	97
2.5	The variation of energies, in a.u. of the inner cell and the outer shell with the charge flow, ΔZ_e for the univalent elements with core radii, $r_c = 1.0, 1.6$ and 2.6 a.u.	98
2.6	The difference in behaviour of the total energy, E_n in a.u. with the charge flow from the inner cell to outer shell, (a) for low core radius, $r_c = 1.0$ a.u. and (b) for high core radius, $r_c = 1.6$ a.u. in valency $Z=1$.	99
2.7	The change of different energy terms involved in step model with the charge flow, ΔZ_e from inner cell to outer shell in an atom with valency, $Z = 1$ and core radius, $r_c = 1.0$ a.u.	100
2.8	The change in the density of electrons in the inner cell, n_0 and the outer shell, n_1 with the flow of charge, ΔZ_e to the outer spherical shell for the element with valency, $Z = 1.0$ and core radius, $r_c = 1.0$ a.u.	101

<u>Fig. No.</u>	<u>Title</u>	<u>Page</u>
2.9	The variation of radius of the inner cell, R_o in a.u. and the radius of the spherical shell, R_a in a.u. with the charge in the outer shell, ΔZ_e for valency, $Z=1$ and core radii, $r_c = 1.0$ and 1.6 a.u.	102
2.10	The change in total energy, E_n in a.u. with core radius, r_c in a.u. for various valencies, $Z=1$ to 3 in step model and the uniform gas model	103
2.11	The change in total energy, E_n in a.u. with core radius, r_c in a.u. for various valencies, $Z=4$ to 7 in the step model and the uniform gas model	104
2.12	The variation of the charge, ΔZ_e in the outer spherical shell, with core radius, r_c in a.u. for the elements with valencies, $Z = 1$ to 4 .	105
2.13	The variation of electron density in a.u. (a) in the inner cell, n_o and (b) the outer spherical shell, n_1 with core radii, r_c in a.u. for different valencies, $Z = 1$ to 4 .	106
2.14	The variation of total energy, E_n in a.u. with atomic radii, R_a in a.u. for various valencies, $Z = 1$ to 4 .	107

<u>Fig. No.</u>	<u>Title</u>	<u>Page</u>
3.1	The variation of total energy, E_n in a.u. with core radius, r_c in a.u. in continuous density model for valencies, $Z=1$ to 4. The arrow mark indicates the boundary with the uniform gas model.	126
3.2	The electron density distribution, $n(\bar{r})$ in the step model-S, the continuous density model-C and the uniform gas model - U for the core radius, $r_c = 0.6$ in a.u. and valency, $Z=4$.	127
3.3	The electron density distribution, $n(\bar{r})$ in the step model -S, the continuous density model -C and the uniform gas model -U, for the core radius, $r_c = 1.6$ a.u. and the valency, $Z=4$.	128
3.4	The variation of maximum to minimum ratio of electron densities with the core radius, r_c in a.u. for the valencies, $Z=1$ to 4.	129
3.5	The change in cross-over core radius, r_c^* in a.u. with valency, Z (—) line for step and continuous density models and (----) line indicates the limits of stability of the uniform gas model	130

<u>Fig. No.</u>	<u>Title</u>	<u>Page</u>
3.6	The variation in the difference in total energy, ΔE_n^{CD-U} as obtained from the continuous density model and the uniform gas model for valencies, $Z=1$ to 4.	131
3.7	The difference in total energy, ΔE_n^{S-CD} between the step model and the continuous density model with the difference in electron density Δn in the atomic cell of the step model for the valencies, (a) $Z = 1$ & 3 and (b) $Z = 4$.	132
3.8	The variation of the parameters [(a) X and (b) Y] of the linear least square fit of total energy with valency.	133
4.1	The variation of energies in a.u. of the ion core cell and electron cell with flow of charge, ΔZ_e for valency, $Z=4$ and core radii, $r_c = 0.6, 0.1, 1.6$ a.u.	154
4.2	The variation of the total energy, E_n in a.u. with charge flow, ΔZ_e for the valency, $Z = 4$ and core radii, $r_c = 0.6, 1.0, 1.6$ a.u.	155
4.3	The change in the different energy terms with the flow of charge, ΔZ_e relating to the ion core cell and the electron cell for the valency, $Z = 4$ and core radius, $r_c = 0.6$ a.u.	156

<u>Fig. No.</u>	<u>Title</u>	<u>Page</u>
4.4	The change of density of electrons in the ion core cell, n_o in a.u. and the electron cell, n_e in a.u. with the flow of charge, ΔZ_e for valency, $Z = 4$ and core radii, $r_c = 0.6, 1.0, 1.6$ a.u.	157
4.5	The variation in the radius of the ion core cell, R_o in a.u. and the radius of the electron cell, R_e in a.u. with the flow of charge, ΔZ_e for valency, $Z = 4$ and core radii, $r_c = 0.6, 1.0, 1.6$ a.u.	158
4.6	The variation of total energies, E_n in a.u. with core radii, r_c in a.u. for valencies, $Z = 2$ to 4.	159
4.7	The variation of total energies, E_n in a.u. with core radii, r_c in a.u. for valencies, $Z = 5$ to 7.	160
4.8	The change in the cross-over core radii, r_c^* in a.u. with the uniform gas model for different valencies.	161
4.9	The variation of total energies, E_n in a.u. at the cross-over core radii, r_c^* in a.u. for different valencies.	162

<u>Fig.No.</u>	<u>Title</u>	<u>Page</u>
4.10	The variation of charge flow, ΔZ_e with core radii, r_c in a.u. for the valencies, $Z = 2$ to 7 .	163
4.11	The variation of electron densities in the ion core cell, n_o in a.u. and the electron cell, n_e in a.u. with core radii, r_c in a.u. for the valencies, $Z = 2$ to 4 .	164
4.12	The variation of electron densities in the ion core cell, n_o in a.u. and the electron cell, n_e in a.u. with core radii, r_c in a.u. for the valencies, $Z = 5$ to 7 .	165
4.13	The difference in total energy in a.u. with Madelung constant, $\alpha_m = 1.76$ and 1.386 scaled with total energy obtained with $\alpha_m = 1.76$ for valency, $Z = 4$.	166
4.14	The difference in the atomic radius in a.u. obtained from $\alpha_m = 1.76$ and 1.386 , scaled with atomic radius obtained from $\alpha_m = 1.76$ for valency, $Z = 4$.	167
5.1	The range of stability of various models in terms of core radius, r_c in a.u. for valencies, $Z = 1, 2, 3$ and 4 .	176
5.2	The range of stability of various models in terms of total energy, E_n in a.u. for valencies $Z = 1, 2, 3$ and 4 .	177

LIST OF TABLES

<u>Table No.</u>	<u>Title</u>	<u>Page</u>
2.1	The total energies of different elements obtained in various models compared with the experimental values.	108
2.2	The total energies E_n of different elements obtained from step model and compared with those obtained from the uniform gas model and experiments.	110
3.1	The various energy terms involved in uniform gas, step and continuous density model, for the valency, $Z = 2.$, at $r_c = 0.6$ and 2.0 a.u.	134
3.2	The total energies of different elements calculated in the continuous model and compared with the experimental values and uniform gas model.	135
5.1	The values of core radius, r_c , for various elements obtained by matching the experimental total energy.	178

CONTENTS

<u>Chapter</u>		<u>Page</u>
	CANDIDATE'S DECLARATION	
	SYNOPSIS	i
	ACKNOWLEDGEMENT	xiii
	LIST OF FIGURES	xiv
	LIST OF TABLES	xxi
1	LITERATURE REVIEW	1
	1.1 Introduction	2
	1.2 Density functional formalism	4
	1.2.1 Hohenberg-Kohn theorem	5
	1.2.2 Local density approximation	8
	1.3 Determination of electron density	11
	1.3.1 Wave function sampling method	14
	1.3.2 The wave function gradient or Kohn-Sham method	15
	1.3.3 Potential sampling method	17
	1.3.4 Potential gradient method	19
	1.4 Pseudopotentials	22
	1.4.1 Philosophy of pseudopotential	23
	1.4.2 First principle pseudopotential	25
	1.4.3 Empirical model potential	26
	1.5 Bonding in pure solids	30

<u>Chapter</u>		<u>Page</u>
	1.5.1	Metallic bonding 30
	1.5.1.1	Resonating bond theory 31
	1.5.1.2	Electron gas theory 32
	1.5.2	Covalent bonding 44
	1.5.2.1	Electronic states of small molecules 48
	1.5.2.2	Electronic states in covalent solids 51
		a) Bond orbital theory 51
		b) Pseudopotential theory of covalent bonding 59
2		BONDING IN METALS 65
	2.1	Introduction 66
	2.2	Uniform electron gas model 67
	2.2.1	Formulation 67
	2.2.2	Results and discussion 71
	2.2.3	Stability of uniform gas model 75
	2.3	Inhomogeneous electron gas: Step model 79
	2.3.1	Formulation 81
	2.3.2	Results and discussion 85
	2.4	Summary 91

<u>Chapter</u>		<u>Page</u>
3	CONTINUOUS DENSITY MODEL	111
	3.1 Introduction	112
	3.2 Formulation	113
	3.3 Results and discussion	118
	3.4 Gradient correction to the step model	121
	3.5 Summary	124
4	MODEL FOR COVALENT BONDING	136
	4.1 Introduction	137
	4.2 Formulation	139
	4.3 Results and discussion	142
	4.4 Summary	151
5	CONCLUSION	169
	REFERENCES	181

CHAPTER 1

LITERATURE
REVIEW

1.1 Introduction

The electronic theory of chemical bonding started with the pioneering contribution of G.N.Lewis [1] . He postulated that a chemical bond forms due to sharing of two electrons between the two atoms. The detailed picture for various modes of bonding like ionic bond, covalent bond, co-ordinative bond etc. has been outlined. But the development of quantum mechanics raised serious doubts about the earlier conceptions about bonding. The principle of indistinguishability invalidates the assignment of electrons to a bond. Any two nuclei in the ensemble of a molecule are always interacting with the electron cloud around and are not permitted to have any special interaction with any two particular electrons. The earlier concepts of bonding have been salvaged by considering it in terms of electron distribution in real space rather than specific electrons. The electron distribution of molecules have been calculated to understand the type of bonding but the complexity of these calculations increases manifold as the number of atoms in a molecule increases. Still, the electron distribution characteristic of a type of bonding has been identified.

The prevalent theories for different types of bonding have adopted different approaches. For example, the ionic bonding is explained in the Born-Mayer theory

by accounting for the electrostatic energies between different ionic species. But the covalent bonding requires the consideration of electron states through either orbital theories or that of inhomogeneous electron gas. There are a large number of compounds exhibiting a mixed ionic-covalent type of bonding which cannot be described within the framework of either of the theories. For all the types of bonding a single theoretical framework is necessary for describing even the intermediate bond types.

In the present investigation the Density Functional Formalism proposed by Hohenberg and Kohn [2] has been applied to describe the bonding in pure solids. The description here is limited to metallic and covalent bonding but it can be easily extended to ionic bonding also. The model developed for covalent bonding partitions the crystal space into charged cells around ions and cells containing bonding electrons. If the electron cells partially overlap with charged cells of a certain species a mixed ionic-covalent bond will result. A complete overlap will cause the ionic bonding. Thus, the Density Functional Formalism has the potential to provide a unified framework for all types of bonding. However, the present investigation has sacrificed rigour in order to retain the simplicity of calculations. Because the primary objective has been to test the workability of the framework rather than its

capability to churn out good numbers.

1.2 Density Functional Formalism

A great deal of attention has been devoted to using electron density as a basic variable in applied quantum mechanics. This basic variable is a better alternative to the quantum mechanical wave function mainly in three ways :

Firstly, the electron density describes the three dimensional distribution of electrons in a system, and hence is a function of only the three coordinates and independent of the number of co-ordinates of the electrons present. This density-based formalisms offer great simplification over the usual wave function approach because, difficulty in solving the Schrodinger equation increases very rapidly as the number of electrons increases. Secondly, the electron density being a physically observable quantity, the accuracy of the quantum mechanical calculations and approximations can be tested directly. Thirdly, it provides a classical picture of quantum phenomena, since the electron density is a function of the three spatial coordinates and enables one to build up various interpretive models.

The electron density can be utilized as a central quantity and the formulation of many particle problem within a single particle like **framework**,. is the essence of

the Density Functional Theory. Starting from the Thomas-Fermi method and its several modifications, Density Functional Theory (DFT) has been rejuvenated by the pioneering works of Hohenberg, Kohn and Sham [2,3], who have laid its strict mathematical foundation and thus provided a formal justification for the use of density as a basic quantity. Since then, a significant body of work has been done to carry out various modifications and extensive applications to a wide variety of problems in atomic, molecular and solid state physics with remarkable practical success.

1.2.1 Hohenberg-Kohn Theorem

Hohenberg and Kohn [2] have proved two theorems. The first one establishes that the nondegenerate ground state of an interacting N-particle system under a static external single particle potential, $v(\vec{r})$, which is completely characterised by the single particle density, $n(\vec{r})$. The second theorem states that, for a given external potential, $v(\vec{r})$, the energy is a unique functional of the particle density, $n(\vec{r})$, and the ground state energy corresponds to a minimum of the energy functional with respect to the variation of the density function. The variation of the particle density is performed under the constraint of conservation of particles as given below

$$\int n(\vec{r}) d\vec{r} = N \quad \dots(1.1)$$

Where N is the total number of particles in the system. The stationary condition

$$\delta \{ E [n] - \mu \int n(\vec{r}) d\vec{r} \} = 0 \quad \dots(1.2)$$

where μ is the lagrangian multiplier, has been used to obtain

$$\frac{\delta E[n]}{\delta n(\vec{r})} - \mu = 0 \quad \dots(1.3)$$

where $(\delta E[n]/\delta n(\vec{r}))$ is a functional derivative of energy functional, E , with respect to the charge density, $n(\vec{r})$. The equation (1.3) forms a key equation of density functional theory and provides a deterministic equation for $n(\vec{r})$. If one considers a collection of an arbitrary number of electrons moving in a system under the influence of an external potential, $v(\vec{r})$, and the mutual coulomb repulsion, then the Hamiltonian can be constructed as a sum of kinetic energy, T , potential energy, V , and coulomb repulsion energy, U , as

$$H = T + V + U. \quad \dots(1.4)$$

where one can write T , V , and U as

$$T = \frac{1}{2} \int \nabla \psi^*(\vec{r}) \nabla \psi(\vec{r}) d\vec{r} \quad \dots(1.5)$$

$$V = \int v(\vec{r}) \psi^*(\vec{r}) \psi(\vec{r}) d\vec{r} \quad \dots(1.6)$$

$$U = \frac{1}{2} \int \frac{1}{|\bar{r}-\bar{r}'|} \psi^*(\bar{r}) \psi^*(\bar{r}') \psi(\bar{r}) \psi(\bar{r}') d\bar{r} d\bar{r}' \dots(1.7)$$

where ψ and ψ^* are the field operator and its conjugate respectively. It has been assumed, for simplicity, that the ground state is non degenerate. Thus, the electron density, $n(\bar{r})$, for the ground state, ϕ , can be written as

$$n(\bar{r}) = (\phi , \psi^*(\bar{r}) \psi(\bar{r}) \phi) \dots(1.8)$$

which is clearly a functional of external potential, $v(\bar{r})$, through ϕ .

In order to write an expression for energy, in terms of density, to take help of this theorem, one requires a knowledge about its functional form. The energy functional, $E[n]$, has been written by Hohenberg and Kohn [2] as

$$E[n] = \int v(\bar{r}) n(\bar{r}) d\bar{r} + F[n] \dots(1.9)$$

where $F[n]$ is a universal functional valid for any number of particles and any external potential, viz.,

$$F[n] = \langle \psi | T + U | \psi \rangle \dots(1.10)$$

assumes its minimum value for the correct $n(\bar{r})$, if the admissible functions are restricted by the condition of equation (1.1). If $F[n]$ is a known functional of n , the problem of determining the ground state energy and density

for a given external potential would be just a problem of the minimization of a functional of the three dimensional density function. However, the determination of $F[n]$, poses a major complexity in the many electron system, because of the long range of the Coulomb repulsion. It is now, convenient to write $F[n]$ as

$$F[n] = \frac{1}{2} \iint \frac{n(\vec{r})n(\vec{r}')}{|\vec{r} - \vec{r}'|} d\vec{r} d\vec{r}' + G[n] \quad (1.11)$$

where $G[n]$ is a universal functional like $F[n]$ and it includes kinetic, $T[n]$, exchange and correlation, $E_{xc}[n]$, energy functionals and can be written as

$$G[n] = T[n] + E_{xc}[n] \quad \dots(1.12)$$

The final expression for $E[n]$ thus becomes,

$$E[n] = \int v(\vec{r}) n(\vec{r}) d\vec{r} + \frac{1}{2} \iint \frac{n(\vec{r}) n(\vec{r}')}{|\vec{r} - \vec{r}'|} d\vec{r} d\vec{r}' + T[n] + E_{xc}[n] \quad \dots(1.13)$$

1.2.2 Local density approximation

Here, the basic idea is to assume the local density to be uniform in an infinitesimal volume element of the space coordinates. The kinetic, exchange and correlation energies for uniform electron gas have been taken within that volume element, and added to the first term in the gradient expansion of the energy functional. Such approximation might

work well only when one assumes the density slowly varying in space.

From equation (1.12), one can get the universal functional, $G[n]$, consisting of kinetic, exchange and correlation energy functionals representable in terms of a general gradient expansion, and can be written as,

$$G[n] = \int g_0(\bar{r}) d\bar{r} + \int g_2(\bar{r}) |\nabla n(r)|^2 d\bar{r} + \dots \quad \dots(1.14)$$

In the above expression the first term can be written as,

$$\int g_0(\bar{r}) d\bar{r} = \int t(n) n(\bar{r}) d\bar{r} + \int \epsilon_{xc}(n) n(\bar{r}) d\bar{r} \quad \dots(1.15)$$

where $t(n)$, is kinetic energy and can be written in terms of density, $n(\bar{r})$, or using the linear measure of density, r_s ,

$$r_s = \left(\frac{3}{4\pi n} \right)^{1/3} \quad \dots(1.16)$$

and

$$r(n) = \frac{3}{10} (3\pi^2 n)^{2/3} = \frac{1.105}{r_s^2} \quad \dots(1.17)$$

The ϵ_{xc} , is further separated as the exchange, ϵ_x , and correlation, ϵ_c , energy respectively, where

$$\epsilon_{xc}(n) = \epsilon_x(n) + \epsilon_c(n) \quad \dots(1.18)$$

and ϵ_x , can be represented as

$$\epsilon_x(n) = - \frac{3}{4} \left(\frac{3n}{\pi} \right)^{1/3} = - \frac{0.458}{r_s} \quad \dots(1.19)$$

Different expressions are available for $\epsilon_c(n)$, starting from Wigner[4] to the most recent one by Gunnarson et. al.[5]. But, normally, the expression provided by Nozieres and Pines [6] has been extensively used as

$$\epsilon_c(n) = - 0.0575 + 0.0155 \ln r_s. \quad \dots(1.20)$$

The above equations (1.17), (1.19) and (1.20) are energies per electron of a uniform electron gas density, n_0 , in a.u. The second term in the equation (1.14) is the energy contribution due to gradient in electron density. g_2 has components coming from the kinetic energy, the exchange and correlation energies as given below

$$g_2(r) = g_{xc}[n(\vec{r})] + \frac{\lambda}{8.n(\vec{r})} \quad \dots(1.21)$$

where, λ is a parameter in the kinetic energy contribution to the equation (1.21), which was originally proposed by Weizasacker [7] with $\lambda = 1$. This form has been extensively used in the literature. Jones and Young [8] have compared the response function obtained from the truncated gradient expansion with variable coefficient to the Lindhard response function. They found that by choosing $\lambda = 1$ yields the correct response for perturbations whose wave length is small with respect to Fermi wave length whereas the choice of $\lambda = 1/9$ is appropriate for perturbations (for large wave length with respect to the Fermi wave length.

The $g_{xc}^{(2)}$ is the gradient term of exchange and correlation energy, which can be written as

$$g_{xc}^{(2)} = C(r_s) (n(\bar{r}))^{-4/3} \quad \dots(1.22)$$

where $C(r_s)$ is a variable and is a function of r_s . A plot of $C(r_s)$ versus r_s has been provided by Rasolt et.al., [9] which can be used to estimate the cost in energy due to gradient in the charge density in inhomogeneous electron gas models.

1.3 Determination of Electron Density

The density functional formalism as explained in section 1.2.1 has led to the equation (1.13) which gives the energy functional for the electrons moving in any given external potential, $V(\bar{r})$. When one finds the charge density that minimizes $E[n]$ the corresponding value of energy is the total energy of the electrons in the ground state. The evaluation of charge density of the ground state at a given $V(\bar{r})$ can be difficult in practice. The major problems faced are :

- i) The functional $E_{xc}[n]$, can at present only be approximated.
- ii) On the scale of binding energies, the calculated value of kinetic energy, $T[n]$ is often insufficiently accurate.

- iii) For the general polyatomic systems, the minimization of $E[n]$ with respect to $n(\vec{r})$ in the current searching algorithms are not effective.

The first problem can be overcome by applying the local-density approximation for $E_{xc}[n]$, but for the second problem Kohn and Sham [3] proposed bypassing the evaluation of kinetic energy, $T[n]$, by simultaneously constructing a density $n(\vec{r})$, and its kinetic energy, $T[n]$, from a set of wave functions of non-interacting particles. A theorem proposed by Theophilcu [10], has shown that for any physical charge density $n(\vec{r})$ there exists a potential, $U_{ext}(\vec{r})$, which is an ordinary function of \vec{r} in which the noninteracting particles will have the same charge density, $n(\vec{r})$. Then, the Schrodinger equation for noninteracting particles is

$$\left[-\frac{1}{2} \nabla^2 + U_{ext}(\vec{r}) \right] \psi_j(\vec{r}) = E_j \psi_j(\vec{r}) \quad \dots(1.23)$$

By construction, the charge density of the real system is identical to the charge density of the system of fictitious noninteracting particles given by

$$n(\vec{r}) = \sum_j \omega_j |\psi_j(\vec{r})|^2 \quad \dots(1.24)$$

where ω_j is the occupation numbers. The ground state kinetic energy also constructed in the independent particle approximation is, likewise, constructed from the

orbitals of noninteracting particle as

$$T[n(\vec{r})] = \sum_j \omega_j \langle \psi_j(\vec{r}) | -\frac{1}{2} \nabla^2 | \psi_j(\vec{r}) \rangle \quad \dots(1.25)$$

Theophilou [10] proved a one-to-one-to-one correspondence among the generating potential, $U_{\text{ext}}(\vec{r})$, the ground state charge density, $n(\vec{r})$, and the ground state orbitals, $\{ \psi_j(\vec{r}) \}$, for the noninteracting particles, and a similar correspondence also for electrons in the system. The $U_{\text{ext}}(\vec{r})$ contains information on the external potential, $V(\vec{r})$, experienced by the electrons as given in the equation (1.13), which, together with the number of electrons $N = \sum_j \omega_j$, defines the physical system and $U_{\text{ext}}(\vec{r})$ generates the charge density and kinetic energy from the equations (1.23) to (1.25).

In the density functional equation (1.13), the density $n(\vec{r})$ is, formally, the independent variable. However, for a given $n(\vec{r})$, it is difficult to find $T[n]$, unless approximate gradient series expressions can be used for $T[n]$ [11,12]. Theophilou's theorem, however, opens the way to treating either the orbitals $\{ \psi_j(\vec{r}) \}$, as done originally by Hohenberg, Kohn and Sham [2,3], or the generating potential $U_{\text{ext}}(\vec{r})$ as the independent variable for minimizing the total energy in density functional equation.

The choice between the two possible independent variables and their type of variation used to minimize the Hohenberg-Kohn-Sham (HKS) [2,3] total energy, can be seen under the four fundamentally different approaches as given below.

1.3.1 Wave function sampling method

In this method, one must select a trial parameter set $\{a_{ij}\}$ for the equation (1.23) and the wave functions $\Psi_j(\vec{r}; \{a\})$ are constructed, on the basis of this wave functions, the density $n(\vec{r})$ and the kinetic energy are evaluated from equations (1.24) and (1.25) respectively. With this, one can calculate the $E[n;V]$ of the density functional equation (1.13). By repeating the above procedure, one obtains the minimum of $E[n\{a_{ij}\}, V]$ as a function of $\{a_{ij}\}$. In this process one does not require any solution of the eigenvalue problem and construction of energy can be conveniently dealt with non-linear parameters $\{a_{ij}\}$, and the interelectronic correlation effects can be evaluated directly from the wave functions. This method has been applied extensively to calculate many body interaction energies, for the systems of bosons [13], nuclear matter [14], Fermi liquids [15], solids [16] and molecules [17]. However, the number of parameters increases with the number of occupied single

particle orbitals $\{\psi_j\}$ and it requires a good search method to converge. So, this method is suitable for independent particle problems only when the number of occupied states is small, and many problems in contemporary one-electron solid-state physics do not satisfy this condition.

1.3.2 The Wave function gradient or Kohn-Sham method

Kohn-Sham [3] have proposed, single particle equation for the variational wave functions of the fictitious non-interacting particles as

$$\left\{ -\frac{1}{2} \nabla^2 + v_{ks} [n(\bar{r})] \right\} \psi'_j(\bar{r}) = \epsilon_j \psi'_j(\bar{r}) \quad \dots(1.26)$$

where $v_{ks} [n(\bar{r})]$ is the potential, the equation (1.26) is identical to the equation (1.23) and is obtained from the wave function variational principle $\delta E [n] / \delta \psi = 0$ that generates orbitals $\{\psi_j\}$. Unlike $U_{ext}(\bar{r})$ in equation (1.23), which is a function of \bar{r} , the $v_{ks} [n(\bar{r})]$ is a function of charge density, $n(\bar{r})$, which can be written as

$$v_{ks} [n(\bar{r})] = v(\bar{r}) + \int \frac{n(\bar{r}')}{|\bar{r} - \bar{r}'|} d\bar{r}' + \frac{\delta E_{xc} [n(\bar{r})]}{\delta n(\bar{r})}$$

$$\text{or} \quad = v(\bar{r}) + v_{coul} [n(\bar{r})] + v_{xc} [n(\bar{r})] \quad \dots(1.27)$$

where $v_{coul} [n(\bar{r})]$ and $v_{xc} [n(\bar{r})]$ are interelectronic coulomb, exchange and correlation potentials respectively.

The dependence of V_{ks} on the charge density requires that the equations (1.27) and (1.26) have to be solved iteratively. The wave functions are constructed by selecting the trial set $\{a_{ij}\}$ in the equation (1.23). Then the charge density, $n(\vec{r})$, and kinetic energy $T[n(\vec{r})]$ are evaluated from equations (1.24) and (1.25). The Kohn-Sham potential, $V_{ks}[n(\vec{r})]$, of equation (1.27) is calculated from the charge density and the eigenvalue problem can be solved from equation (1.26), to obtain new wave functions. The above procedure has to be repeated until the input and output wave functions are equal or within a desired limit.

This method has advantage over the wave-function sampling method, as an arbitrary m^{th} iteration it yields solutions for a set of wave function, $\{\psi_{ij}^{(m)}(\vec{r})\}$, which contain more information than a single number $E^{(m)}[n]$ provided by the wave function sampling, scheme. This information, then, can be used as a guide to select the next wave functions. This procedure has been used with various computational approximations like,

- a) the size and form of the basis set describing $\{\Psi_j\}$,
- b) the calculation of Kohn-Sham potential from the charge density,
- c) the solution of the eigenvalue problem,

- d) specification of a consistency between input and output wave functions.

The difficulties often faced in solving Kohn-Sham problem are due to the high sensitivity of charge density to computational fluctuations in finding Kohn-Sham potential, $V_{ks} [n(\vec{r})]$, and the large size of the subspace $\{a_{ij}\}$ needed to obtain results with the desired accuracy [18]. Also, there is a problem of convergence, when the trial wave functions in the m^{th} iteration $\psi_j^{(m)}(\vec{r})$ is simply the solution of the eigenvalue equation in the $(m-1)^{\text{th}}$ iteration. Several methods of mixing Kohn-Sham potentials obtained in prior iterations have been used to improve the convergence [19,20,21,22].

1.3.3 Potential sampling method

The potential sampling method uses a generating potential in equation (1.23) to arrive at wave functions and density. This method proceeds as follows :

Selection of the trial set of $\{\mu_\rho\}$ in equation (1.24) and the $U_{\text{ext}} [\vec{r}; \{\mu_\rho\}]$; solving equation (1.23) to get the wave function $\psi_j(\vec{r})$; calculation of the charge density, $n(\vec{r})$, and kinetic energy, $T[n(\vec{r})]$, from equation (1.24) and (1.25) respectively, and the evaluation of $E[n(\mu_\rho); V]$.

The above procedure is repeated until the minimum energy is obtained as a function of $\{ \mu_p \}$. In this procedure, the $U_{\text{ext}}[\bar{r}; \{ \mu_p \}]$ is used merely for generating the wave functions only. Whereas the physical potential $V(\bar{r})$ is used to find the total energy.

The primary advantages of this method are its conceptual simplicity and the ease of getting crude solution to simple problems. It does not have complex problem of calculating $V_{\text{KS}}[n(\bar{r})]$ unlike wave function gradient method. However, as it is true for any sampling method, the potential sampling method also faces the problem of constructing the trial effective potential for the subsequent iterations, as it provides at each iteration only one $E^{(m)}[n]$. So, the convergence becomes more difficult and the problem of convergence increases manifold as the number of variables $\{ \mu_p \}$ increases, so in most applications only a small number of parameters are used [22]. But, with very little variational freedom in the potential, the results are not accurate enough in comparison with those obtained by Kohn-Sham wave function gradient method [23]. This method is applied recently in the density functional context, to the problem of Jellium surface [23] and electron hole drops [24] and in the calculation of energies of isolated ions [25, 26]. However, no application of this method on the electronic structure of real solids is yet reported.

1.3.4 Potential gradient method

In this method, the advantages of wave function gradient method and potential-sampling method have been incorporated. The analytic gradient of the total energy of equation (1.13) with respect to the variational parameter $\{ \mu_\rho \}$ of the potential is put equal to zero and the resulting equations are solved. The potential is used to generate only the independent particle energies and wave functions ; the resulting values are used throughout this approach. The response of energies and wave-functions to a change in potential can be obtained by perturbation theory, but for first derivatives, it is sufficient to use first-order perturbation theory.

This gives

$$\frac{\partial \epsilon_j}{\partial \mu_\rho} = \langle \psi_j | \frac{\partial U_{\text{ext}}(\vec{r})}{\partial \mu_\rho} | \psi_j \rangle = \int n_j(\vec{r}) \frac{\partial U_{\text{ext}}(\vec{r})}{\partial \mu_\rho} d\vec{r} \quad \dots(1.28)$$

and

$$\frac{\partial \psi_j(\vec{r})}{\partial \mu_\rho} = \sum_{j \neq j'} \psi_{j'}(\vec{r}) \frac{1}{\epsilon_{j'} - \epsilon_j} \langle \psi_{j'} | \frac{\partial U_{\text{ext}}(\vec{r})}{\partial \mu_\rho} | \psi_j \rangle \quad \dots(1.29)$$

The response of the charge density can be obtained from equation (1.24) as follows ,

$$\frac{\partial n(\vec{r})}{\partial \mu_\rho} = \sum_j \omega_j^2 \operatorname{Re} \left[\psi_j^+(\vec{r}) \frac{\partial \psi_j(\vec{r})}{\partial \mu_\rho} \right] = \sum_j \omega_j$$

$$\cdot \sum_{j' \neq j} \frac{2}{\epsilon_{j'} - \epsilon_j} \operatorname{Re} \left[\psi_j^+(\vec{r}) \psi_{j'}(\vec{r}) \langle \psi_{j'} | \frac{\partial U_{\text{ext}}(\vec{r})}{\partial \mu_\rho} | \psi_j \rangle \right]$$

and the equation (1.23) can be manipulated to obtain $-\frac{1}{2} \nabla^2 \psi_j(\vec{r})$. This can be inserted in equation (1.25) and the variation giving the change in kinetic energy as

$$\begin{aligned} \frac{\partial T[n(\vec{r})]}{\partial \mu_\rho} &= \sum_j \left\{ \frac{\partial \epsilon_j}{\partial \mu_\rho} - \int [n_j(\vec{r}) \frac{\partial U_{\text{ext}}(\vec{r})}{\partial \mu_\rho} + \right. \\ &\quad \left. + U_{\text{ext}}(\vec{r}) \frac{\partial n_j(\vec{r})}{\partial \mu_\rho}] d\vec{r} \right\} \omega_j \\ &= - \int U_{\text{ext}}(\vec{r}) \frac{\partial n_j(\vec{r})}{\partial \mu_\rho} d\vec{r} \quad \dots(1.31) \end{aligned}$$

for the remaining terms in density functional equation(1.13), the only term in the derivatives comes from a change in charge density, $n(\vec{r})$, so one can get

$$\begin{aligned} \frac{\partial E[n]}{\partial \mu_\rho} &= \int d\vec{r} \left[-U_{\text{ext}}(\vec{r}) + V(\vec{r}) + \int d\vec{r}' \frac{n(\vec{r}')}{|\vec{r} - \vec{r}'|} \right. \\ &\quad \left. + \frac{\partial E_{\text{xc}}[n(\vec{r})]}{\partial n(\vec{r})} \right] \frac{\partial n(\vec{r})}{\partial \mu_\rho} \quad \dots(1.32) \end{aligned}$$

which is,

$$\frac{\partial E [n]}{\partial \mu_\rho} = \sum_j \omega_j \sum_{j' \neq j} \frac{2}{\epsilon_{j'} - \epsilon_j} \text{Re} \{ \langle \psi_j | V_{ks} - U_{\text{ext}} | \psi_{j'} \rangle \langle \psi_{j'} | \frac{\partial U_{\text{ext}}(\bar{r})}{\partial \mu_\rho} | \psi_j \rangle \} \quad \dots(1.33)$$

where V_{ks} is given by the equation (1.27) and $U_{\text{ext}}(\bar{r})$ is an ordinary local function of \bar{r} ,

$$U_{\text{ext}}(\bar{r}) = U_{\text{ext}}(\bar{r}; \{ \mu_\rho \}) \quad \dots(1.34)$$

This is the fundamental equation in this approach, and is variationally equivalent to the Kohn-Sham condition, the gradients become zero while satisfying the condition that

$$V_{ks}(\bar{r}) - U_{\text{ext}}(\bar{r}; \{ \mu_\rho \}) = 0 \quad \dots(1.35)$$

The steps in this approach are as follows :

Firstly the trial set $\{ \mu_\rho \}$ has to be selected and the $U_{\text{ext}}(\bar{r}; \{ \mu_\rho \})$ is constructed by the equation (1.23), and then, the independent particles eigenvalue equation (1.24) is solved to obtain $\{ \psi_j(\bar{r}) \}$ and $\{ \epsilon_j \}$. The charge density, $n(\bar{r})$, is constructed from the orbitals, $\{ \psi_j(\bar{r}) \}$, by equation (1.25) and from $n(\bar{r})$, the $V_{ks} [n(\bar{r})]$, of the equation (1.27) is found, by repeating the above in steps, until the condition of the equation(1.35) is satisfied.

This gives advantage over the selection on next trial potential, $U_{\text{ext}}^{(m+1)}(\bar{r})$ since, each iteration yields the function $V_{\text{KS}}^{(m)}(\bar{r}) - U_{\text{ext}}^{(m)}(\bar{r})$, rather than the single $E^{(m)}[n]$. So it is easy to find the unique self-consistent potential. At the same time, one can include enough free parameters in the potential to obtain accurate results.

1.4 Pseudopotentials

Any electronic property of a solid is determined by the energy states, and the associated wave functions of the electrons obtained by solving the schrodinger equation,

$$H\psi = (T + V)\psi = E\psi \quad \dots(1.36)$$

where, ψ is the wave function and H is the Hamiltonian which contains, kinetic energy operator, T , and potential energy operator, V . In any solid, the potential, V , contains coulombic contributions from various nuclei and from all the core and valence electrons as it is included in Hartree and Hartree Fock equation [27]. In addition, exchange and correlation energies are also included in the latter equation.

In a solid, the eigenstates can be classified as valence states and core states. The valence states are the ones which are involved in the chemical bonding. Now, it is desirable to construct a pseudo Hamiltonian, which has the

same valence eigen values as that of the original Hamiltonian but has no core states of lower energies. In other words, the Hamiltonian is simulated to give the energies of the valence electron eigenstates and to remove the atomic-like oscillations of valence electron wave functions inside the core.

1.4.1 Philosophy of pseudopotential

On the basis of the work of Herring [28] who found that the valence electron wave functions can be expanded in a rapidly convergent series of plane waves orthogonalised to the core wave functions. Phillips and Kleinmann [29] constructed the potential energy operator for the pseudo Hamiltonian. This potential is called the pseudopotential and has been represented as

$$V_{ps}(E) = V + \sum_c | \psi_c \rangle \langle \psi_c | (E - E_c) \quad \dots(1.37)$$

where $| \psi_c \rangle$ is the core state eigen function with an eigenvalue of E_c . If E_i is an eigenvalue of the valence state of H corresponding to the true wave function, ψ_i , then, by direct substitution, it is evident that E_i is also an eigenstate of $H_p = T + V_{ps}$ with eigen function $| \phi_i \rangle$, ie

$$E_i | \phi_i \rangle = H_p | \phi_i \rangle = [T + V_{ps}(E_i)] | \phi_i \rangle \quad \dots(1.38)$$

with

$$| \phi_i \rangle = | \psi_i \rangle - \sum_c | \psi_c \rangle \langle \psi_c | \psi_i \rangle \quad \dots(1.39)$$

From the basic philosophy of the above approach, as explained earlier, one can see that the pseudopotential, $V_{ps}(E_i)$, is not a unique operator and one can choose a variety of pseudopotential with the property that the same eigen value spectrum of valence electrons will be obtained corresponding to different eigenfunctions. This approach has been pursued extensively by Harrison [30] and Heine et. al., [31] .

In general, any pseudopotential can be presented with any arbitrary, complete set of functions, F_c , as

$$V_{ps} = V + \sum_c | \psi_c \rangle \langle F_c | \quad \dots(1.40)$$

The above equation (1.40) will have the same properties as the pseudopotential specified in equation (1.37). This allows one to choose $\langle F_c |$ in any form. Austin et.al., [32] and Pick et.al., [33] have chosen the following form

$$\langle F_c | = - \langle \psi_c | V \quad \dots(1.41)$$

This leads to the pseudopotential as given below

$$V_{ps} = (1 - \sum_c | \psi_c \rangle \langle \psi_c |) V \quad \dots(1.42)$$

This V_{ps} is different from the original potential energy

operator, V . Since the projection operator corresponding to the core states eliminates the corresponding components from the true wave function, there is an additional potential term when the eigen value equation is written in terms of this transformed wave function. In a metal with a substantial number of core levels, the pseudopotential, V_{ps} , which has been given in equation (1.42), is relatively very weak, as compared with the original potential, V , and does not result in any bound core states. This can also be understood from the point of view of scattering in terms of phase shifts [34]. One can define pseudopotential as the one having phase shifts δ_1 's obtained by subtracting the integral multiples of π from the phase shifts of the original potential. Thus it has no bound states.

1.4.2 First principle pseudopotential

Since the pseudopotential is weak, the perturbation theory may be applied quite successfully. Apart from Austin et.al., [32] Pick et.al., [33], a variety of such pseudopotentials are given by Harrison [30], Hafner [35], Shaw. Jr, [36], Appapillai et.al., [37], Williams et. al., [38] and Zunger et.al., [39] .

The pseudopotential proposed by Phillips-Kleinmann [29], and others results in a normalised pseudo-wave function having the same shape as the normalised ortho-

gonalised plane wave (OPW) eigen function in the region of space outside the cores, but with different amplitudes. These potentials are generally 'hard core' in character, i.e., strongly repulsive at the origin. The pseudopotential developed by Hamann and coworkers [40,41], matches the true wave function outside the core both in shape and amplitude. These pseudopotentials are called Norm-conserving pseudopotentials.

In a practical calculation, the pseudopotential is usually selected by one of the two broad methods:

- a) by calculating from first principle, or,
- b) by fitting to experiments.

1.4.3 Empirical model potentials

These pseudopotentials are specifically designed for application to specific elements or compounds or ions. The ionic pseudopotentials are usually parametric functions and the parameters are determined by fitting with the observed values of some properties as discussed in detail by Cohen and Heine [42], in their review paper on this subject. The pseudopotential applicable to specific elements or compounds are numerous and only a few popular pseudopotentials are discussed below.

The pseudopotential operator given in equation (1.37)

can be written as

$$V_{ps} | \phi \rangle = V | \phi \rangle - \sum_c | \psi_c \rangle \langle \psi_c | V | \phi \rangle \quad \dots(1.43)$$

where $\langle \psi_c | \phi \rangle$ has nonzero contributions for the core states ψ_c with angular quantum number, l , and spin quantum number, m , because ϕ has component having the same l and m due to the orthogonality of spherical harmonic, $Y_{lm}(\theta, \psi)$, which are the angular part of the core wave functions. Thus, the potential becomes very weak in the core region due to the negative term in equation (1.43) and this is called cancellation. If the core states are more and the cancellation is better and conversely, if there is no cancellation, then, the electron sees the full potential. For example, in carbon, the 2s state electrons see a cancelled pseudo-potential, but the 2p state electrons see the full potential, which is as it should be, since ψ_{2p} has no corresponding p-states in the core for causing cancellation. Thus, the 2p electrons are relatively tightly bound compared to the 2s electrons.

Thus, if for a given l , there are no core states, then the pseudopotential for that l is equal to the real potential. But, if there are core states, then, the answer is that V_{ps} is almost zero inside core region of radius, r_c , for that l . This conclusion is derived from empirical experience as well as from the above theoretical arguments

often referred to as the cancellation theorem. Ashcroft [43] set V_{ps} equal to zero inside some radius, R_M , which he adjusted to fit some experimental data and the resulting values of R_M were close to the accepted ionic radii respectively, r_c . Abarenkov et.al., [44] chose R_M at some arbitrary radius, set $V_{ps}(\bar{r})$ to a constant, A , inside R_M , and adjusted A to fit the spectroscopically observed energy levels of an electron in the field of the ion, and again, A was found close to zero for $R_M \approx r_c$. Therefore, one can arrive at the empty core model for the ionic pseudopotential

$$V_{ps} = \begin{cases} 0 & \text{for } r < R_M \\ -\frac{Z}{r} & \text{for } r > R_M \end{cases} \dots(1.44)$$

Here, the empty core parameter R_M is approximately the radius, r_c , of the physical atomic core and may vary somewhat around that value.

A similar model used by Harrison [30], termed the delta function core model, which is a pure Coulomb potential of charge, Z , with a repulsive delta function of adjustable strength, D . In Fourier transform with screening, it yields the pseudopotential which does not tend to zero even at large q , as it should be. One can correct the large q -behaviour by smearing the delta function out a bit and can be written as

$$V_{ps}(\bar{q}) = \left[- \frac{4 \pi Z}{\bar{q}^2} + \frac{D}{(1 + \bar{q}^2 R_H)^2} \right] / \Omega \epsilon(\bar{q}) \dots (1.45)$$

where R_H is Harrison's radius which can be varied as a second parameter and $\epsilon(\bar{q})$ is dielectric constant due to screening in a crystal, varied as a second parameter. If R_H is chosen around, r_c , the potential given by equation (1.45) does not differ much from the Fourier transform of Ashcroft's empty core pseudopotential [43] except at $\bar{q} > 3 \bar{k}_F$.

Simons and Bloch (SB) [45] introduced a potential by a given l-dependent ion-core radii derived from free-ion quantum defects. The SB effective potential is

$$V_{SB}^l(\bar{r}) = V_r^l(\bar{r}) + V_v(\bar{r}) \dots (1.46)$$

The repulsive potential part $V_r^l(\bar{r})$, originating from the relaxation of core-valence orthogonality is chosen as

$$V_r^l(\bar{r}) = \frac{B_i}{r^2} \dots (1.47)$$

Here, B_i is an adjustable constant and $V_v(\bar{r})$ is potential field experienced by the valence electrons. When this potential is written for the case of a single-valence-electron system, the complicated valence-valence inter-electronic interactions vanish and $V_v(\bar{r})$ is given in the central field limit as

$$V_v(\bar{r}) = - \frac{Z}{r} + \frac{l(l+1)}{2r^2} \dots (1.48)$$

where Z is the valency. An expression for orbital radii in this case as obtained by putting $V_{SB}^1(\bar{r})$ equal to zero in equation (1.46) is given below

$$r_1^0 = B_1/Z + \frac{1(1+1)}{2Z} \quad \dots(1.49)$$

These orbital radii are characteristic of the atomic core and structural indices [46].

1.5 Bonding in pure solids

The chemical bond in a solid is concerned with mutual interaction of the valence electrons of the atoms in the lattice. The nature of the bond is characterised by the spatial distribution of the valence charges around the atoms in the crystal lattice. The bonding in pure solids, thus, has been classified in two basic forms- metallic and covalent bonds.

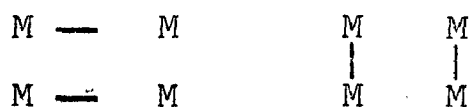
1.5.1 Metallic bonding

The valence electrons of atoms in the metallic crystal is spread over throughout the solid, thereby achieving a high electrical and heat conduction. The electrons moving about are said to be delocalized because, the valence electron wave function, ψ_v , extends over the entire solid. So, the valence electrons are always closer to one or another nucleus as compared to its position in free atoms. Thus,

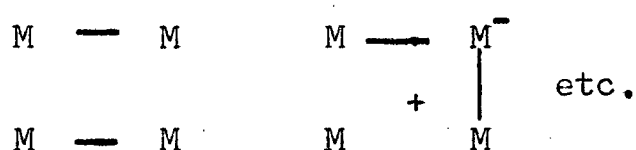
the potential energies of the electrons are lowered in a solid. Similarly, the kinetic energy of the metallic valence electron is also lowered because the wave function is extended more in space. These two factors contributing to a decrease in energy are primarily responsible for metallic bonding. Since the valence electrons are delocalized the bonding is nondirectional and the lattice ions can be thought of as embedded in the valence electron gas, which holds the lattice together. In absence of the directional forces the lattices of the most of the metals are closely packed. The bonding energy or the cohesive energy of the metal, is defined as the energy required to break the metal down into neutral atoms.

1.5.1.1 Resonating bond theory

The bonding of metals, as suggested by Pauling [47], results from the metallic orbitals permitting the resonance of electron pair bonds from one interatomic position to another by the jump of one electron from one atom to an adjacent atom, leading to stabilization due to resonance energy. For each atom to remain electrically neutral by retaining its valence electrons, the stabilization occurs through permitted synchronized bond resonance,



which is analogous to that of benzene molecule. But the stabilization caused would be relatively small and will not explain the extent of stabilization observed in metals. So, it has been assumed that there are unsynchronized resonances as well.



This unsynchronized resonance would require the use of an additional orbital on the atom, called metallic orbital, receiving an extra bond. This type of metallic orbital has been considered in the calculation of interatomic distances by Pauling [47] .

1.5.1.2 Electron gas theory

In electron gas theory of metals, some of the basic premises of Pauling's [47] theory is retained. Equal bonds are formed with all the nearest neighbours and that the electrons resonate between them in a complex way. In physics, this complex movements of the electrons have been portrayed as that obtained from an electron gas. There is a voluminous literature on the calculation of energy in an electron gas which is far more quantitative than the theories for metals based on chemical approach.

If a metal crystal is conceived as an array of positive charges embedded in a nearly uniform sea of negative charges, the total energy of such a system may be written as

$$E_{\text{crystal}} = E[n] + E_w + E_{\text{bs}} \quad \dots(1.50)$$

where, the first term is the total energy of the atom in the crystal, which is related to separated ions and electrons explained in equation (1.13). The second term is the Ewald electrostatic energy of point ions in an uniform electron gas. The bulk of the electrostatic energy of the system has already been included in the $E[n]$ of equation (1.13) and E_w accounts for the structure dependent part of the electrostatic energy. The coulomb repulsion favours simple symmetrical structures, for which E_w is quite small. Since, the Wigner - Seitz cell is not far from a sphere and E_w increases rapidly with any distortion, it stabilizes the simple structures to avoid distortion of Wigner-Seitz cell.

The E_{bs} is the band structure energy which is the effect of band gaps in the band structure, i.e., the deviation of electron gas from free electron gas.

If one considers a single Brillouin zone plane \bar{g} , and $v(\bar{g})$ is positive then the usual nearly free electron treatment of the band gap in terms of 2x2 secular equations, gives the state at the bottom of the gap as $\psi = \sin\left(\frac{1}{2}\bar{g}\cdot\bar{r}\right)$.

This can be termed as purely p-like state, because that is its symmetry about the atomic site $\vec{r}=0$. It is infact a p-bonding state with maximum density $|\psi|^2$ half way between the atom. Similarly, the other states near the bottom of the gap have also larger p-like components as compared to the simple plane-wave state, $\exp(i \vec{g} \cdot \vec{r})$ and pile up charge between the atoms. In other words, the reduction in their energy comes from forming s-p hybridized bonds. However in the metallic bond, one can not assign localized electrons and the heaping up of charge is a modulation on the density of the electron gas involving all the electrons 'resonating' between the bonds. These bonds are not oriented in a particular direction with respect to one another. The charge density in the bond arises from the overlapping of these metallic atoms [48,30] and one can form any number of such bonds independently in any direction desired. When $v(\vec{g})$ is negative, the state at the bottom of the band gap is s-like antibonding one, $\psi = \text{Cos}(\frac{1}{2} \vec{g} \cdot \vec{r})$, which subtract the charge from the region between the atoms and the same will be true for the electron gas as a whole. However, the lowering of the energy, E_{bs} does not depend upon the sign of $v(\vec{g})$ so that these anti-bonds provide just as strong links as the others. In this the electrons move towards the lower potential energy. When $v(\vec{g})$ is positive, the bonds are formed in the region away from the centre, i.e.,

half way between the atoms. The pseudopotential for small \bar{r} is relatively high, because of the core level, as in Animalu and Heine [49] square well potential characterised by its depth, A_0 . When $v(\bar{g})$ is negative the electron density increases at the centre of the atom either because the core radius is so small, that the Ashcroft's empty core does not materially effect much or because the A_0 of Animalu and Heine's [49], square well potential is also relatively low for some atoms in keeping with their atomic and chemical properties. Due to the tendency for the electrons to move towards the centre of the atom, normally one gets tightly bound s-orbitals in these regions.

The energy involved in these inhomogeneous distribution of electrons has been estimated by the second order perturbation theory. The deviation in energy per atom over that of the uniform electron gas can be written as

$$E_{bs} = N^{-1} \sum_{\bar{k} < \bar{k}_F} \sum_{\bar{g}}' \frac{|\langle \bar{k} + \bar{g} | V | \bar{k} \rangle|^2}{\frac{1}{2}|\bar{k}|^2 - \frac{1}{2}|\bar{k} + \bar{g}|^2} \quad \dots(1.51)$$

where, the inner summation excludes $\bar{g} = 0$ state and N is the number of atoms. V is the total potential of the crystal. From this expression one can find that it is sufficient to sum over the free electron Fermi sphere. The total potential, V , is in the form of pseudopotential, arising from the positive ions into the uniform electron gas

at the atomic sites R_j and can be written as

$$V = (\text{Const}) + \sum_{\bar{g}}' s(\bar{g}) v^{\text{ion}}(\bar{g}) \exp(i \bar{g} \cdot \bar{r}) \quad \dots(1.52)$$

where, s is the structure factor and $v^{\text{ion}}(\bar{g})$ is the potential of a single ion, which can be written in Fourier transform as

$$v^{\text{ion}}(\bar{g}) = \Omega^{-1} \int v^{\text{ion}}(\bar{r}) \exp(-i \bar{g} \cdot \bar{r}) d\bar{r} \quad \dots(1.53)$$

where Ω is the atomic volume. The structure factor for the unit cell can be written as

$$s(\bar{g}) = n^{-1} \sum_j \exp(i \bar{g} \cdot \bar{R}_j) \quad \dots(1.54)$$

The summation on j being over the n equivalent atoms in the unit cell. When the electron gas relaxes, i.e., the electron gas now can take up inhomogeneity, the total potential gets screened. Each Fourier component $s(\bar{g}) v^{\text{ion}}(\bar{g})$ is reduced by some screening factor, $\epsilon(\bar{g})$, giving the total pseudopotential as

$$V(\bar{r}) = (\text{Const}) + \sum_{\bar{g}}' s(\bar{g}) v(\bar{g}) \exp(i \bar{g} \cdot \bar{r}) \quad \dots(1.55)$$

where, $v(\bar{g})$ is the screened ionic pseudopotential as given below,

$$v(\bar{g}) = v^{\text{ion}}(\bar{g}) / \epsilon(\bar{g}) \quad \dots(1.56)$$

The summation in equation (1.55) excludes $\bar{g} = 0$. The screening factor $\epsilon(\bar{g})$ for a free electron gas can be written in terms of Lindard dielectric function

$$\epsilon(\bar{q}) = 1 - \left(\frac{8\pi\epsilon^2}{\Omega\bar{q}^2} \right) \left[1 - \frac{\bar{q}^2/2}{|\bar{q}^2 + \bar{k}_F^2 + \bar{k}_S^2|} \right] \chi(\bar{q}) \quad \dots(1.57)$$

where, $\chi(\bar{q})$ is the form factor, k_F is the radius of the Fermisphere of the free electron and \bar{k}_S^2 is the screened coulomb interaction with screening constant which can be written as

$$\begin{aligned} \chi(\bar{q}) &= N^{-1} \sum_{\bar{k} < \bar{k}_F} \left[\frac{1}{2} |\bar{k}^2| - \frac{1}{2} (\bar{k} + \bar{q})^2 \right]^{-1} \\ &= -\frac{1}{2} Z \left(\frac{2}{3} E_{F0} \right)^{-1} \quad \dots(1.58) \end{aligned}$$

$$\cdot \left[\frac{1}{2} + \frac{4\bar{k}_F^2 - \bar{q}^2}{8\bar{q}\bar{k}_F} \log \left| \frac{\bar{q} + 2\bar{k}_F}{\bar{q} - 2\bar{k}_F} \right| \right] \quad \dots(1.59)$$

The summation being over both spin states, the $\chi(\bar{q})$ is also called the perturbation characteristics, because, $\epsilon(\bar{q})$ is derived by simple perturbation calculation with the summation extending over all NZ electrons. The factor in parenthesis in equation (1.57) is twice the Fourier transform of the coulomb potential of the electrons which is responsible for the screening. The matrix element in the numerator of the equation (1.51) becomes just $S(\bar{g}) v(\bar{g})$.

So one can write E_{bs} as

$$E_{bs} = \frac{1}{N} \sum_{\bar{k} < \bar{k}_F} \sum_{\bar{g}} \frac{|S(\bar{g})|^2 [v(\bar{g})]^2}{\left[\frac{1}{2} |\bar{k}|^2 - \frac{1}{2} (\bar{k} + \bar{g})^2 \right]} \dots(1.60)$$

Further, it is necessary to modify equations (1.51) and (1.60) which are incomplete as they stand, because the coulomb repulsion has been counted twice in the summation of one electron energies, so electrostatic self energy of the system as given below, will have to be subtracted once.

$$v_{coul} = \frac{1}{2\Omega} \sum_{\bar{g}} n(\bar{g}) v^{sc}(\bar{g}) \dots(1.61)$$

where, $v^{sc}(\bar{g})$ is the screening potential of the electron gas and $n(\bar{g})$ is the corresponding electron charge density, i.e., deviation from the uniform electron gas density. From equation (1.56) one can write

$$\begin{aligned} v^{sc}(\bar{g}) &= V(\bar{g}) - v^{ion}(\bar{g}) \\ &= S(\bar{g}) [v(\bar{g}) - v^{ion}(\bar{g})] \\ &= S(\bar{g}) \cdot v(\bar{g}) [1 - \epsilon(\bar{g})] \dots(1.62) \end{aligned}$$

The total charge density obtained from the perturbed wave function is

$$n(\bar{g}) = 2^{-1} s(\bar{g}) v(\bar{g}) \chi(\bar{g}) \quad \dots(1.63)$$

substituting equations (1.63) and (1.62) into equation (1.61) and subtracting it from equation (1.60) yields the energy per atom as

$$E_{bs} = \sum_{\bar{g}} |s(\bar{g})|^2 [v(\bar{g})]^2 \chi(\bar{g}) \varepsilon(\bar{g}) \quad \dots(1.64)$$

in place of equation (1.66) the equation (1.64) is the corrected one and it correctly includes the correlation and exchange contributions from non uniform electron gas.

The charge density in equation (1.63) has the form of a sum of overlapping spherical pseudoatom charge distribution [30,50,51]. The total charge per atom is the $\bar{q} \rightarrow 0$ limit of $2v(\bar{q}) \chi(\bar{q})$. The limit of $v(\bar{q})$ is $-\frac{2}{3} E_{F0}$ and limit of $\chi(\bar{q})$ is $-\frac{3}{4} Z E_{F0}^{+1}$, [52,42,53,54] giving a charge of Z electrons per atom as one would expect.

In equation (1.64) the last three factors $v(\bar{q})$, $\chi(\bar{q})$ and $\varepsilon(\bar{q})$ which can be grouped together as,

$$\phi_{bs}(\bar{q}) = [v(\bar{q})]^2 \chi(\bar{q}) \varepsilon(\bar{q}) \quad \dots(1.65)$$

This product is named the energy-wave number characteristics. These three factors depend solely on the element considered and not on the crystal structure. The reciprocal lattice vectors come in sets of n_g equivalent ones with the same $|S|^2$, e.g., the eight (111) reciprocal lattice vectors, and it is useful to lump them together giving a total structural

weight

$$W(\bar{g}) = n_g |s(\bar{g})|^2 \quad \dots(1.66)$$

for the set. Now the equation (1.64) becomes

$$E_{bs} = \sum_{\bar{g}} W(\bar{g}) \phi_b(\bar{g}) \quad \dots(1.67)$$

where, the summation is only over the modulus \bar{g} and not all individual \bar{g} 's. This form is most convenient for computing. Now, let us return to perturbation theory and define a $\chi(\bar{q})$ for one dimension from equation (1.58). It diverges for $\bar{q} = 2\bar{k}_F$. Therefore one can say that it is energetically very favourable to introduce a reciprocal lattice vector at $2k_F$. But this ignores the fact that $\epsilon(\bar{q})$ in equation (1.57) also contains a factor $\chi(\bar{q})$ and hence, so does $v(\bar{q})$ through equation (1.56). From equation (1.64) E_{bs} is proportional to

$$[v^{ion}(\bar{g})]^2 \chi(\bar{g}) / \epsilon(\bar{g}) \quad \dots(1.68)$$

and the divergence of $\chi(\bar{g})$ cancels in the numerator and denominator. The function $\chi(\bar{q})$, has a logarithmic singularity in the derivative at $\bar{q} = 2\bar{k}_F$, but as Harrison [30] has pointed out that, this singularity is so weak, that one can never see it on a figure. However, $\chi(\bar{q})$ is always negative and it decreases rapidly beyond $2\bar{k}_F$. So, the zone planes far from the Fermi sphere hardly affect the E_{cryst}

of the equation (1.50) and the band structure energy, E_{bs} . Zone planes with $\bar{g} < 2\bar{k}_F$ cut the Fermi sphere and contribute substantially. The plane $\bar{g} = 2\bar{k}_F$ just touches the Fermi sphere and does not make an abnormally large contribution, in fact less than that obtained when $\bar{g} < 2\bar{k}_F$, but the derivative is maximum there. The form factor χ , depends only on the electron concentration, Z and the $\epsilon(\bar{g})$ is near unity in the range of \bar{g} of interest and $v(\bar{g})$ can be treated as a constant, M , in the present case. Under this approximation one can expect reasonable results for those metals with a reciprocal vector for zero potential considerably smaller than the first reciprocal lattice vectors, i.e., for Berillium, Magnisium, Zinc and Aluminium. One can therefore approximate χ very crudely by a step function as

$$\begin{aligned}\chi(\bar{g}) &= 0 & \text{for } \bar{g} \geq 2\bar{k}_F \\ \chi(\bar{g}) &= -M & \text{for } \bar{g} < 2\bar{k}_F\end{aligned}\quad \dots(1.69)$$

In such cases E_{bs} will become,

$$E_{bs} \propto -M \sum_{\bar{g}} W(\bar{g}) \quad \dots(1.70)$$

with $\bar{g} < 2\bar{k}_F$. Now one can read off from Figure 1.1 which of the three common structures has the lowest energy. For $Z = 1$, $2\bar{k}_F$ is just greater than the smallest \bar{g} of the hcp structure, which therefore has the lowest energy with a total W of 1.5. This corresponds to the observance of the

hcp structure of Lithium and Sodium at the lowest temperatures. For $Z = 1.5$, the bcc structure has the largest total $W = 12$ below $2\bar{k}_F$, which is in accordance with the observed structure of the β -brass type of alloys. For $Z=2$, the hcp structure has the lowest energy again according to equation (1.70) as found in elements like Berillum, Magnesium, Zinc and Cadmium and the fcc structure is energetically favourable for elements like Aluminium with valency $Z = 3$. A more complete investigation of the fcc and hcp structures has been carried out by Blandin [55], who considered their stability against twinning and various types of stacking faults. Since the number and distance of nearest neighbours remains unaltered, the asymptotic form of the atomic interaction was used. The results are qualitatively in accordance with the Figure 1.1. But, the bcc structure is left out of account. One may represent the E_{bs} in terms of real space version of the theory, which is also mathematically equivalent to its reciprocal space version. However, most calculations are carried out conveniently in reciprocal space. Though the calculations in real space encounters the convergence difficulties in interatomic potentials, it confirms the existence of a fairly well defined hard core diameter $2 R_0$ such that the interatomic potential is strongly repulsive for $R \leq 2 R_0$ but this potential is comparatively weak and oscillatory for $R > 2 R_0$. This

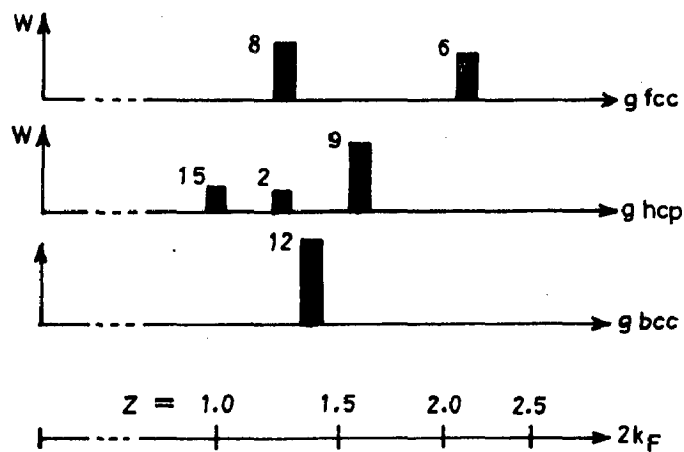


Fig.1.1: MAGNITUDES OF THE RECIPROCAL LATTICE VECTORS, g WITH STRUCTURAL WEIGHTS, $W(g)$ FOR THE fcc, hcp and bcc STRUCTURES, RELATIVE TO $2k_F$ FOR VARIOUS ELECTRON-PER-ATOM RATIOS, Z .

puts the limitation on the configurations of nearest neighbours that can be taken up at constant volume. But, the comparison of fcc and hcp structures which have the same distribution of the nearest neighbours, are simplified to some extent when considered in real space. The real space calculations are applicable : firstly, to rearrangements at constant density only ; secondly, they are strictly meaningful in situations where perturbation theory is valid. The assumption of its validity is difficult to justify without considering the situation in reciprocal space, especially when one deals with strong perturbations.

1.5.2 Covalent bonding

There have been two seemingly incompatible schools of thought on the physical reasons for chemical binding. One school goes back to H.Hellmann [56] who held that interatomic binding is due to a lowering of the kinetic energy upon molecule formation. This idea appears plausible when one compares the molecular wave function in certain types of molecules [56] with the atomic wave functions. But the other school criticizes this approach by pointing out that the virial theorem is known to hold for the molecules as well as for free atoms, so that the binding energy, E_B , has the form

$$E_B = \Delta V + \Delta T < 0 \quad \dots(1.68)$$

where ΔV , the change in potential energy is less than zero and the kinetic energy, ΔT , is greater than zero. The lowering of energy comes about because of the drop in the potential energy inspite of an increase in the kinetic energy. According to the proponents of this critique, the lowering of potential energy is caused by accumulation of extra charge in the bond which is attracted by both the nuclei giving rise to a lower potential energy in the molecule.

Most frequently the argument is made to appeal to physical insight as follows : firstly, it is observed that the molecular Hamiltonian operator is more negative every where, and in particular between the nuclei, so that there is an accumulation of higher charge. Secondly, it is observed that the accumulation of charge in the bond results due to overlap. But, it should be realised that simultaneously there is a depopulation of charge near the nuclei resulting in a rise in potential energy. Also, the nuclear repulsions come into play when the atoms are brought together in the molecule. The crucial question is however, whether or not the lowering in potential energy between the nuclei can outweigh the nuclear repulsions, the additional electronic repulsion and the rise in the potential energy due to a depopulation near the nuclei.

In addition, it should also be noted that the electron distribution in the bonded state can not be conceived as due

to overlap of electrons in the atomic state. The covalent bond is the classical electron pair or homopolar bond as conceived by the chemists. It is a strong bond, in the sense that it has a high cohesive energy comparable with that in ionic crystals, although the covalent bond acts between neutral atoms. Normally this bonding in crystals is expected between nonmetallic atoms like Nitrogen, Oxygen, Carbon, Fluorine and Chlorine. Other elements like Silicon, Germanium, Arsenic and Selenium form bonds that are partially covalent and partially metallic.

A prerequisite for strong covalent bonding is that each atom have at least one half filled orbital. For example, an isolated carbon atom in its ground state contains two 2s electrons and two 2p electrons. In diamond crystal every carbon atom forms four equivalent bonds to the neighbouring atoms. Pauling [47] conceived the covalent bonding in the following way. The energy required to promote a 2s electron to the 2p state is small and it results in four unpaired electrons in four sp^3 hybrid orbitals, which will overlap strongly with the orbitals of the neighbouring atoms in tetrahedral directions. The lowering of energy caused by the overlap of these orbitals is much more than the increase in energy caused by promoting an s- electron to p-state. The more the bonding orbitals overlap, the more is the lowering of energy, or, the stronger is the bond.

The amount of overlap is limited either by electrostatic repulsion or by exclusion principle repulsion. The theory of covalent bond is, thus, one of co-ordination number, bond lengths and bond angles, all in real space. However, the study of electrons in crystals through the concept of Bloch functions and Brillouin zone is in reciprocal space. So, the manifestation of covalency in k-space has been described by several investigators [57] .

A covalently bonded material is usually an insulator or semiconductor with a band gap between the occupied bonding states called valence states and the unoccupied antibonding orbitals called conduction states. A suitable Jones' zone containing the correct number of electrons per atom was constructed by Mott and Jones [58] for diamond and graphite. Since Fermi sphere is enveloped by a number of zone planes there is an extra lowering of energy. For an example, in Gallium (113), (211), (202), (022) and (004) reciprocal lattice vectors cluster in the range of $g/2k_F = 0.95 - 0.99$. It is because of the energy advantage near the singularity of $\chi(\bar{q})$ at $\bar{q} = 2k_F$ with a finite $v(\bar{q})$. But, the structure of covalently bonded solids are more open with a relatively large unit cell. The reciprocal lattice vectors, \bar{g} , are relatively small and the corresponding potentials, $v(\bar{q})$, are large due to the general shape of $v(\bar{q})$. So, the second order perturbation theory

breaks down.

1.5.2.1 Electronic states of small molecules

In a system containing several isolated atoms, a composite set of electron states will be the collection of all the states from all the atoms, but if the atoms are brought together closely enough so that the wave functions of one atom, overlaps with those of the others, the energies of these states will change. However, the number of the states will be conserved. If the total energy of the system is lowered due to the overlap, the atoms are said to be bound forming a molecule.

The electronic states of the molecule, Ψ , is written approximately as a linear combination of the atomic orbitals as given below,

$$|\Psi\rangle = \sum_{\alpha} U_{\alpha} |\alpha\rangle \quad \dots(1.69)$$

where U_{α} 's are the coefficients and $|\alpha\rangle$ represents the set of the normalised orthogonal atomic states. The coefficients, U_{α} , and the energy of the system, E , are determined variationally as,

$$\delta \frac{\langle \Psi | H | \Psi \rangle}{\langle \Psi | \Psi \rangle} = 0 \quad \dots(1.70)$$

From this equation (1.70), one can write the secular determinant as,

$$\det (H_{\beta\alpha} - E\delta_{\beta\alpha}) = 0 \quad \dots(1.71)$$

where, $H_{\beta\alpha} = \beta |H|\alpha\rangle$ and $\delta_{\beta\alpha}$ is the unit matrix. If one considers the simplest case of covalent bonding of Hydrogen molecule with two electrons, the equation (1.71) becomes

$$\begin{aligned} (\epsilon_s - E) U_1 - V_2 U_2 &= 0 \\ -V_2 U_1 + (\epsilon_s - E) U_2 &= 0 \end{aligned} \quad \dots(1.72)$$

where one uses two orbitals $|1\rangle$ and $|2\rangle$, which represents 1s states on atom 1 and 2 respectively and $\epsilon_s = \langle 1|H|1\rangle = \langle 2|H|2\rangle$ and $V_2 = -\langle 1|H|2\rangle = -\langle 2|H|1\rangle$. The matrix element representing the overlap, i.e., V_2 is called the covalent energy. The equation (1.72) can, now, be solved to give a low energy solution called the bonding state with energy $(\epsilon_s - V_2)$ and a high energy solution called the antibinding state with the energy $(\epsilon_s + V_2)$.

This simple treatment can also be extended to polar covalent bond like LiH, where the bonding takes place in 1s orbital of hydrogen and 2s orbital of Lithium having two different energies in their atomic states - ϵ_s^1 and ϵ_s^2 , the lowering state being called the energy of the anion, ϵ_s^1 , and the high energy state the energy of the cation, ϵ_s^2 .

The secular equation (1.72) can, easily, be modified to apply to this case and half of the difference in the values of the anion and cation energies is called the polar energy, V_3 . The energy states of the molecule can be written as,

$$E = \bar{\epsilon} \pm (V_2^2 + V_3^2)^{1/2} \quad \dots(1.73)$$

representing the energies of the bonding and the anti-bonding states and V_2 is the covalent energy as define earlier.

The evaluation of U_1 and U_2 will enable to determined the charge density associated with the bonding and anti-bonding states. In the case of Hydrogen molecules, as discussed earlier, $U_1 = U_2 = 2^{-1/2}$ for the bonding state and $U_1 = -U_2 = 2^{-1/2}$ for the antibonding state. But, for polar covalent solid one obtains $U_1 = U_2 V_2 / ((V_2^2 + V_3^2)^{1/2} - V_3)$ for the bonding state. If the atomic wave functions do not overlap, the probability of finding an electron on atom 1 will be $U_1^2 / (U_1^2 + U_2^2)$ and that on atom 2 will be $U_2^2 / (U_1^2 + U_2^2)$. Now, in the case of molecule this probability is modified to $(1 + \alpha_p) / 2$, the probability of finding electron on atom 1 and, $(1 - \alpha_p) / 2$, the probability of finding electron on atom 2, where α_p is defined as polarity given by $\alpha_p = V_3 / (V_2^2 + V_3^2)^{1/2}$, and the dipole that develops in this bond is proportional to α_p , and the complimentary quantity, α_c , defined as

covalency is given by

$$\alpha_c = v_2 / (v_2^2 + v_3^2)^{1/2}.$$

In the above simple example, only s states have been combined to form bonds through the overlap of the atomic states. However, this concept can be extended even when other atomic states are involved.

1.5.2.2 Electronic states in covalent solids

(a) Bond orbital theory

The solids can be conceived as a giant molecule containing large number of atoms. Here also, the orbitals can be constructed by linear combination of atomic states. It has already been explained that in the tetrahedral solids the bonding takes place between the sp hybrid orbitals and this natural choice has been made by chemists by looking at the tetrahedral symmetry of bonding [59]. The sp^3 hybrids are formed by the linear combination of the wave functions of atomic $|s\rangle$ orbitals and three p orbitals - $|p_x\rangle$, $|p_y\rangle$ and $|p_z\rangle$ in the following manner.

$$\begin{aligned}
 |h_1\rangle &= \left[\frac{1}{2} |s\rangle + |p_x\rangle + |p_y\rangle + |p_z\rangle \right] \\
 |h_2\rangle &= \left[\frac{1}{2} |s\rangle + |p_x\rangle - |p_y\rangle - |p_z\rangle \right] \\
 |h_3\rangle &= \left[\frac{1}{2} |s\rangle - |p_x\rangle + |p_y\rangle - |p_z\rangle \right] \\
 |h_4\rangle &= \left[\frac{1}{2} |s\rangle - |p_x\rangle - |p_y\rangle + |p_z\rangle \right]
 \end{aligned}$$

(1.74)

These four hybrid orbitals have the largest charge density in (111) , $(1\bar{1}\bar{1})$, $(\bar{1}\bar{1}1)$ and $(\bar{1}1\bar{1})$ respectively. These orbitals are called sp^3 hybrids because the probability of finding an electron in p-state is three times that of finding it in s state. It is noted that these hybrids are not the energy eigenstates and the expectation value of energy, called the hybrid energy, is given by

$$\epsilon_h = (\epsilon_s + 3\epsilon_p) / 4 \quad \dots(1.75)$$

$$\text{where } \epsilon_s = \langle s|H|s\rangle \quad \dots(1.76)$$

and,

$$\epsilon_p = \langle p_x|H|p_x\rangle = \langle p_y|H|p_y\rangle = \langle p_z|H|p_z\rangle \quad \dots(1.77)$$

For polar covalent solids, the hybrids can be constructed on each of the atom types present and treated in terms of the lesser hybrid energy ϵ_h^1 , the greater energy ϵ_h^2 and a hybrid polar energy, V_3^n , defined as

$(\epsilon_h^2 - \epsilon_h^1)/2$. Since the hybrids are not the eigen states, the non-zero matrix elements of the Hamiltonian can exist between the hybrids. The magnitude of the resulting matrix elements is called the metallic energy, V_1 , and can be written as

$$V_1 = - \langle h_i | H | h_j \rangle = - \frac{1}{4} (\epsilon_p - \epsilon_s). \quad \dots(1.78)$$

The matrix elements between the hybrids on two neighbouring atoms pointed to each other is called the hybrid covalent energy as given below,

$$\begin{aligned} V_2^h &= - \langle h^1 | H | h^2 \rangle \\ &= (-V_{ss\sigma} + 2\sqrt{3} V_{sp\sigma} + 3 V_{pp\sigma}) / 4 \quad \dots(1.79) \end{aligned}$$

and these terms are explained in figure (1.2).

To calculate the band structure of the covalent solids, it is possible to use these hybrids for constructing Bloch states or else, the electron eigen state, $|k\rangle$, which can be written approximately as a linear combination of the atomic orbitals $|\alpha\rangle$, as

$$|k\rangle = \sum_{\alpha} U_{k\alpha} |\alpha\rangle. \quad \dots(1.80)$$

The variational solution of the equation (1.80) will lead to a set of algebraic equation like

$$\sum_{\alpha} \langle \beta | H | \alpha \rangle U_{k\alpha} - E_k U_{k\beta} = 0 \quad \dots(1.81)$$

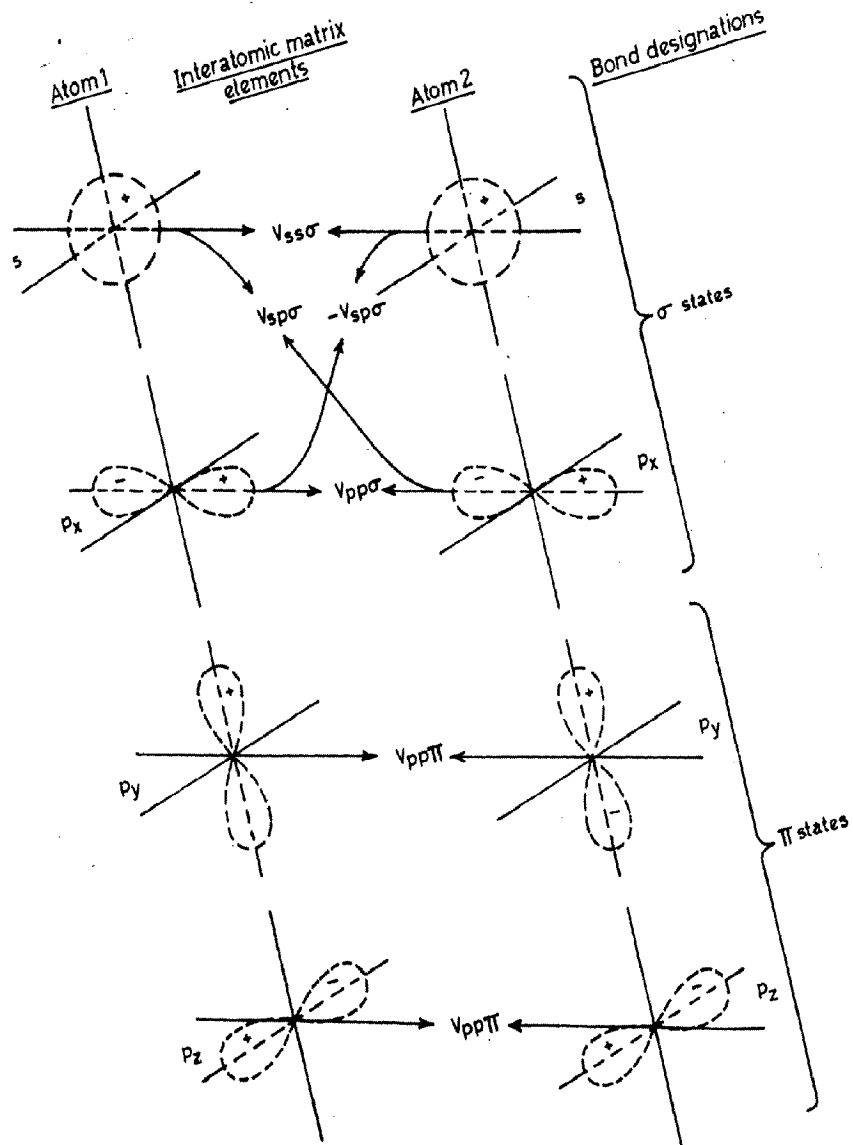


Fig.1.2: THE COUPLING OF ATOMIC ORBITALS IN LITHIUM-FLUORINE DIATOMIC MOLECULES AND THE RESULTANT BOND DESIGNATIONS.

The solution of these algebraic equations can be obtained by diagonalizing the Hamiltonian matrix, $\langle \beta | H | \alpha \rangle$, through unitary transformation.

The solution for the above equations are possible in principle but several approximations have been made to overcome the computational difficulties. The bond orbital [60] approximation neglects all matrix elements coupling the bonding states and the antibonding states. In other words, the k^{th} valence band state is written as a linear combination of bond orbitals.

$$|k\rangle = \sum_i U_{ki} |b_i\rangle \quad \dots(1.82)$$

where $|b_i\rangle$, represents the bond orbital. The error introduced by the neglect of the bond-antibond matrix elements has been corrected in perturbation theory by constructing extended bond and antibond orbitals, $|B\rangle$, and $|A\rangle$ respectively in the following manner;

$$|B\rangle = |b\rangle + \sum_a |a\rangle V_{ab} / (\epsilon_b - \epsilon_a), \quad \dots(1.83)$$

$$|A\rangle = |a\rangle + \sum_b |b\rangle V_{ba} / (\epsilon_a - \epsilon_b). \quad \dots(1.84)$$

The electronic states of the covalent solid corresponding to valence and conduction bands are formed by the linear combinations of their extended bonding and antibonding states respectively. The secular determinant can be set and the band structure can be evaluated completely.

Cohesive energy of covalent solids

The cohesive energy of covalent solids is obtained by calculating three component energies. Firstly, a promotion energy for preparing the isolated atoms; secondly, an overlap interaction energy between atoms as they are brought together without bonding . and lastly, an energy gained in bond formation.

The promotion energy can easily be calculated by considering the energies of the atomic states and the hybrid states. Taking the specific case of Silicon which has two electrons in the atomic s states and two electrons in the atomic p states, the sp^3 hybrid states, when constructed, have the total energy of $4 (\epsilon_s + 3\epsilon_p)/4$. The total energy of the electrons in the free atom is $2 (\epsilon_s + \epsilon_p)$ and, thus, an additional energy of $(\epsilon_p - \epsilon_s) = 4 V_1$ has been required to promote the electrons from the states of a free atom to the hybrid states.

After promotion, a quarter of the charge density arises from s orbitals and three quarters from p orbitals but, there is no change in electrostatic energy because, the atoms remain neutral. When the atoms are brought together the hybridized electron densities are superimposed leading to a change in the potential, kinetic and the exchange energies. The overlap interaction in Silicon has been carried out by Harrison and Sokel [61] as shown

in figure (1.3). The change in kinetic energy and the sum of coulomb and exchange interaction have also been plotted in the same figure. The calculation of the overlap energy has been carried out assuming that all the electrons have the same spin and there is no distortion of the atoms. It is evident from the figure (1.3), that the overlap interaction as conceived, provides a simple interatomic repulsion. Now, if the bonds are allowed to form, the energy of each electron is lowered by the difference between the bond energy, ϵ_b , and the hybrid energy, ϵ_h , and for a nonpolar system, this energy change per bond is $2(\epsilon_h - \epsilon_\beta) = 2V_2^h$. However, the hybrid energies will change due to the influence of overlap potential but this could be included in the electrostatic contribution of the overlap energy.

All this contributions to the energy can be combined to give the cohesive energy of the covalent solid, E_{coh} , as

$$E_{coh} = -E_{pro} - V_o(d) + E_{bond} \quad \dots(1.85)$$

where E_{pro} , is the promotion energy and $V_o(d)$, is the energy of atomic overlap as a function of interatomic distance, d . E_{bond} , is the energy due to bond formation which also depends upon bond length. The expression of the cohesive energy can be minimised to find out the

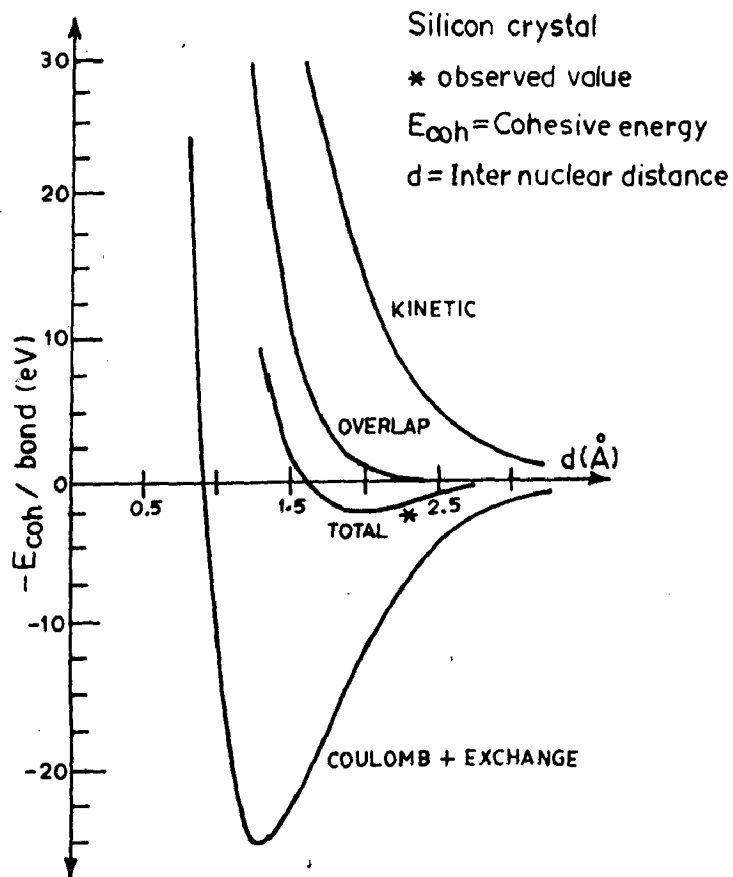


Fig.1.3 : VARIOUS CONTRIBUTIONS TO THE TOTAL ENERGY PER BOND.

equilibrium bond length and the bulk modulus.

(b) Pseudopotential theory of covalent bonding

The pseudopotential theory has been used to describe semiconductors but the pseudopotential perturbation theory as applied to metals in section (1.5.1.2) is quite inappropriate for semiconductors. For metals the perturbation expansion is written in terms of the ratio of the pseudopotentials to the kinetic energy, which is small. For covalent solids, on the contrary, the ratio of kinetic energy to the pseudopotential should be treated as small. This distinction is important only in the case of approximate theories using pseudopotentials.

If one considers the specific example of Silicon and begin with a nearly free electron gas of 4 electrons per ion and calculate the energies of the states by writing it as a linear combination of four plane waves with wave numbers (110) , $(\bar{1}\bar{1}0)$, $(00\bar{1})$ and $(00\bar{1})$, the Hamiltonian matrix, H , can be constructed as given below

$$H = \begin{bmatrix} \hbar^2 k_{110}^2 / 2m & W_{220} & W_{110}^* & W_{111}^* \\ W_{220} & \hbar^2 k_{\bar{1}\bar{1}0}^2 / 2m & W_{111} & W_{111} \\ W_{111} & W_{111}^* & \hbar^2 k_{00\bar{1}}^2 / 2m & 0 \\ W_{111} & W_{111}^* & 0 & \hbar^2 k_{00\bar{1}}^2 / 2m \end{bmatrix}$$

Harrison [62] has diagonalized the above Hamiltonian, to show that the two pairs of energies appearing in the diagonals are split into four levels. The energies of these levels have been matched with the four lowest energy levels at 'X' in the band structure of Silicon and the agreement is quite impressive. The splitting of the upper two levels has given the band gap between the valence and the conduction bands which has arisen primarily from the pseudopotential matrix elements W_{111} , suggesting that a simple theory may be formulated by neglecting all other matrix elements except W_{111} . Band structure of group IV and III-V covalent semiconductors have also been studied successfully by using orthogonalised plane wave pseudopotentials by Garoff and Kleinman [63] .

Cohesive energy

Cohesive energy of covalent semiconductors with treatments based on Heitler-London type methods has been carried out by Schmid, [64] Asano-Tomishina [65] and Goto [66] . Since these treatments involve large overlaps between bonding orbitals, a thorough going orthogonalization of atomic functions and the evaluation of multi-centered Coulomb integrals are inevitable. The task becomes quite laborious.

The concept of pseudopotential proposed originally for band calculations, has opened the possibilities of calculating various crystal properties directly and the stability of metals systematically as discussed in section (1.5.1.2). But, in applying pseudopotential perturbation theory to covalent materials, there are two difficulties : firstly, the cohesive energy of these crystals are large compared to those of simple metals; and secondly, there is an energy gap on the Jones Zone-face corresponding to the Fermi surface. These characteristics of covalent crystals require higher order terms in the perturbation theory.

Morita et.al., [67] developed third order perturbation theory of covalent crystals in terms of pseudopotential to calculate cohesive energies and compressibilities of group IV and III-V covalent crystals.

A crystal consisting of ions located on the lattice points, R_i , 's and an electron gas with four valence electrons per atom (especially in the case of Carbon, Silicon and Germanium), the pseudopotential seen by a valence electron is essentially nonlocal. But local Ashcroft's [43] empty core pseudopotential has been taken as ionic potential for reasons of simplicity. The parameter corresponding to the empty core radius is determined from the first zero of the pseudopotential form

factor interpolated from Cohen and Bergstresser's [68] pseudopotential.

The calculated values of the binding energy of Silicon in second order theory has been shown by Morita et.al., [67] , in which it corresponds to the values in metallic, fcc, bcc and hcp structures and compared with the experimental values. It has been observed that the Ewald energy, E_W , is unfavourable for the open diamond structure compared to those for the close packed metallic structures. The band structure energy, E_{bs} , is favourable for the former structure in comparison to the latter ones. These two opposing tendencies almost balance each other but the diamond structure becomes a little more favourable when compared with the metallic structures. This fact might be considered to suggest that the diamond structure is stable in second order perturbation theory. Even the calculated values of the binding energy is only a little less compared to the experimental values [69]. But, the calculations of phonon dispersion curves in Silicon and Germanium show the diamond structure is unstable against shear stress in the second order perturbation approximation and all transverse acoustic modes have imaginary frequencies. In order to have a consistent theory for covalent crystals one has to go beyond the second order perturbation theory and take into account higher order terms

producing covalent bonding effects.

In covalent crystals with diamond or zinc blende structures, $W(111)$ is only one large pseudo-potential Fourier transform and the effect of $W(111)$ in second order is comparable to that of other $W(\bar{q})$'s is first order. Heine and Jones [70] also have shown that the band gap at the point X ($k_x = (110)$ in $2\pi/a$ unit) on the Jones Zone-faces, is given approximately

$$E_g^{(x)} = 2 | W_{\text{eff}}(220) |$$

where,

$$W_{\text{eff}}(220) = W(220) + \sum'_{\bar{g}} \langle -\bar{k}_x | W | \bar{k}_x - \bar{g} \rangle$$

$$\frac{\langle \bar{k}_x - \bar{g} | W | \bar{k}_x \rangle}{[\bar{k}_x^2 - (\bar{k}_x - \bar{g})^2]} \quad \dots(1.87)$$

where, the summation $\sum'_{\bar{g}}$ is limited to the strong Fourier transform $W(111)$, i.e., $\bar{k}_x - \bar{g} = (0, 0, \pm 1)$. The energy gap calculated from the above equation (1.87) is in good agreement with observed values, so one can therefore assume the energy gap as constant over the Jones Zone-faces. The number of states whose energies are substantially lowered by the presence of the band gap is about $E_g/2$ times the free electron density of states per atom at the Fermi surface, $n(E_F) = 6/E_F$. On an

average, their energies are lowered by $E_g / 2$.

Consequently, the covalent bond correction to the crystal energy, E_{cov} , is given by

$$E_{cov} = - n (E_F) \{ |W_{eff}(220)|^2 - |W(220)|^2 \} \dots(1.88)$$

CHAPTER **2**

BONDING IN METALS

2.1 Introduction

The Hohenberg-Kohn (H.K) theorem states that, for a given external potential, $v(\vec{r})$, the ground state energy is a unique functional of the particle density, $n(\vec{r})$. The energy functional can be minimized with respect to the variation in particle density. The corresponding minimum in energy will be the ground state energy, E_n , of the system which can be written as

$$E_n = \int v(\vec{r}) n(\vec{r}) d\vec{r} + \frac{1}{2} \iint \frac{n(\vec{r})n(\vec{r}')}{|\vec{r} - \vec{r}'|} d\vec{r} d\vec{r}' + G[n] \quad \dots(2.1)$$

where $G[n]$ is a universal functional of density, $n(\vec{r})$, containing the kinetic, the exchange and the correlation energies. The external potential, $v(\vec{r})$, the Ashcroft's [43] empty core pseudopotential has been chosen as a model potential, as it yields the cohesive energy values of the real systems quite in agreement with their experimental values. This indicates that the empty core pseudopotential may provide a sufficiently good model potential. This potential separates the core region of zero potential from the outer region where the coulomb potential is operative.

The model potential is represented as

$$v(\vec{r}) = \begin{cases} 0 & r \leq r_c \\ \frac{Z}{r} & r > r_c \end{cases} \quad \dots(2.2)$$

where r_c is the core radius, beyond which the full ionic potential, $\frac{Z}{r}$, is operative.

Bonding in metals has been investigated both in the homogeneous and the inhomogeneous electron gas model within the framework of density functional formalism. The formulation of the problem and the results have been discussed in the following sections.

2.2 Uniform electron gas model

Due to the volume dependency and a lack of directionality in metallic bonding, the simplest electron distribution assumed is that of a homogeneous electron gas. The ground state energy of a given metal characterised by the valency, Z and the core radius, r_c , has been determined by using the Hohenberg-Kohn [2] theorem. The systematic variation of energy with valency and core radius has been calculated to match it with the observed trend in the periodic table.

2.2.1 Formulation

The electron density in the uniform gas model, n_0 , is independent of the space coordinates. The size of n_0 is the variational parameter which in turn determines the lattice constant or the atomic volume. The system is neutral electrically and each atomic cell has a valence

charge equal to its valency, Z , as expressed below

$$\int_0^{R_a} n_0 d\bar{r} = Z \quad \dots(2.3)$$

or,

$$n_0 = \left(\frac{3Z}{4\pi R_a^3} \right) \quad \dots(2.4)$$

where R_a , is the atomic radius, with these choices of $v(\bar{r})$ as given in equation (2.2). One can write E_n per atom from the Hohenberg-Kohn equation (2.1) as

$$E_{n_0} = -2\pi n_0 Z (R_a^2 - r_c^2) + \frac{16}{15} \pi^2 n_0^2 R_a^5 + G[n_0] \quad \dots(2.5)$$

where the first term is the energy of interaction of electrons with the ion, the second term is the electron-electron repulsion energy and the third term, $G[n_0]$, is a universal functional giving the kinetic, exchange and correlation energy and is expressed in the local density approximation as

$$G[n_0] = \frac{3}{10} (3\pi^2 n_0)^{2/3} Z - \frac{3}{4} \left(\frac{3}{\pi} n_0 \right)^{1/3} Z + Z \left\{ -0.0575 + 0.0155 \ln \left(\frac{3}{4\pi n_0} \right)^{1/3} \right\} \dots(2.6)$$

By combining equations (2.5) and (2.6) and substituting the value of n_o from equation (2.4) one arrives at the following expression for energy as a function of only the atomic radius, R_a , for a given element with valency, Z , and core radius, r_c .

$$\begin{aligned}
 E_{n_o} = & - 1.5 Z^2 \left\{ \frac{1}{R_a} - \frac{r_c^2}{R_a^3} \right\} + \frac{0.6 Z^2}{R_a} \\
 & + \frac{3}{10} \left(\frac{9 \pi Z}{4 R_a^3} \right)^{2/3} Z - \frac{3}{4} \left(\frac{9 Z}{4 \pi R_a^3} \right)^{1/3} Z \\
 & + Z \left\{ -0.0575 + 0.0155 \ln \left(R_a / Z^{1/3} \right) \right\} \\
 & \dots(2.7)
 \end{aligned}$$

The valency of an element is known but the core radius, r_c , is an unknown parameter of its ionic potential. The exact value of r_c can be determined by fitting certain observed physical quantities like term values of energy obtained from spectroscopy, resistivity, the volume per atom in the solid etc. Here, r_c has been determined by demanding that the minimum of E_{n_o} as given by equation (2.7) exists at the observed values of R_a .

The first derivative of the equation (2.7) with respect to R_a can be expressed as

$$\begin{aligned} \frac{dE_{n_0}}{dR_a} = & \frac{1.5 Z^2}{R_a^2} - \frac{4.5 Z^2}{R_a^2} \left(\frac{r_c^2}{R_a^2} \right) - \frac{0.6 Z^2}{R_a^2} \\ & - \frac{2.21 Z^{5/3}}{R_a^3} + \frac{0.458 Z^{4/3}}{R_a^2} + \frac{0.0155 Z}{R_a} \end{aligned} \quad \dots(2.8)$$

At equilibrium $\frac{dE_{n_0}}{dR_a} = 0$

The last term, which is the contribution from correlation energy, can be neglected since its contribution towards the equation (2.8) is less than 5%, and one can get the radius ratio of core versus atomic radius as

$$\frac{r_c}{R_a} = \left\{ 0.2 - \frac{2.21}{4.5} \frac{Z^{-1/3}}{R_a} + \frac{0.458}{4.5} Z^{-2/3} \right\}^{1/2} \quad \dots(2.9)$$

By substituting equation (2.9) in equation (2.8) one can get the above mentioned equilibrium condition. Now the ground state energy, as given by equation (2.7), is a unique function of the atomic radius, R_a . For the observed atomic radius, R_a , one can get the core radius, r_c , for a given element. At a valency, Z , and atomic radius, R_a , for a given element the energy, E_{n_0} , can be determined from equation (2.7) and compared with the experimental values. Thus, one can get an idea as to how good this uniform density

assumption is for a given element.

2.2.2 Results and discussion

The table-2.1 gives the comparison of experimental total energies of simple metals, with those obtained from the present uniform gas model. The energies from various other models using different potentials and charge densities have also been included. The extent of success achieved by the uniform electron gas in explaining the experimental values of total energy has been analysed in the light of its limitations.

The results of Weaire as discussed by Heine [71] give the total energy of various elements which are higher compared to the experimental values. These results are calculated on the basis of Animalu-Heine [49] , model potential, neglecting the terms with $l > 0$. The calculations are purely volume dependant and structure independant, because, the energy has been calculated for a uniform density of electrons. The parameters of the potential has been determined from the term values of energy and so the atomic energy is not an input parameter. The atomic radii of different elements as calculated in this model have large deviations from the observed values. Heine [71] argues that the cohesive energy is proportional to the square of the band gap $\{ 2 v(\bar{q}) \}$ and a

neglect of the band structure part has resulted in a large shift in the calculated atomic radius, R_a , as shown in figures 2.1 and 2.2. These figures show the variation in total energy, E_{n_0} , with the atomic cell radius, R_a . The experimental results, the calculated results of Weaire [71], and those of the present investigation have been presented for elements of Group IA and IIA of the periodic table.

In figure 2.1, the total energy obtained by Ashcroft et.al., [72] for alkali metals have also been included. Ashcroft et.al., [72], in their model have included the band structure term in the calculation of total energy. However the total energy has been estimated by demanding the optimum at the observed values of atomic radius by keeping $\alpha_A = 2\pi Z r_c^2$, a floating parameter. At the same time the band structure term has been calculated by a core radius from liquid resistivity or Fermi Surface(FS) data. In effect it means that Ashcroft et.al., [72] has used two different core radii for the volume dependant and structure dependant terms.

From these figures 2.1 and 2.2, it is quite evident that although the energies obtained by Weaire [71] are higher compared to the experimental results, but the energy versus atomic radius curves for both the calculations of Weaire [71] and the present one lie below the experimentally observed values. If one includes now the band structure

term, the calculated curves will be pushed further below, but simultaneously, a change in the R_a will also take place as anticipated by Heine [71] , causing a lateral shift of the curve. This is borne out by the trend in the calculation of Ashcroft et.al., [72] and is indicated by him.

The total energy as reported by Ashcroft et.al., [72] , is higher than the experimental values except for regions of lower atomic radii containing elements like Lithium. The inclusion of the band structure term has resulted in a part of the calculated energy versus atomic radii curve being above the experimental curve, due to a lateral shift. The discrepancy for elements with lower atomic radii however, can be attributed to a bad choice of potential, an inadequacy of second order perturbation theory and the ignoring of the non local term in the potential. The choice of potential on the basis of the data on Fermi Surface or liquid resistivity are dependant only on states near $\bar{k} \sim \bar{k}_F$. It has obviously not given a good approximation for the states in the entire band. However, for total energy, the energies of all the states are important.

Our calculations with uniform gas model have been lower energies than the values obtained experimentally [69] . This may have resulted from a neglect of the inhomogeneous nature of electron distribution and/or from a bad pseudo-potential when calculated on the basis of observed atomic

radius excluding inhomogeneity. To examine the model further, the pseudopotential of a bare ion of Sodium used by Ashcroft et.al., [72], Weaire [71] and the one used in the present investigation have been compared in figure 2.3. In this figure the potential used by Weaire [71] has been plotted with a well depth, A_0 inside the radius, R_M , as obtained by Animalu and Heine [49]. Also, the empty core pseudopotential with a core radius derived from calculations of Ashcroft et.al., [72] and the one used in the present calculations have been presented. It is observed that the core radii in the model of Ashcroft et.al., [72] is very near to that obtained in the present model. Thus, the potential obtained in the present investigation is not much different from that of Ashcroft et.al., [72]. If one calculates the equivalent core radii for the Animalu and Heine [49] potential used by Weaire [71] one gets

$$r_c^2 = R_M^2 - \frac{2}{3} A_0 \frac{R_M^3}{Z} \quad \dots(2.10)$$

For Sodium $r_c = 1.889$ a.u. is equivalent in energy to the given Animalu and Heine [49] potential. Thus, the potential used in the present investigation lies below that of Ashcroft et.al., [72] and is equivalent to the Animalu and Heine [49] potential. So it may be inferred that the potential used here is not bad. The energy versus atomic radii, R_a , curve should shift above the experimental curve

if inhomogeneity in electron distribution is allowed, as it is expected similarly for the calculations of Weaire [71].

It should be noted that with more detailed calculations the energy values improved by only a small extent, as it is evident from the calculations of Janak et.al., [73], and Moriarty [74]. Since the objective of the present investigation is not to obtain accurate cohesive energy, but to understand bonding behaviour, further refinement in the calculation has not been undertaken. The inhomogeneity has been included in a manner relevant from the point of view of bonding, as it will be explained in the next sections.

2.2.3 Stability of uniform gas model

The expression of E_{n_0} , as given in the equation (2.7) lays down a restriction that every atomic cell must necessarily have the negative charges equal to the valency, making the cell neutral. It implies that the solid does not have the option to accommodate additional space outside the atomic cell and accommodate part of the charge from the atomic cell in this space. Even if it leads to a lowering of energy. To examine this tendency, it is necessary to write the expression for energy of the atomic cell when an amount of charge, ΔZ_e , has moved away from the atomic cell. Now the charge $(Z - \Delta Z_e)$, if uniformly distributed in the

atomic cell will give rise to a uniform density, n_o , as given below,

$$\int_0^{R_o} n_o d\bar{r} = (Z - \Delta Z_e)$$

or

$$n_o = \frac{3(Z - \Delta Z_e)}{4 \pi R_o^3} \quad \dots(2.11)$$

The energy expression can now be obtained, by substituting the expression for n_o from the equation (2.11), into equations (2.5) and (2.6), to give

$$\begin{aligned} E_{n_o} = & -1.5 Z (Z - \Delta Z_e) \left\{ \frac{1}{R_o} - \frac{r_c^2}{R_o^3} \right. \\ & + \frac{0.6 (Z - \Delta Z_e)^2}{R_o} \\ & + \frac{3}{10} \left(\frac{9\pi}{4R_o^3} \right)^{2/3} \cdot (Z - \Delta Z_e)^{5/3} \\ & - \frac{3}{4} \left(\frac{9}{4\pi^2 R_o^3} \right)^{1/3} (Z - \Delta Z_e)^{4/3} \\ & \left. + (Z - \Delta Z_e) \left\{ -0.0575 + 0.0155 \ln \left(\frac{R_o}{(Z - \Delta Z_e)^{1/3}} \right) \right\} \right\} \end{aligned}$$

... (2.12)

The condition that the atomic cell is stable with respect to the flow of charge away from the cell to outside is

given by

$$\frac{dE_{n_0}}{d\Delta Z_e} \Big|_{\Delta Z_e = 0} \geq 0 \quad \dots(2.13)$$

when,

$$\begin{aligned} \frac{dE_{n_0}}{d\Delta Z_e} = & 1.5 \left\{ \frac{1}{R_0} - \frac{r_c^2}{R_0^3} \right\} - \frac{1.2 (Z - \Delta Z_e)}{R_0} \\ & - 1.105 \frac{5}{3} \frac{(Z - \Delta Z_e)^{2/3}}{R_0^2} \\ & + 0.458 \frac{4}{3} \frac{(Z - \Delta Z_e)^{1/3}}{R_0} \quad \dots(2.14) \end{aligned}$$

In the above equation, correlation energy is neglected, due to its negligible contribution (<5%) to the total expression.

Thus,

$$\begin{aligned} \frac{r_c}{R_0} \leq & \left\{ 1 - \frac{1.2(Z - \Delta Z_e)}{1.5 Z} - 1.105 \frac{5}{3} \frac{(Z - \Delta Z_e)^{2/3}}{Z R_0} \right. \\ & \left. + 0.458 \frac{4}{3} \frac{(Z - \Delta Z_e)^{1/3}}{1.5 Z} \right\}^{1/2} \quad \dots(2.15) \end{aligned}$$

Since the energy of the uniform electron gas should, in addition, satisfy the condition for minimum with respect to R_0 at the observed radius of the atomic cell, the equations (2.9) and (2.15) have to be satisfied simul-

taneously. Transferring the value of $\frac{r_c}{R_a}$ from equation (2.9) into equation (2.15) one obtains

$$r_s = Z^{-1/3} R_a > 2.4127 \quad \dots(2.16)$$

Thus, it is clear that only when the uniform electron gas has a density satisfying equation (2.16), it is possible to have stability in the uniform electron gas model.

In this context, one can examine the segment of periodic table where equation (2.16) will be satisfied. The figure 2.4 shows the stability range in the uniform gas model by plotting core radius, r_c , versus the radius of the spherical volume containing one electron, r_s , for the elements with valencies, $Z = 1$ to 7. The elements occurring with the lowest core radius and the highest core radius are shown in each valency. A line of separation has been drawn at $r_s = 2.4127$ a.u. to show the limit beyond which the uniform gas model is stable. It is observed that all the elements with valency, $Z = 1$, lie in the uniform gas model region. For valency, $Z = 2$, the elements with core radius less than 1.14 a.u. lie in the region of instability of uniform gas. The elements with the core radius greater than 1.14 a.u. should conform to uniform gas model as indicated by its success in explaining their cohesive energy. Almost all the elements with valency $Z = 3$ fall in the region where r_s is less than 2.4127 a.u.

except the element Thallium. In case of valencies, $Z \geq 4$, all the elements in the periodic table lie in the region where electron distribution is inhomogeneous and the validity of the uniform gas model is doubtful. Such elements demand the application of inhomogeneous electron gas model as it has been carried out and presented in the following sections.

2.3 Inhomogeneous Electron Gas : Step model

The study of the stability of uniform electron gas model has shown that at $r_s > 2.4127$ a.u. the uniform electron gas model works. But a large number of simple metals in the periodic table have $r_s < 2.4127$ a.u., (See fig. 2.4) for which the uniform electron gas model is not stable. There is a tendency of some amount of charge ΔZ_e , to be away from the uniform bas atomic cells spontaneously. If the metallic bonding still persists the next model should be evolved by violating the assumption of the uniform distribution of electrons within the atomic cell. The step model developed in this context assumes the existence, electron gases of two different densities in the inner and the outer region of the cell. But, it will lead to a discontinuity in the boundary. As a result, the gradient term in the expression for energy will diverge. The realistic electron distribution will result by readjusting the dis-

tribution at the boundary so as to eliminate the infinite gradient. However, this model will be instructive to yield information about the gross behaviour of the electrons from the point of view of bonding. The model here approximates an inhomogeneous electron gas in metal in terms of homogeneous electron gas in two segments of the atomic cell. The size of the segments and the corresponding charge density is dictated by the principle of minimization of total energy. The advantage of this approach lies in the ability to build a large non-uniformity in charge, in case it leads to a lowering in energy. Also the energy can be calculated more accurately here than that is possible in perturbation theory because the density functional formalism is formally exact. But the representation of the charge density by just two homogeneous segments may be quite insufficient and a poor approximation to the true charge distribution.

An atomic cell consisting of electron gas with two densities as envisaged in this step model will be able to reflect some features of concern to the chemists. If the charge density in the inner cell is higher, the metal has predominantly electrons with s-character. But when the outer shell charge density increases it indicates an increasing p-character of the electrons giving rise to sp bonding. But this sp bonding is distinctly different from covalent sp bonding because the electron distribution here

is nondirectional. It is more a reflection of the nature of states occupied by the electrons in a overlapping s-p band.

In the following sections the density functional energy has been expressed as a parametric function of the density parameters. For a given valency and core radius the energy function has been optimized by Davidon Fletcher and Powell method [75] to get the ground state energy and the corresponding charge distribution.

2.3.1 Formulation

With the choice of Ashcroft's [43] empty core pseudopotential, $v(\vec{r})$, from the equation (2.2), one proceeds to choose a parametric function for electron density, $n(\vec{r})$. Here, the density has a step discontinuity as given below

$$n(\vec{r}) = \begin{cases} n_0 & \text{for } r \leq R_0 \\ n_1 & \text{for } R_0 \leq r < R_a \end{cases} \quad \dots(2.17)$$

where, n_0 is the density of the electrons in the inner cell of radius, R_0 , within the atomic cell and n_1 is the electron density in the outer spherical shell of inner radius, R_0 and outer radius, R_a . The density has four parameters n_0, n_1, R_0 and R_a . One of these parameters is fixed by using the principle of charge neutrality in the atomic cell

consisting of the inner cell and the outer shell. Thus, there remains three parameters or variables for minimizing the energy. The inner cell contains an amount of charge, $(Z - \Delta Z_e)$. Since the electron distribution, n_o , in the inner cell is uniform the equation (2.11) and the energy of the inner cell as given in equation (2.12) can be written directly as,

$$\begin{aligned}
 E_{n_o} = & - 1.5 Z (Z - \Delta Z_e) \left\{ \frac{1}{R_o} - \frac{r_c^2}{R_o^3} \right\} \\
 & + \frac{0.6(Z - \Delta Z_e)^2}{R_o} + \frac{3}{10} \left(\frac{9\pi}{4 R_o^3} \right)^{2/3} (Z - \Delta Z_e)^{5/3} \\
 & - \frac{3}{4} \left(\frac{9}{4\pi^2 R_o^3} \right)^{1/3} (Z - \Delta Z_e)^{4/3} \\
 & + (Z - \Delta Z_e) \left\{ - 0.0575 + 0.0155 \ln \left(\frac{R}{(Z - \Delta Z_e)^{1/3}} \right) \right\} \\
 & \dots(2.18)
 \end{aligned}$$

where, the first term is the energy of interaction of electrons with the ionic pseudopotential and r_c , is the core radius. The second term is the electron-electron repulsion energy and the rest of the terms are kinetic, exchange and correlation energies respectively.

The remaining ΔZ_e charge of the atomic cell is now distributed homogeneously in the outer shell around the

inner cell to make the atomic cell neutral. But the charge density in the spherical outer shell may be different from that in the inner cell and thus, there is a step discontinuity in electron distribution at $r = R_0$. If the charge density of the electrons in the outer shell is n_1 , the charge neutrality of the atomic cell demands that

$$\int_{R_0}^R n_1 d\vec{r} = \Delta Z_e$$

or

$$n_1 = \frac{3 \Delta Z_e}{4 \pi (R_a^3 - R_0^3)} \quad \dots(2.19)$$

Following Hohenberg-Kohn[2] theorem, the energy of the outer shell can be written as

$$E_{n_0, n_1}^{\text{shell}} = \int_{R_0}^R v(\vec{r}) n_1 d\vec{r} + \frac{1}{2} \int_{R_0}^R \int_{R_0}^R \frac{n_1 n_1}{|\vec{r} - \vec{r}'|} d\vec{r} d\vec{r}'$$

$$+ \int_{R_0}^R \int_{R_0}^R \frac{n_0 n_1}{|\vec{r} - \vec{r}'|} d\vec{r} d\vec{r}' + G[n_1] \quad \dots(2.20)$$

In this equation, the first term represents the interaction of the ionic pseudopotential, with the outer shell electron density, n_1 . The second term is the electron-electron repulsion within the outer shell. The third term is the electron-electron repulsion between the inner cell electrons with those in the outer shell. The fourth term $G[n_1]$ is the universal functional representing the kinetic, exchange

and correlation energy of the electrons in the outer shell with a density, n_1 .

Using equation (2.19) in (2.20) and the expression for $G [n_1]$ for the uniform electron gas, one arrives at the following expression,

$$\begin{aligned}
 E_{n_0, n_1}^{\text{shell}} = & - \frac{1.5 Z \cdot \Delta Z_e (R_a^2 - R_o^2)}{(R_a^3 - R_o^3)} \\
 & + \frac{4.5 \Delta Z_e^2}{(R_a^3 - R_o^3)^2} \left\{ \frac{2}{15} R_a^5 - \frac{1}{3} R_a^2 R_o^3 + \frac{2}{10} R_o^5 \right\} \\
 & + 1.5 (Z - \Delta Z_e) \Delta Z_e \frac{(R_a^2 - R_o^2)}{(R_a^3 - R_o^3)} \\
 & + \frac{1.105 \Delta Z_e^{5/3}}{(R_a^3 - R_o^3)^{2/3}} - \frac{0.458 \Delta Z_e^{4/3}}{(R_a^3 - R_o^3)^{1/3}} - 0.0575 \Delta Z_e \\
 & + \frac{0.0155}{3} \Delta Z_e \left\{ \ln(R_a^3 - R_o^3) - \ln \Delta Z_e \right\} \\
 & \dots(2.21)
 \end{aligned}$$

The total energy of the pure metal in the step model can now be written by combining the energy of the inner cell given in equation (2.18) and the energy of the outer shell as given by equation (2.21).

$$E_n = E_{n_0} + E_{n_0, n_1}^{\text{shell}} \dots(2.22)$$

Now, the total energy, E_n , is a function of the inner cell radius, R_o , the outer shell radius, R_a , and the charge contained in the outer shell, ΔZ_e . To derive the energy for a metal with a given valency, Z , and core radius, r_c , under this model the expression for energy as given by equation (2.22) is optimized with respect to the variables R_o , R_a and ΔZ_e .

2.3.2 Results and discussion

The variation of energies of the inner atomic cell and the outer shell with ΔZ_e have been shown for a given univalent metal with $r_c = 1.0, 1.6, \text{ and } 2.6 \text{ a.u.}$ in figure 2.5. It is observed that the energy of the inner cell is increasing from a highly negative value of zero as the charge in this cell reduces. On the contrary, the energy of the outer shell is reducing from zero to a negative value with the increase in charge in this shell, ΔZ_e , as shown in figure 2.5. However, the configuration of electron gas of two different densities will be stable only when there is a minimum in the total energy for a specific value of ΔZ_e . In addition to this, the configuration will become energetically favourable compared to the uniform electron gas only when the value of total energy, which is the sum of the energies of the atomic inner cell and the outer shell, at the minimum is lower than the energy of the atomic cell

with uniform electron gas .

The difference in behaviour of the total energy with ΔZ_e , for low r_c and high r_c have been explored as shown in figures 2.6a and 2.6b. For $r_c = 1.0$ and 1.6 a.u., one observes that the total energy decreases as the charge in the outer spherical shell increases. However, beyond the optimum the total energy starts increasing. The depth of the energy minimum reduces as ionic pseudopotential becomes weak i.e., r_c increases from 1.0 to 1.6 a.u. At still higher values of r_c , the minima disappears.

Figure 2.7 shows the details of different energy terms of the inner cell and the outer spherical shell. It is observed that the kinetic energy and the electron - electron repulsion energy of the inner cell reduces with the charge flow to the outer shell and similarly, the magnitude of the negative energy terms like the potential, exchange and correlation energy also reduces. But, the kinetic energy, the electron - electron repulsion energy of the outer spherical shell increase and the magnitude of the negative energy terms like, potential energy, exchange and correlation energy increase as the outer shell acquires charge. The increase in the potential energy and the decrease in the electron - electron repulsion energy of the inner cell almost balance for small ΔZ_e and thus the decrease in kinetic energy of the inner cell and the exchange

and correlation energy of the outer spherical shell provide a major impetus for the lowering of energy. However, the change in energy in the spherical shell starts dominating the terms favouring the charge transfer outside the inner cell, but soon the increase in potential energy of the inner cell grows relatively strongly, disfavouring further charge transfer. As a result of these two opposing tendencies a minimum in total energy is obtained for a given quantity of charge flowing to the outer spherical shell.

The change in the density of electrons in the inner cell and the outer spherical shell with the increase in charge in the spherical shell have been shown for the element $Z = 1.0$ and $r_c = 1.0$ a.u. in figure 2.8. In the outer shell, the electron density, n_1 , has been observed to rise steadily with ΔZ_e but, that in the inner cell, n_0 , has two peaks. The smaller initial peak is the reflection of a tendency to recover some potential energy while kinetic and electron-electron repulsion energies are dominating, but due to the change of domination from electron-electron repulsion to kinetic energy at $\Delta Z_e = 0.40$, there is a corresponding peak in n_0 . However, the increased magnitude of the change in potential energy at $\Delta Z_e > 0.40$ stimulates a buildup of charge in an effort to partly compensate for it. The electron density of the outer spherical shell, n_1 , increases steadily due to the dominance of the negative

energy terms like potential energy, exchange and correlation energy.

The radius of the inner cell, R_0 , and the outer radius of the spherical shell, R_a , vary with the charge in the outer shell as shown in figure 2.9. The inner cell radius decreases continuously in order to give an advantage of higher ionic pseudopotential to electrons in spherical shell. However, the outer radius increases initially to restrict the electron density to a level beyond which, the kinetic and the electron-electron repulsion energy will become prohibitive. But, an increase in ΔZ_e and a decrease in R_0 strengthens the potential energy term to such an extent that the outer spherical shell radius starts decreasing.

In this investigation, a configuration having no electrons in the inner core region and all the electrons in the outer spherical shell has been ruled out as an artifact of Ashcroft's pseudopotential. The prevalent s-p bond can not result in such an extreme electron distribution unless a large number of states with higher quantum number are involved. The last possibility is not physically sound because the promotion energies will forbid such an occurrence.

The figures 2.10 and 2.11 show the total energy of the inhomogeneous electron gas leading to metallic bonding,

optimized with respect to R_o , ΔZ_e and R_a for a given valency, Z , and the core radius, r_c . The change in energy with core radius, r_c , for a given valency, $Z = 1$ to 7, has been shown in figures 2.10 and 2.11. It has been observed that, at lower core radii, the total energy is large and more negative compared to that observed for higher core radii for a particular valency, Z . As valency increases, the total energy becomes more negative. The total energies obtained in the uniform electron gas model have also been plotted with dotted lines for comparison with the step model as shown in figures 2.10 and 2.11. The step model yields a slightly higher value for the negative total energy for a particular valency, Z , at lower ranges of core radii. But, the deviation in total energy in the uniform gas model and step model becomes smaller for higher core radii. This trend has been maintained for all valencies.

The variation of the charge in the outer spherical shell for different elements characterised by valency and core radius of the ionic pseudopotential is shown in figure 2.12. It is observed that, for stronger pseudopotentials the values of ΔZ_e are higher for a given valency but, it increases in certain rapid steps and remains steady before the next increase at some appropriate lower r_c . This stair-like characteristic has been observed for all valencies with a larger number of steps for higher

valencies in the same range of r_c under investigation. But, the electron densities vary smoothly without any of the above characteristics as observed in the case of ΔZ_e . The figure 2.13, shows the increase in the density of electrons in the inner cell, n_0 , and the outer spherical shell, n_1 , for a decrease in the value of r_c . However, n_0 increases at a much faster rate compared to n_1 in the outer shell. For large r_c the uniform electron gas model is approached and the density difference between n_0 and n_1 reduces.

Figure 2.14 shows the variation of energy with the radii of the atomic cell including the spherical shell around. It is observed that for a given valency and a low atomic radius the step model yields an energy considerably lower compared to that obtained in the uniform gas model. However, the difference in energies become negligible beyond a given limiting value of the atomic radius for a given valency. These limiting values of radii increase with an increase in valency. Since the density functional theory is an exact theory it could create, in its framework, a strong inhomogeneity in charge distribution if it is favoured by a lowering in energy.

A comparison of the results obtained in the step model with those observed experimentally shows that the

step model has invariably given a higher total negative energy as shown in table 2.2. The total energy obtained by uniform gas model has been nearer to the values observed experimentally in the case of metals with lower valency, but for higher valency metals, the uniform electron gas model gives an energy which is higher than the observed ones. The step model shows energy values lower than the experimental ones. It should be pointed out that in the step model, the positive gradient energy contribution has been ignored. This energy term would have checked the extent of difference in electron densities in the outer shell and the inner cell considerably. Also, its positive contribution to the energy is expected to result in higher total energy and thus, the agreement would have been better with experiments. In the next chapter the impact of this gradient energy contribution will be examined in a continuous electron density model and compared with the results of the step model in order to devise appropriate correction.

2.4 Summary

The ground state energy and the cohesive energy of the elements have been investigated under the assumption that the electron gas around the ion core is uniform and is under the Ashcroft's empty core pseudopotential characterised by a core radius. The ground state energy has been calculated

using Hohenberg-Kohn density functional formalism. The energy functional has been reduced to a parametric function of atomic radius. By knowing the valency of an element, the core radius of the element has been expressed as a function of atomic radius by demanding that the ground state energy corresponds to the minimum of the energy function at the observed values of atomic radius, R_a . The cohesive energies determined by this model have been tabulated and are higher than the experimental values for the corresponding atomic diameter. But if one allows for small inhomogeneity through second order perturbation theory there will be a further lowering of ground state energy but a simultaneous shift in the atomic radius will result in a better matching of the calculated values with the observed ones.

The stability of the uniform electron gas model has been analysed with respect to a movement of the charge away from the atomic cell causing a reduction in the total energy. For elements with $r_s > 2.4127$ a.u. only the uniform electron gas model is stable.

A large inhomogeneity in the electron gas has been introduced in a step model where the atomic cell has been split into two segments with different densities of electron gas. The gradient energy in the density functional expansion has been ignored. The density functional is reduced

to a three parameter function of atomic radius, the radius of the inner segment and the density of electrons in the order segment. The ground state energies calculated are smaller compared to the observed results for different elements. However, a correction to this model introduced by comparing the results with that obtained from continuous density model presented in the next chapter improves the performance of this model remarkably.

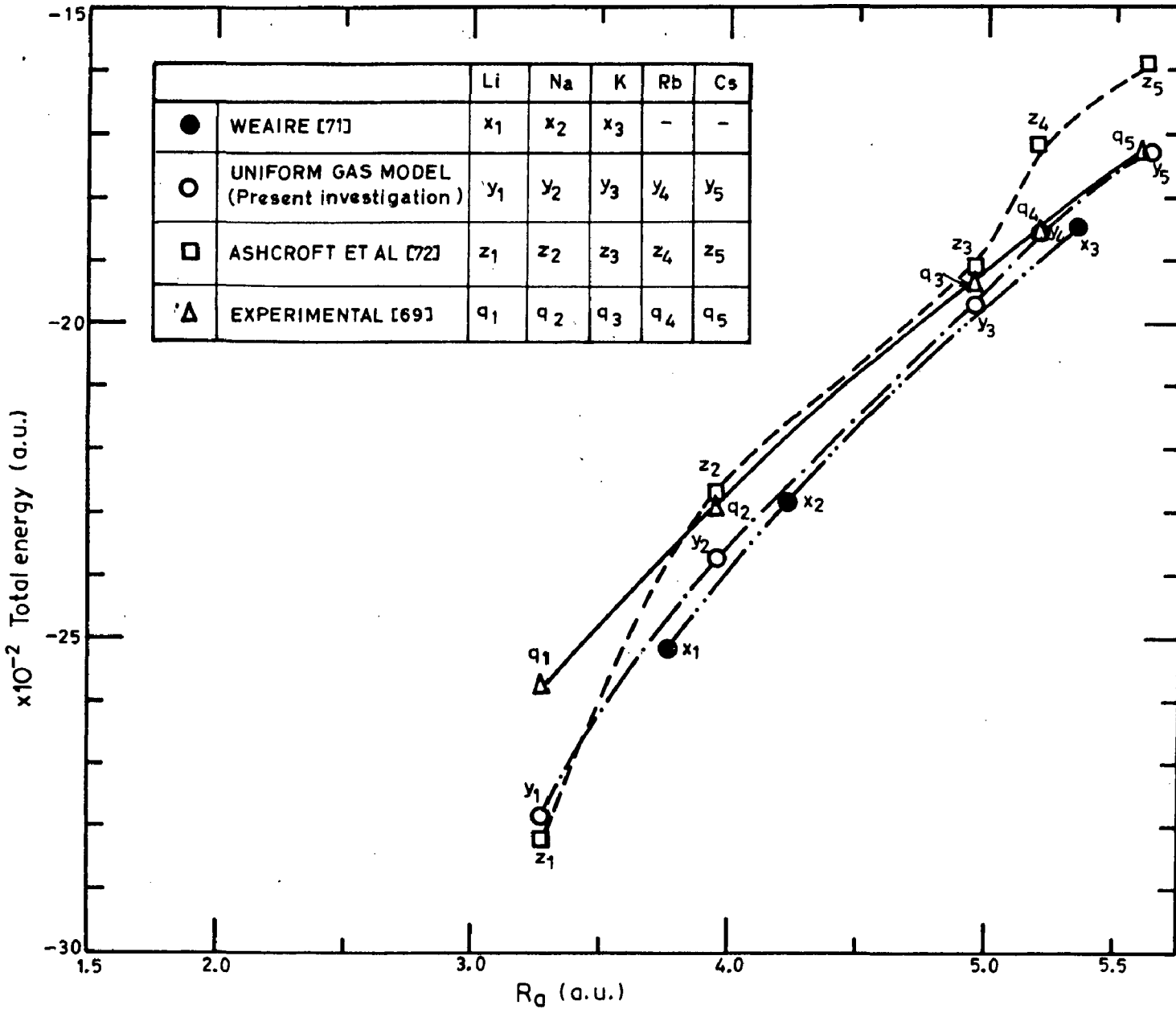


FIG.2.1 : THE VARIATION IN TOTAL ENERGY, E_n in a.u. WITH ATOMIC CELL RADIUS, R_a in a.u. FOR ELEMENTS IN GROUP I OF THE PERIODIC TABLE.

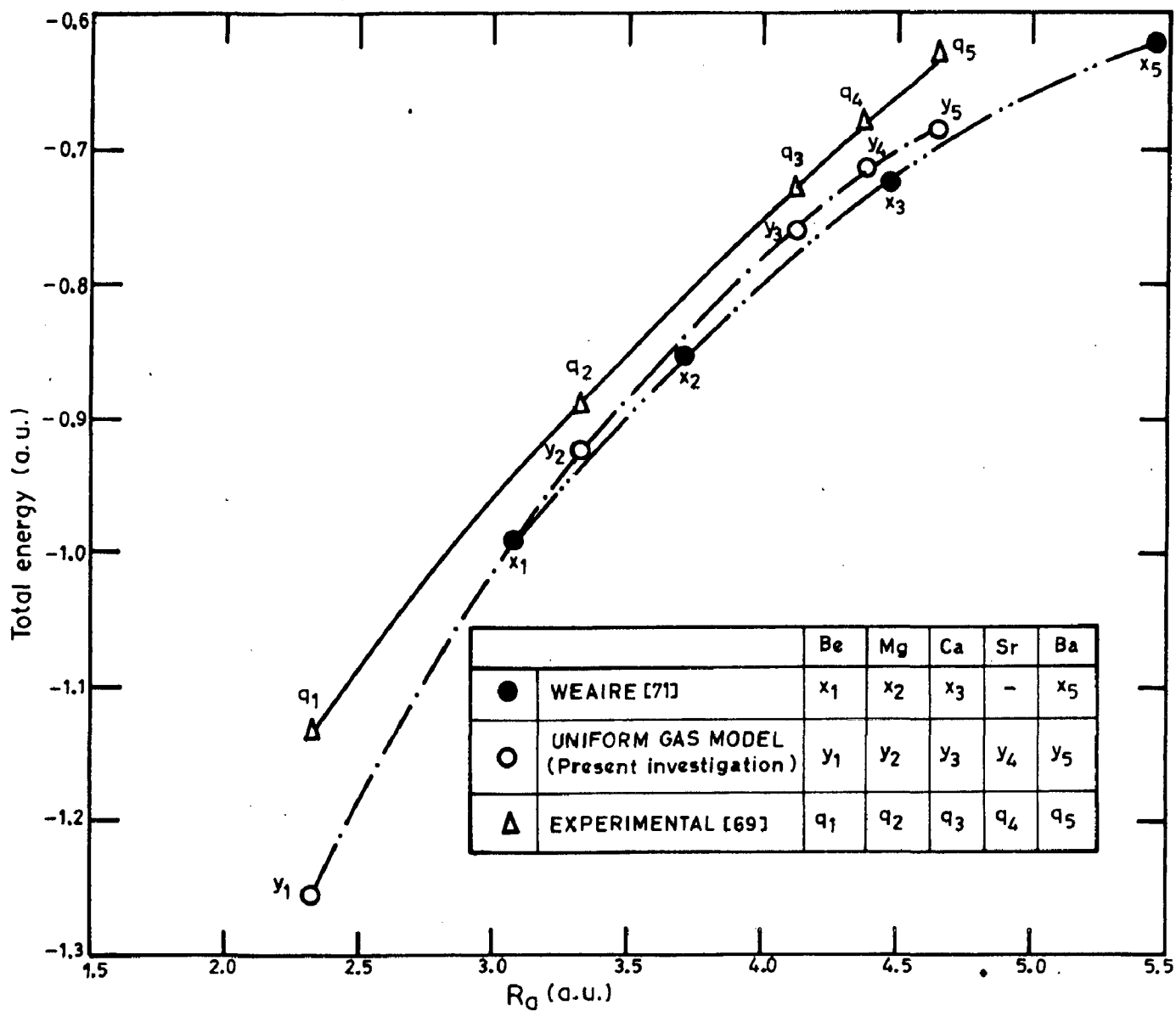


FIG. 2.2: THE VARIATION IN TOTAL ENERGY, E_n in a.u. WITH ATOMIC CELL RADIUS, R_a in a.u. FOR ELEMENTS IN GROUP II OF THE PERIODIC TABLE.

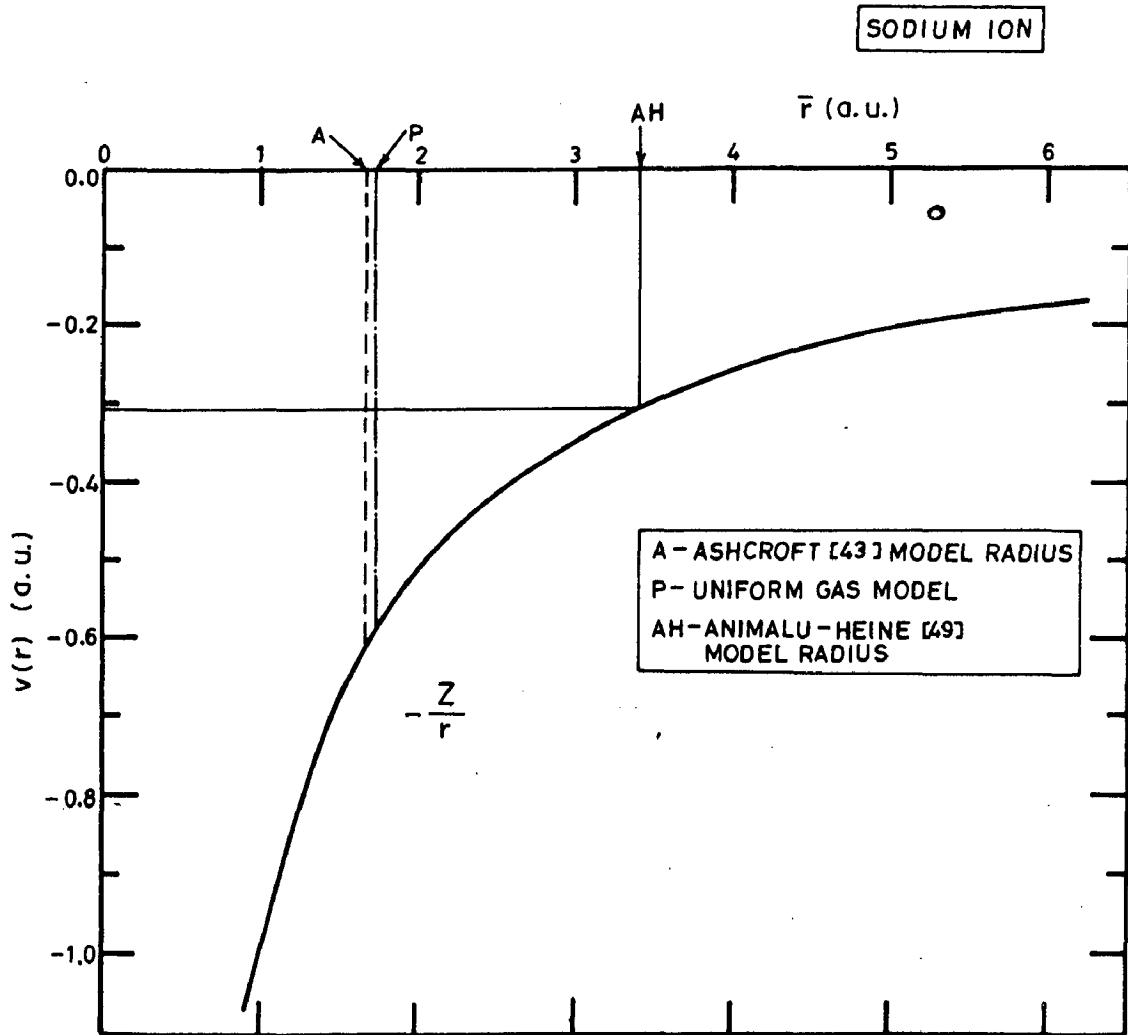


FIG.2.3: THE PSEUDOPOTENTIAL OF A BARE SODIUM ION, SHOWN IN REAL SPACE USED IN THE CALCULATION OF ASHCROFT [43] WEARE [71] AND THE PRESENT INVESTIGATION.

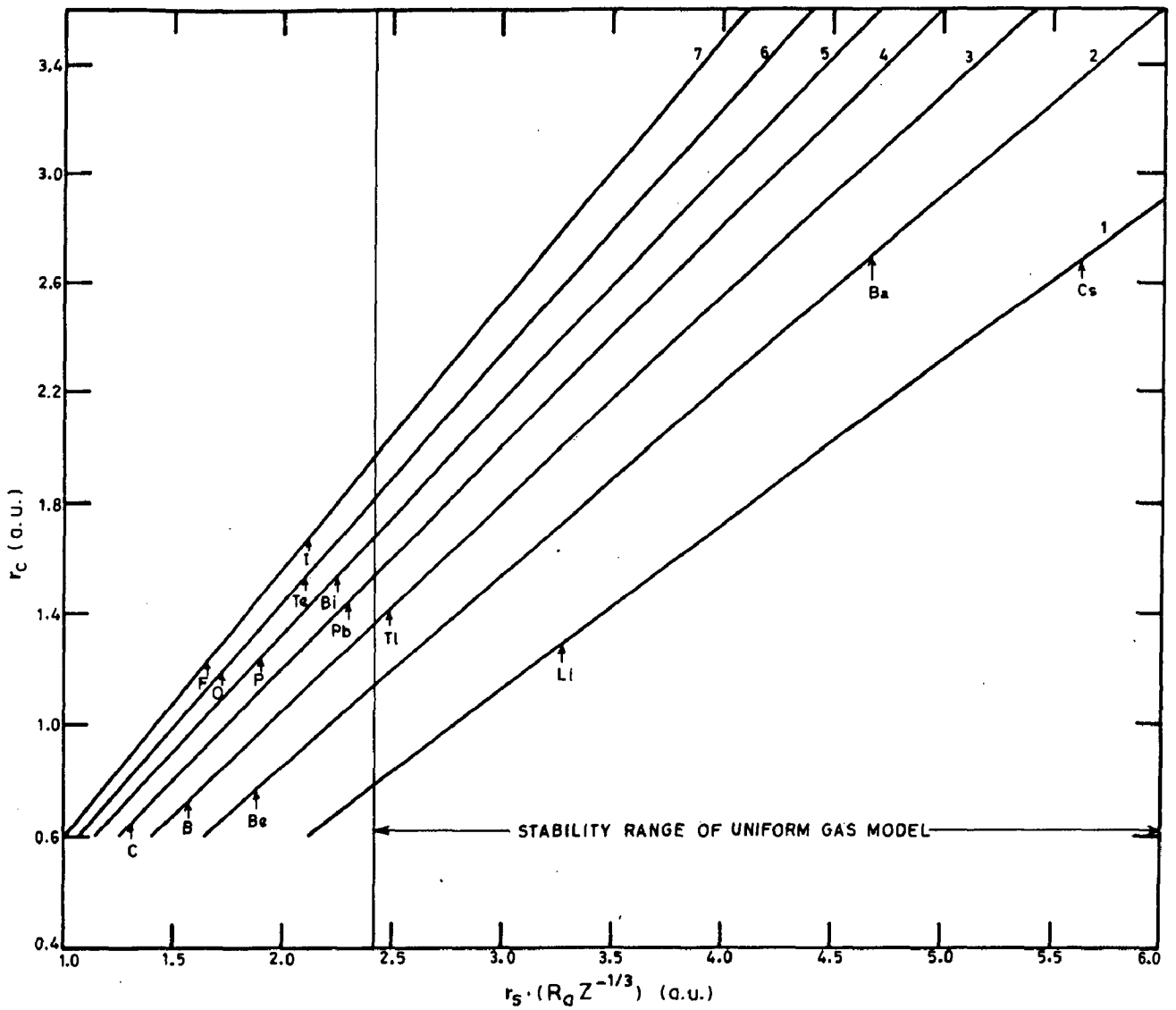


FIG.2.4: THE CHANGE OF CORE RADII, r_c in a.u. WITH r_s in a.u. FOR VARIOUS ELEMENTS WITH VALENCIES, $Z=1$ TO 7 . THE UNIFORM GAS MODEL STABLE AFTER $r_s \geq 2.4127$ a.u.

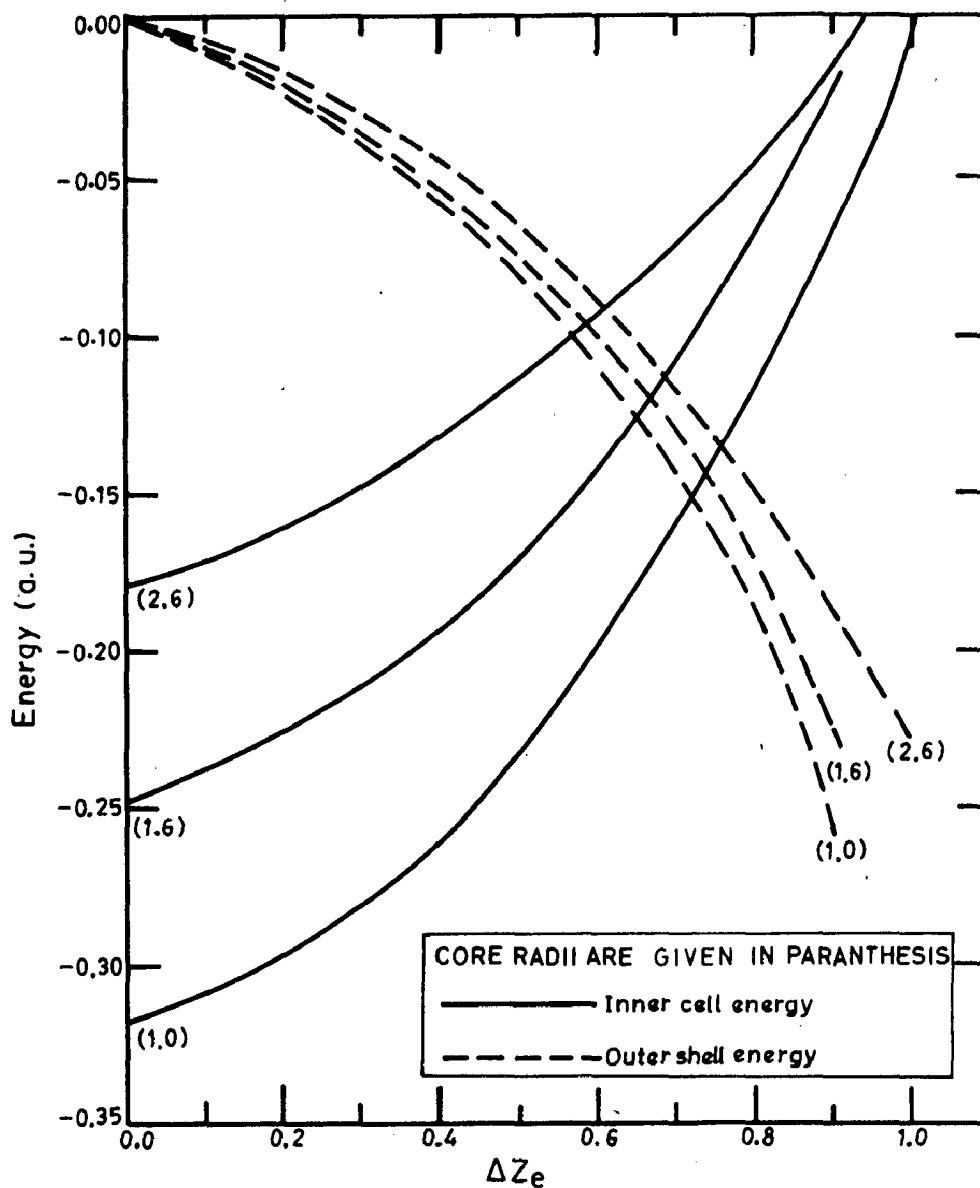


FIG.2.5: THE VARIATION OF ENERGIES, in a.u. OF THE INNER CELL AND THE OUTER SHELL WITH THE CHARGE FLOW, ΔZ_e FOR THE UNIVALENT ELEMENTS WITH CORE RADII, $r_c = 1.0, 1.6$ & 2.6 a.u. .

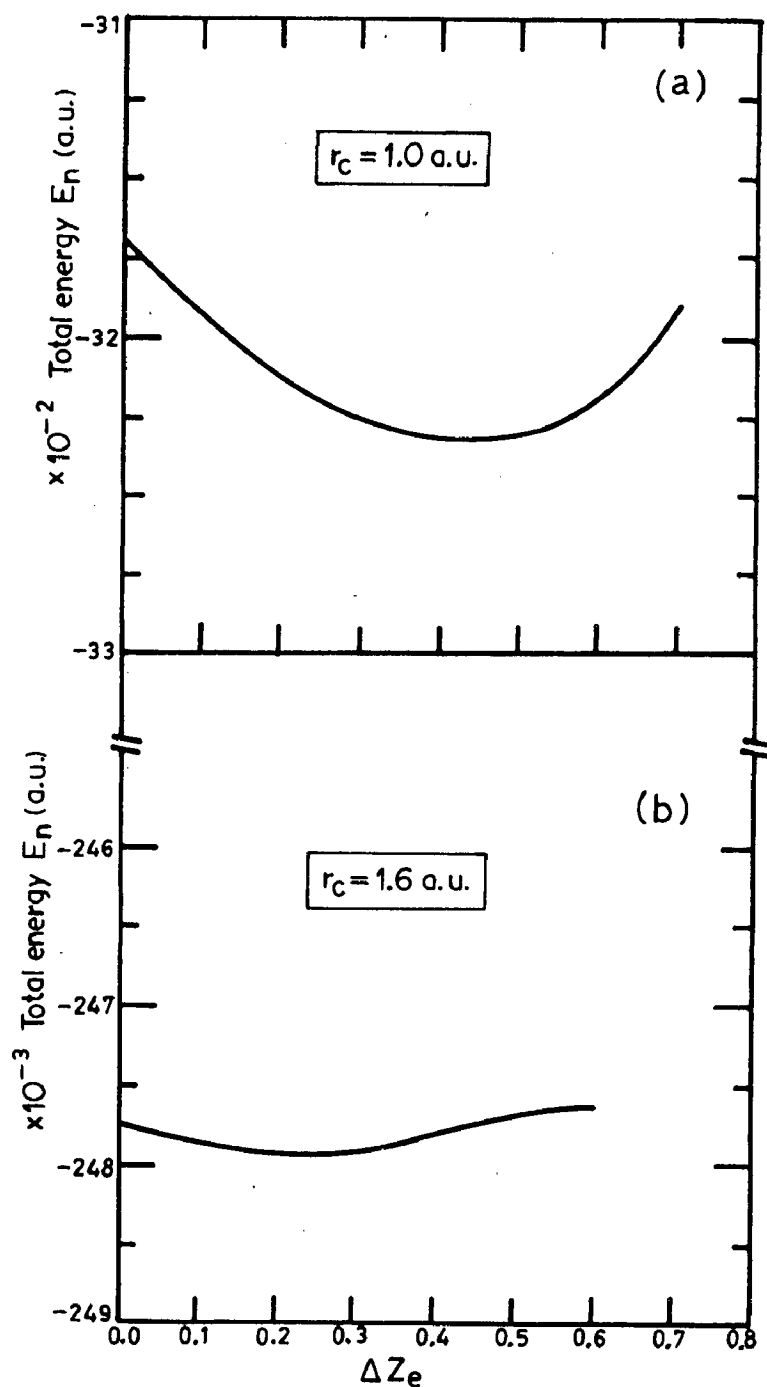


FIG. 2.6: THE DIFFERENCE IN BEHAVIOUR OF THE TOTAL ENERGY, E_n in a.u. WITH THE CHARGE FLOW FROM THE INNER CELL TO OUTER SHELL, (a) FOR LOW CORE RADIUS, $r_c = 1.0$ a.u. AND (b) FOR HIGH CORE RADIUS, $r_c = 1.6$ a.u. IN VALENCY, $Z = 1$.

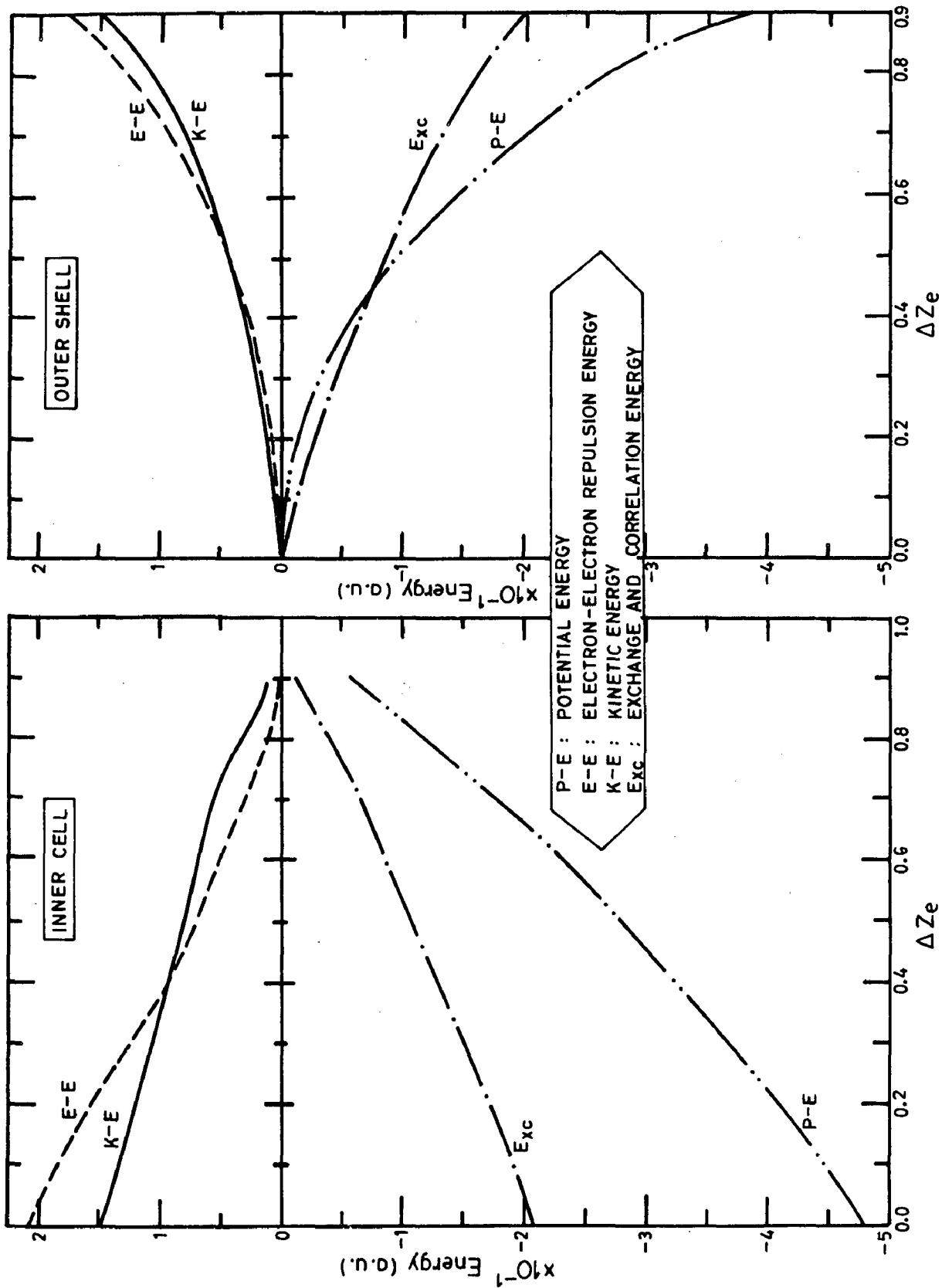


FIG.2.7: THE CHANGE OF DIFFERENT ENERGY TERMS INVOLVED IN STEP MODEL WITH THE CHARGE FLOW, ΔZ_e FROM INNER CELL TO OUTER SHELL IN AN ATOM WITH VALENCY, $Z=1$ AND CORE RADIUS, $r_c=1.0$ a.u. .

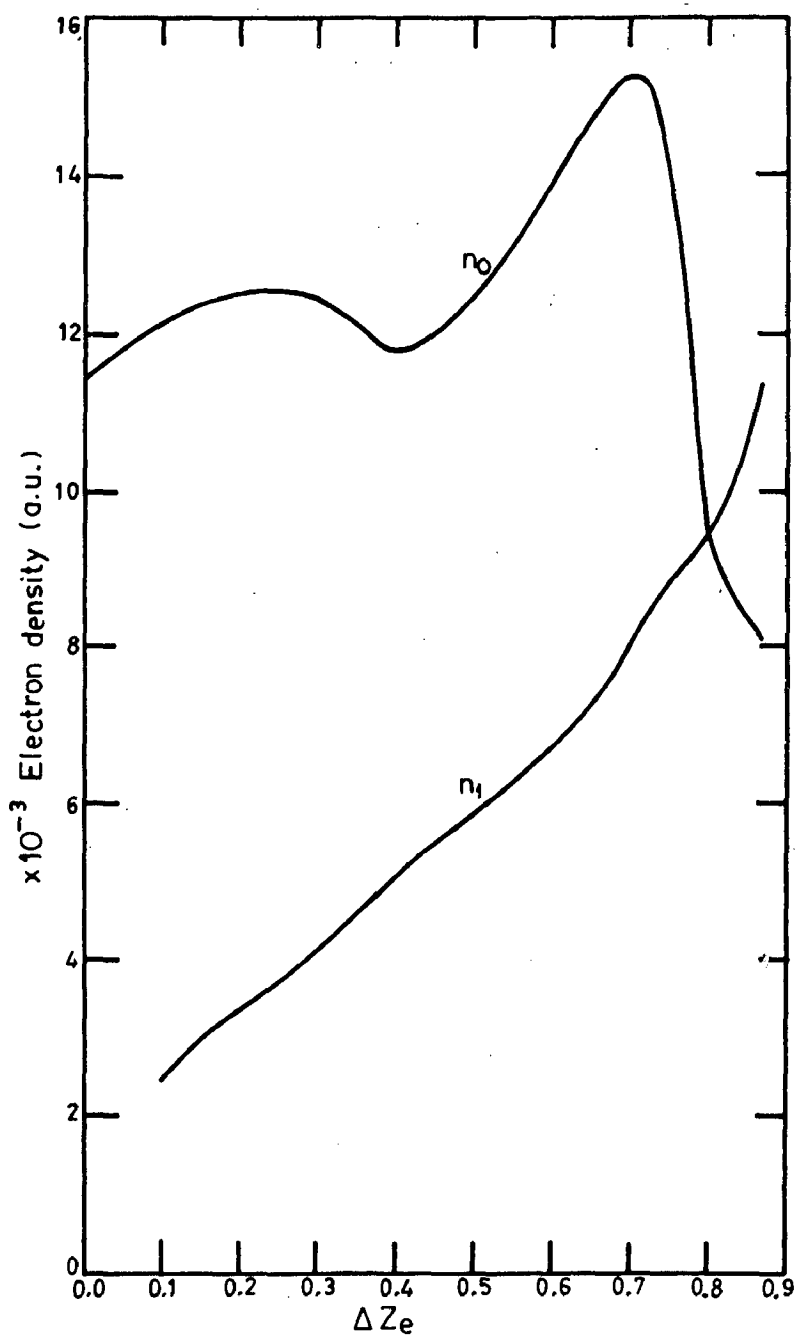


FIG.2.8: THE CHANGE IN THE DENSITY OF ELECTRONS IN THE INNER CELL, n_0 AND THE OUTER SHELL, n_1 WITH THE FLOW OF CHARGE, ΔZ_e TO THE OUTER SPHERICAL SHELL FOR THE ELEMENT WITH VALENCY, $Z = 1.0$ AND CORE RADIUS, $r_c = 1.0$ a.u. .

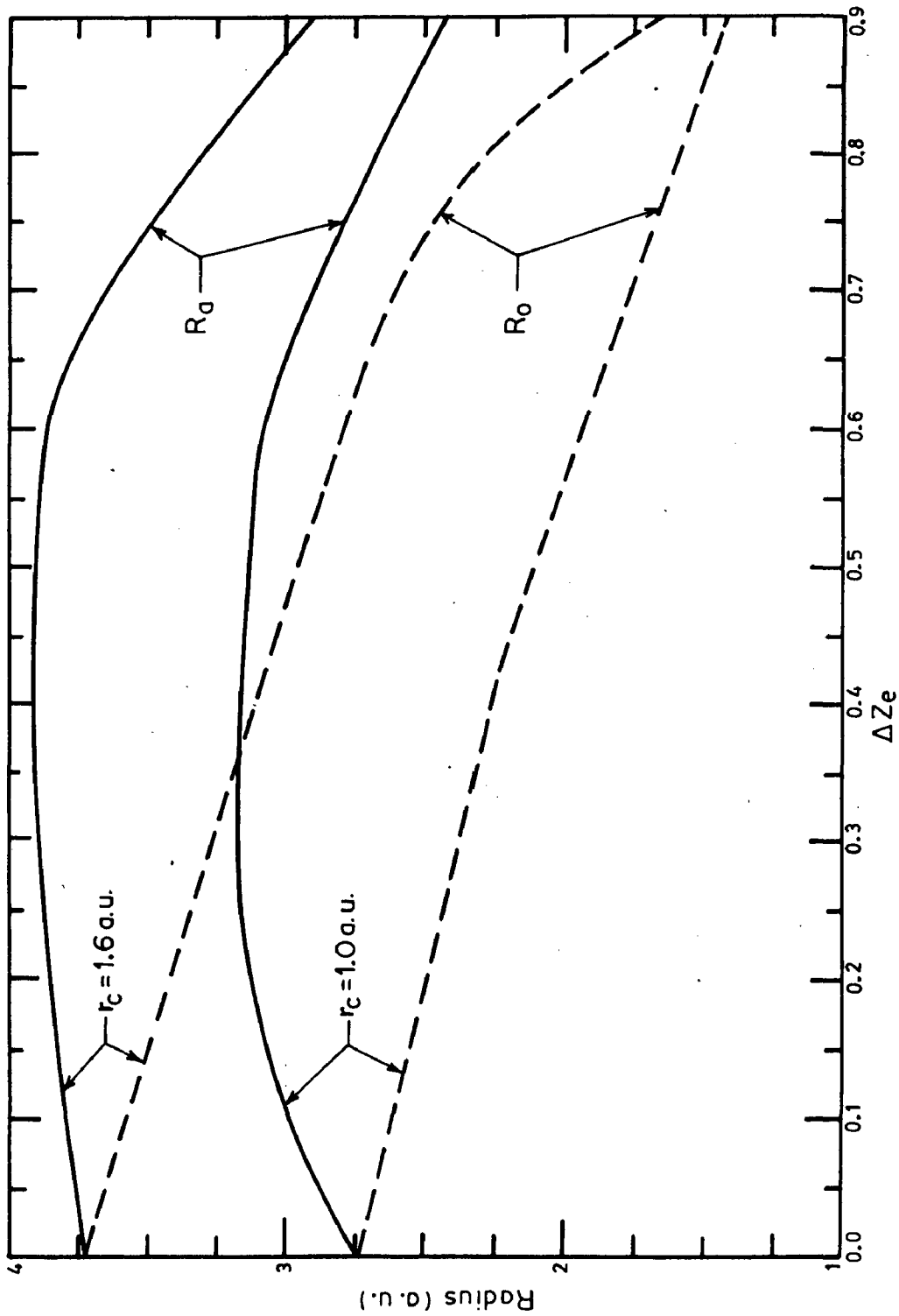


FIG.2.9: THE VARIATION OF RADIUS OF THE INNER CELL, R_0 in a.u. AND THE RADIUS OF THE SPHERICAL SHELL, R_G in a.u. WITH THE CHARGE IN THE OUTER SHELL, ΔZe , FOR VALENCY, $Z=1$ AND CORE RADII, $r_c = 1.0$ & 1.6 a.u. .

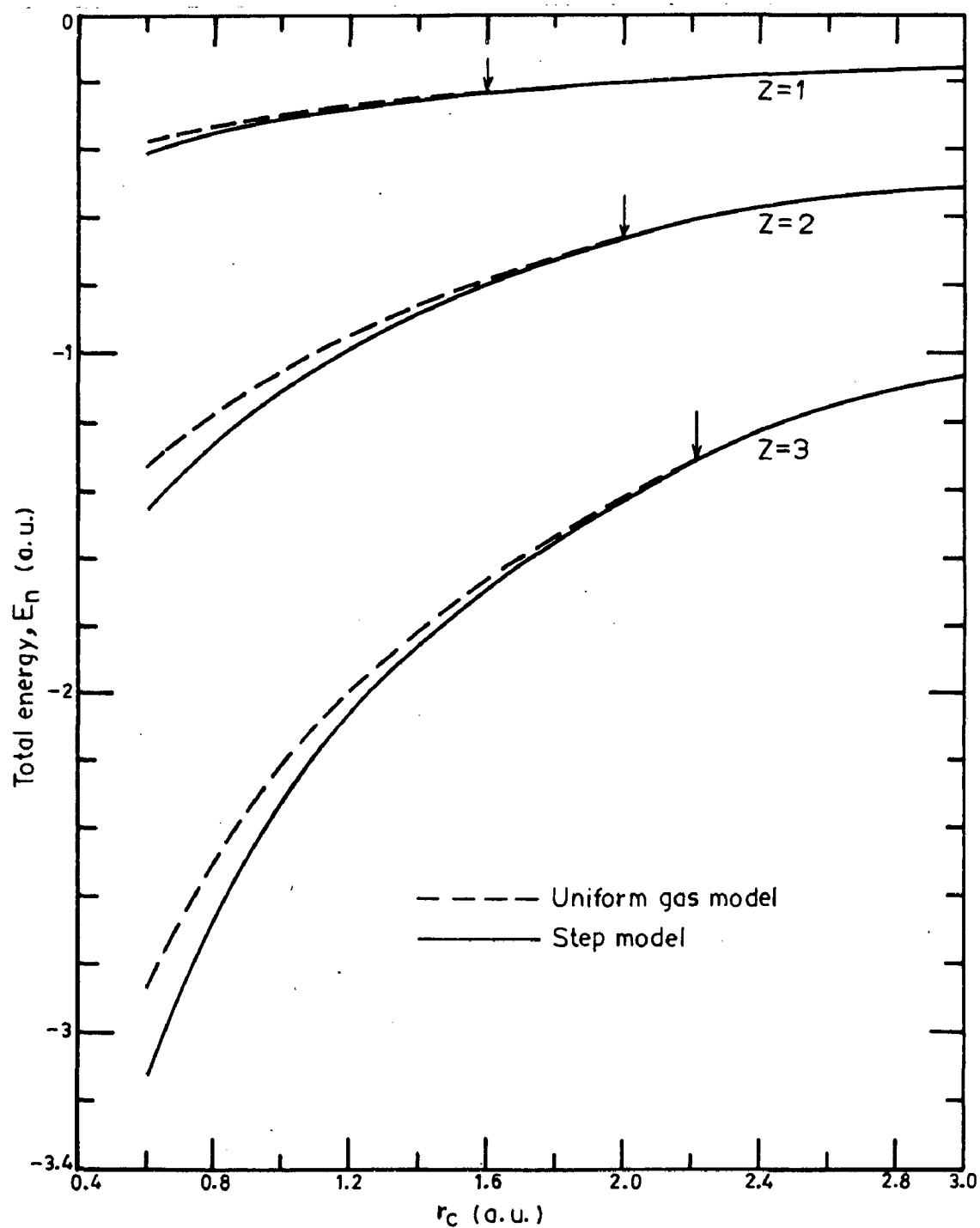


FIG. 2.10: THE CHANGE IN TOTAL ENERGY, E_n in a.u. WITH CORE RADIUS, r_c in a.u. FOR VARIOUS VALENCIES, $Z=1$ TO 3 IN STEP MODEL AND THE UNIFORM GAS MODEL.

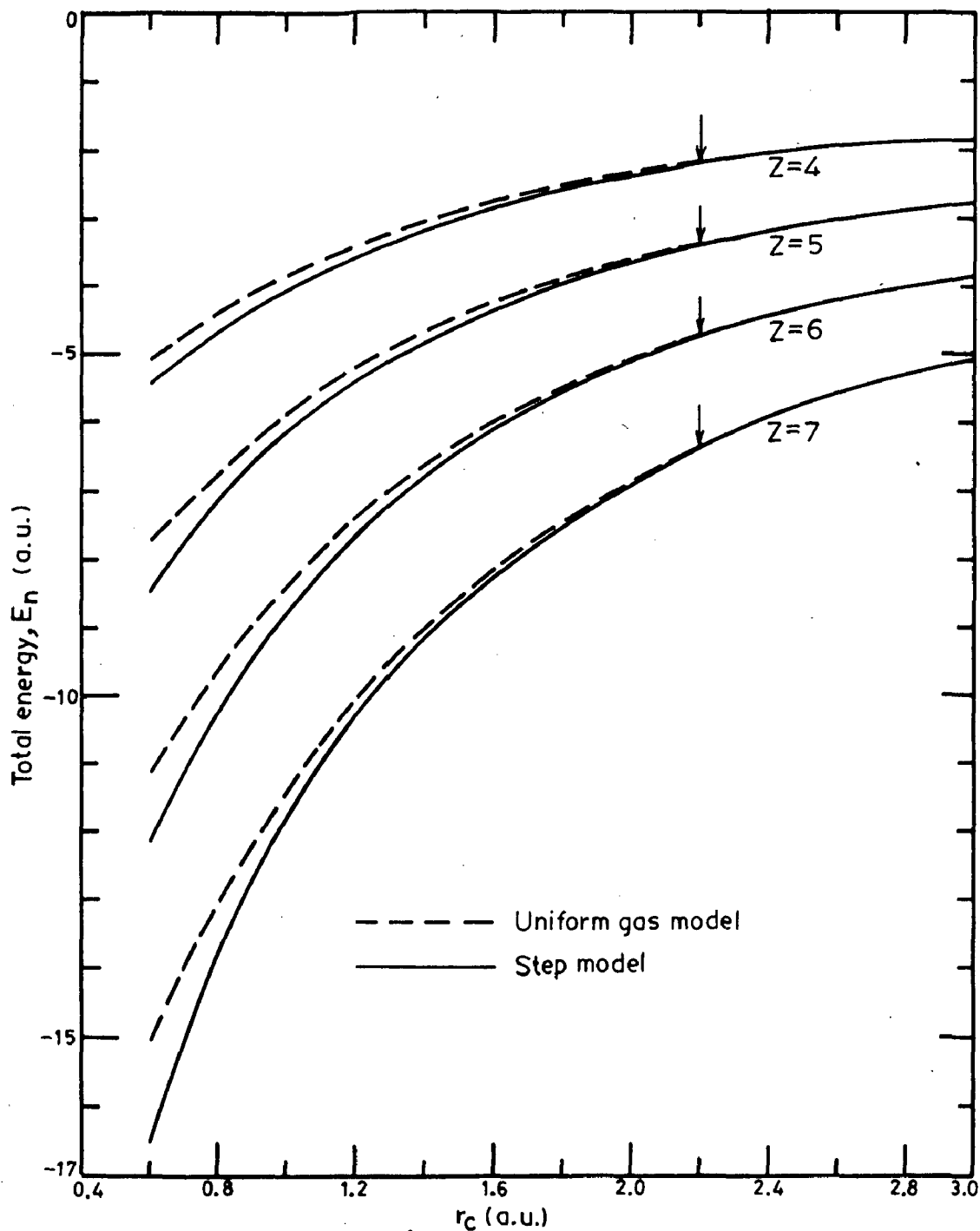


FIG.2.11: THE CHANGE IN TOTAL ENERGY, E_n in a.u. WITH CORE RADIUS, r_c in a.u. FOR VARIOUS VALENCIES, $Z=4$ TO 7 IN THE STEP MODEL AND THE UNIFORM GAS MODEL.

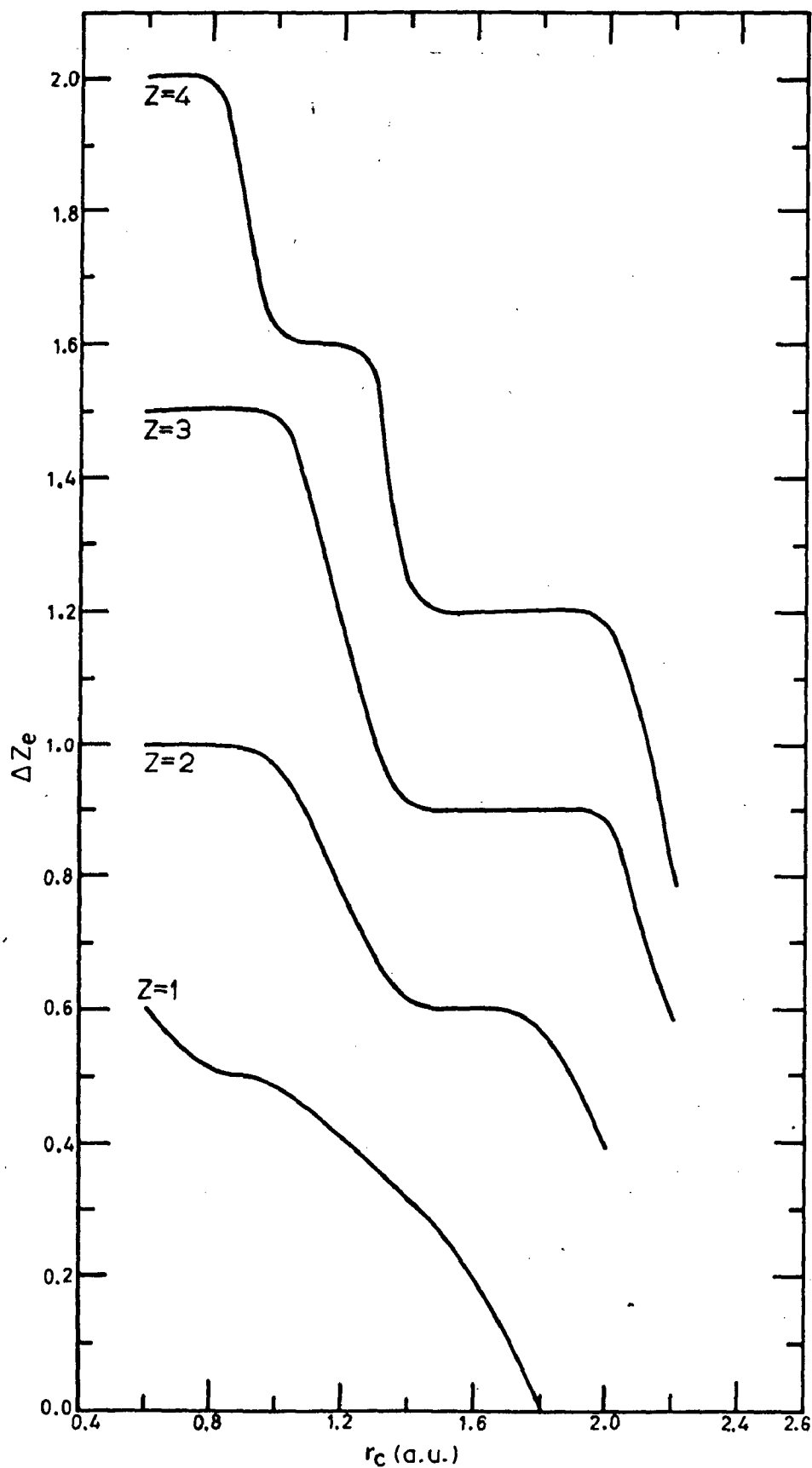


FIG. 2.12 : THE VARIATION OF THE CHARGE, ΔZ_e IN THE OUTER SPHERICAL SHELL, WITH CORE RADIUS, r_c in a.u. FOR THE ELEMENTS WITH VALENCIES, $Z=1$ TO 4.

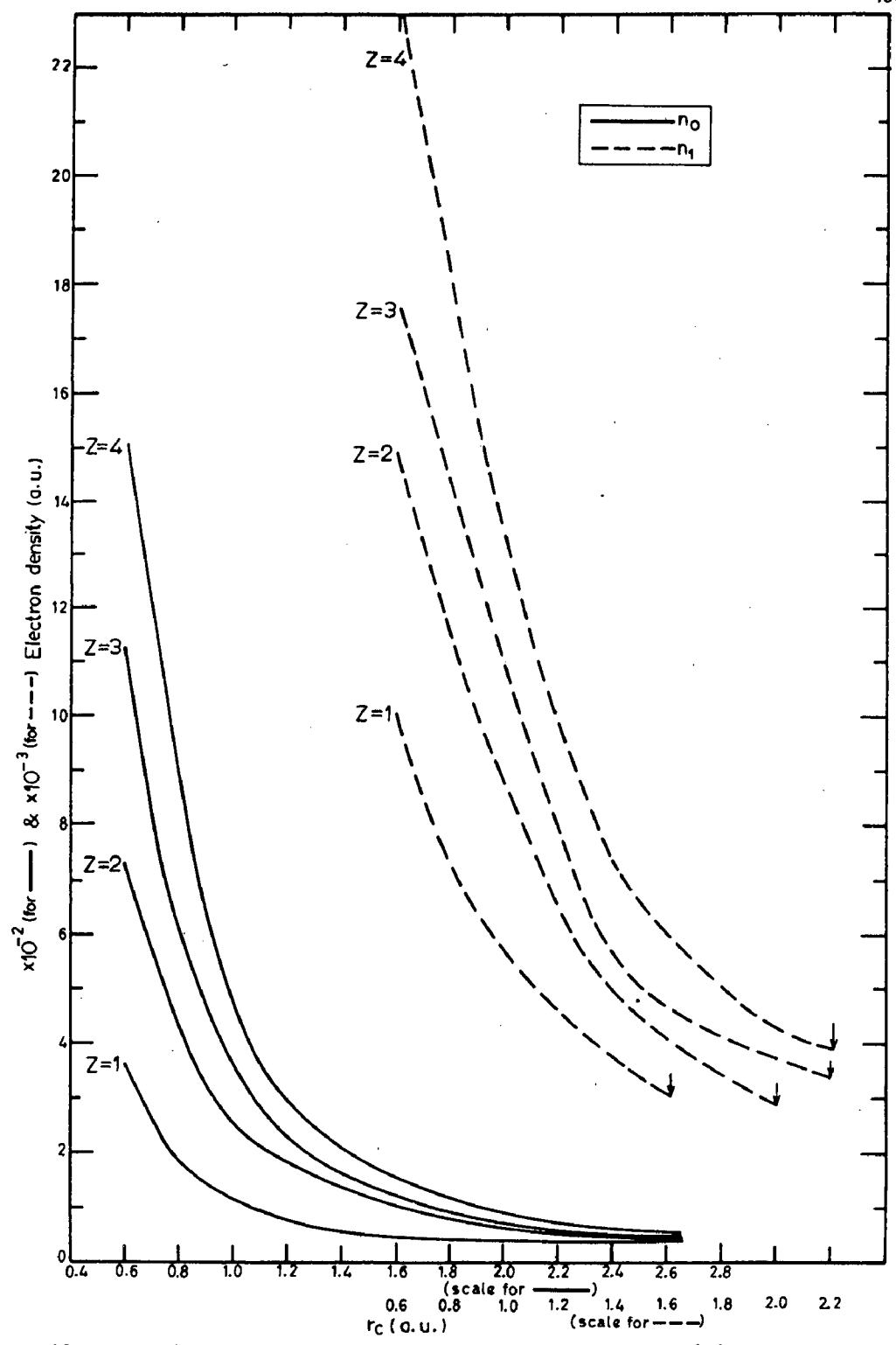


FIG.2.13: THE VARIATION OF ELECTRON DENSITY IN a.u. (a) IN THE INNER CELL, n_0 AND (b) THE OUTER SPHERICAL SHELL, n_1 WITH CORE RADII, r_c IN a.u. FOR DIFFERENT VALENCIES, $Z = 1$ TO 4.

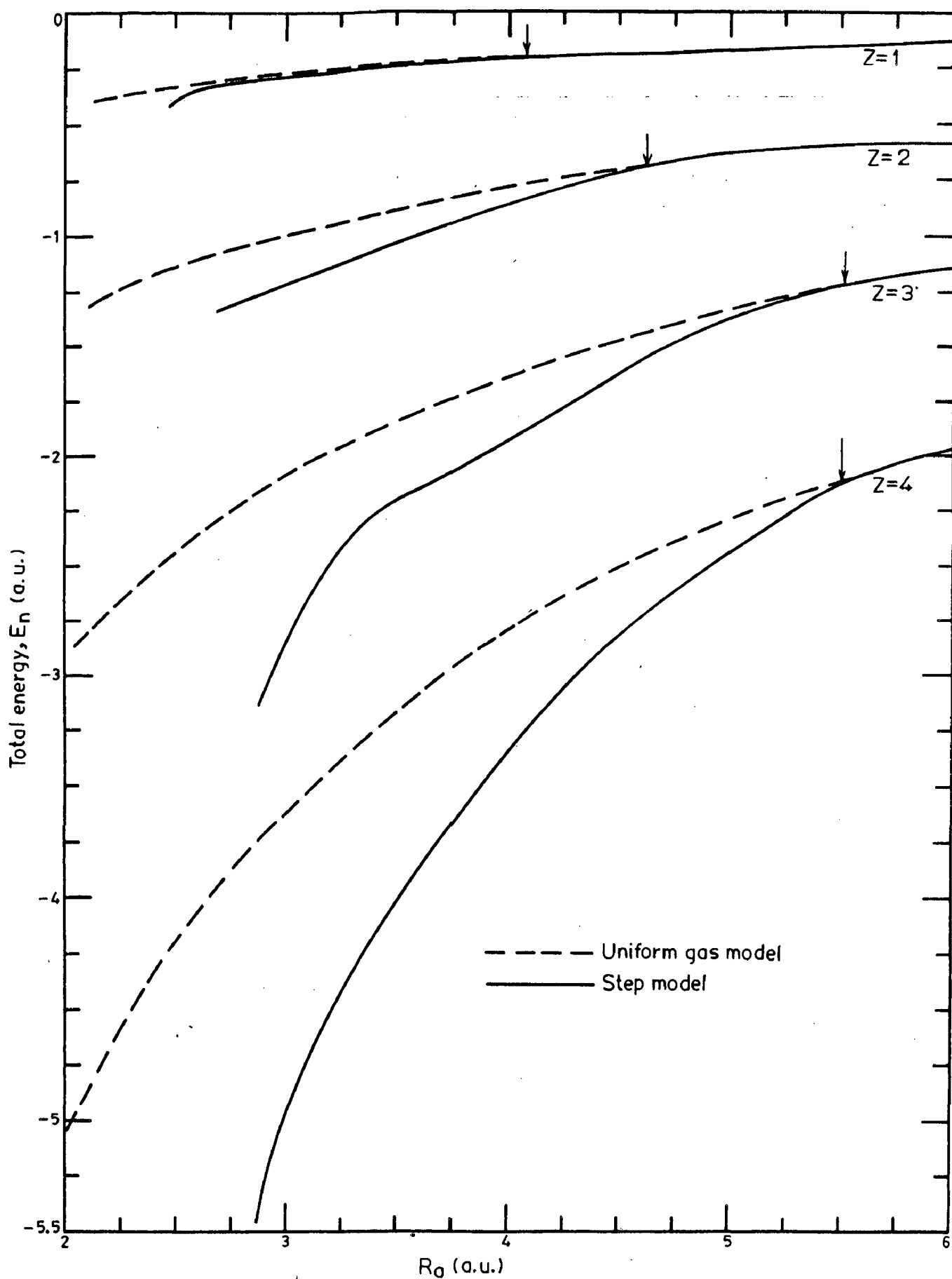


FIG. 2.14: THE VARIATION OF TOTAL ENERGY, E_n in a.u. WITH ATOMIC RADII, R_a in a.u. FOR VARIOUS VALENCIES, $Z = 1$ TO 4.

Table-2.1 The total energies of different elements obtained in various models compared with the experimental values.

Elements	Valency	Total energy E_n (a.u.) all in negative sign							
		Experimental [69]	Weaire [71]	Ashcroft et.al., [72]	Janaket et.al., [73]	Mariarty [74]	Uniform gas Present	Investigation	
1	2	3	4	5	6	7	8		
Li	1	0.2581	0.2515	0.282	0.2585	0.2569	0.2785		
Na	1	0.2299	0.2285	0.227	0.2294	0.2359	0.2372		
K	1	0.1939	0.1845	0.1915		0.1966	0.1966		
Rb	1	0.185		0.172		0.1848	0.1852		
Cs	1	0.1726		0.159		0.1690	0.1724		
Be	2	1.1342	0.9950		1.1587	1.1039	1.2288		
Mg	2	0.8893	0.852	0.86	0.8940	0.8963	0.9224		
Ca	2	0.7287	0.722		0.7428	0.7376	0.7661		

Table-2.1 Contd.....

1	2	3	4	5	6	7	8
Sr	2	0.6779				0.6754	0.7090
Ba	2	0.6290	0.613			0.6071	0.6860
B	3						
Al	3	2.0815	1.98	2.115	2.0979	2.0851	2.1290
Ga	3	2.2088	2.07			2.2031	2.0299
In	3	2.0294	1.92			1.9668	1.8663
Tl	3	2.1401	2.07			1.9054	1.8177
Si	4	3.9607	3.64				3.475
Ge	4	3.9173	3.66				3.35
Sn	4	3.540	3.38			3.4202	3.1525
Pb	4	3.6275	3.46	3.1		3.2721	3.047

Table-2.2 The total energies E_n of different elements obtained from step model and compared with those obtained from the uniform gas model and experiments

Element	Valency	Atomic Radius R_a (a.u.)	E_n (a.u.)		
			Experimental [69]	Uniform gas	Step
Li	1	3.258	-0.2581	-0.2785	-0.303
Na	1	3.931	-0.2299	-0.2375	-0.2410
K	1	4.862	-0.1939	-0.1966	-0.1966
Rb	1	5.197	-0.185	-0.1852	-0.1852
Cs	1	5.625	-0.1726	-0.1724	-0.1724
Be	2	2.351	-1.1342	-1.2288	
Mg	2	3.339	-0.8893	-0.9224	-1.08
Ca	2	4.123	-0.7287	-0.7661	-0.825
Sr	2	4.494	-0.7090	-0.725	
Ba	2	4.661	-0.629	-0.6860	-0.686
B	3	2.273	-2.8357		
Al	3	2.984	-2.0824	-2.129	-2.85
Ga	3	3.154	-2.2088	-2.0299	-2.55
In	3	3.472	-2.0294	-1.8663	-2.20
Tl	3	3.577	-2.1401	-1.8177	-2.15
Si	4	3.177	-3.9607	-3.475	-4.55
Ge	4	3.309	-3.9173	-3.35	-4.325
Sn	4	3.512	-3.541	-3.1525	-4.05
Pb	4	3.648	-3.6275	-3.047	-3.80

CHAPTER **3**

**CONTINUOUS
DENSITY MODEL**

3.1 Introduction

The step model suffers from a serious handicap, since it is incapable of accommodating the gradient term in the density functional expansion. As in the step model, the representation of the charge density by two homogeneous systems may be a poor approximation to the true charge distribution. However, the inhomogeneity can be incorporated in the atomic cell in a continuous manner to avoid the physically improbable discontinuity at the boundary of the segmented or the step model resulting in the divergence of the gradient term in the energy expression. In a realistic electron distribution, the gradient terms in energy is by no means negligible and a modification to the electron density is called for to improve accuracy. But, a continuous inhomogeneous density will introduce additional optimisation parameters. In the case of pure elements the choice of the density used here is a continuous tangent hyperbolic function similar in form to the one used by Smith [76] to model the charge density at the metal surfaces. The analytical form of the surface charge density has been written as,

$$\begin{aligned}
 n(Z) &= n_+ - \frac{n_+}{2} \exp(\beta Z) \text{ for } Z < 0 \text{ (in metal)} \\
 &= \frac{n_+}{2} \exp(-\beta Z) \text{ for } Z \geq 0 \text{ (out side)} \\
 &\dots(3.1)
 \end{aligned}$$

where, n_+ is determined by charge conservation and β is the free parameter to be determined variationally. The resulting charge distribution for different metals is very similar to a tangent hyperbolic function. The calculation of Lang and Kohn [77] with a jellium model for the metal surface also yields a charge distribution similar in form to that used by Smith [76].

3.2 Formulation

The Ashcroft's empty core pseudopotential [43] has been used here as in the case of step model and the electron density within the cell, $n(\bar{r})$, can be written as,

$$n(\bar{r}) = \frac{1}{2} [(n_0 + n_1) + (n_0 - n_1) \text{Tanh } \beta (\bar{r} - \bar{r}_0)]$$

or

$$n(\bar{r}) = A + B \text{Tanh } \beta (\bar{r} - \bar{r}_0) \quad \dots(3.2)$$

where, A is the uniform component and B is the coefficient of the nonuniform component of the resultant charge density. β is the slope and r_0 is the point of inflection of this distribution. From the charge conservation criterion one can get

$$\int_0^{R_a} [A + B \text{Tanh } \beta (\bar{r} - \bar{r}_0)] d\bar{r} = Z \quad \dots(3.3)$$

where, R_a is the atomic cell radius. For a given R_a , β and

r_0 one can evaluate A, and then B can be evaluated with the help of the charge conservation criteria yielding

$$B = (Z - 4 \pi R_a A/3) / \int_0^{R_a} \text{Tanh } \beta (\bar{r} - \bar{r}_0) d\bar{r} \quad \dots(3.4)$$

The evaluation of A and B completely defines the charge density of the atomic cell, $n(\bar{r})$. Using Hohenberg - Kohn [2] expression for the energy functional and the local density approximation, one can express the energy of the atomic cell, E_n , as,

$$\begin{aligned} E_n = & \int_0^{R_a} v(\bar{r}) [A + B \text{Tanh } \beta (\bar{r} - \bar{r}_0)] d\bar{r} \\ & + \frac{1}{2} \int_0^{R_a} \int_0^{R_a} \frac{[A+B \text{Tanh } \beta (\bar{r} - \bar{r}_0)] [A+B \text{Tanh } \beta (\bar{r}' - \bar{r}_0)]}{|\bar{r} - \bar{r}'|} d\bar{r} d\bar{r}' \\ & + \int_0^{R_a} \frac{3}{10} \cdot (3 \pi)^{2/3} [A+B \text{Tanh } \beta (\bar{r} - \bar{r}_0)]^{5/3} d\bar{r} \\ & + \int_0^{R_a} E_{xc} [A + B \text{Tanh } \beta (\bar{r} - \bar{r}_0)]^{4/3} d\bar{r} \\ & + \int_0^{R_a} g_2(\bar{r}) |\nabla [A+B \text{Tanh } \beta (\bar{r} - \bar{r}_0)]|^2 d\bar{r} \\ & \dots(3.5) \end{aligned}$$

where, the first term is the pseudopotential term and the second is electron- electron repulsion, the third term and

fourth term are the kinetic, the exchange and the correlation energy, E_{xc} , as explained in section 1.2.2 of chapter 1. The last term is the energy due to gradient contribution from the kinetic energy and the exchange and correlation energy.

The potential energy part, E_{PE} , of the equation (3.5) is integrated over atomic cell radius, R_a , from core radius, r_c , and is given below

$$E_{PE} = -2\pi Z (R_a^2 - r_c^2) A \int_{r_c}^{R_a} \frac{Z}{r} B \operatorname{Tanh} \beta (\bar{r} - \bar{r}_0) d\bar{r} \quad \dots(3.8)$$

Then, the electron-electron repulsion term of equation (3.5), E_{ee} , is obtained as,

$$E_{ee} = \frac{16}{15} = \pi^2 A^2 R_a^5$$

$$+ \frac{1}{2} \int_0^{R_a} \left[\int_{\bar{r} > \bar{r}'}^{\bar{r}} \left(\frac{Z}{\bar{r}} \right) B \operatorname{Tanh} \beta (\bar{r} - \bar{r}_0) \cdot B \operatorname{Tanh} \beta (\bar{r}' - \bar{r}_0) d\bar{r}' \right. \\ \left. + \int_{\bar{r} < \bar{r}'}^{\bar{r}} \left(\frac{Z}{\bar{r}} \right) (B \operatorname{Tanh} \beta (\bar{r} - \bar{r}_0)) B \operatorname{Tanh} \beta (\bar{r}' - \bar{r}_0) d\bar{r}' \right] d\bar{r}$$

$$+ \int_0^{R_a} \left[\int_{\bar{r} > \bar{r}'}^{\bar{r}} \left(\frac{Z}{\bar{r}} \right) A B \operatorname{Tanh} \beta (\bar{r} - \bar{r}_0) d\bar{r}' \right]$$

$$+ \int_{\bar{r} < \bar{r}'}^R \left(\frac{2}{\bar{r}'} \right) A B \operatorname{Tanh} \beta (\bar{r}' - \bar{r}) d\bar{r}'] d\bar{r} \dots(3.9)$$

The kinetic energy term, T , is evaluated as,

$$T = \frac{3}{10} (3 \pi^2)^{2/3} \int_0^R [(A+B \operatorname{Tanh} \beta (\bar{r}-\bar{r}_0))]^{5/3} d\bar{r} \dots(3.10)$$

The exchange and correlation energy term, E_{xc} , has been reduced to the following form

$$E_{xc} = -\frac{3}{4} \left(\frac{3}{\pi} \right)^{1/3} \int_0^R [A+B \operatorname{Tanh} \beta (\bar{r}-\bar{r}_0)]^{4/3} d\bar{r} \\ + \int_0^R \left[-0.0575 + \frac{0.0155}{3} \ln \left(\frac{3}{4 \pi [A+B \operatorname{Tanh} \beta (\bar{r}-\bar{r}_0)]} \right) \right] \\ [A+B \operatorname{Tanh} \beta (\bar{r}-\bar{r}_0)] d\bar{r} \dots(3.11)$$

The gradient energy, E_{grad} , of this has been incorporated here as such after substituting the expression for the electron density as given below,

$$E_{grad} = \int_0^R \left[\lambda/8 + C(r_s) (A+B \operatorname{Tanh} \beta (\bar{r}-\bar{r}_0))^{-2/3} \right] \\ [A+B \operatorname{Tanh} \beta (\bar{r}-\bar{r}_0)]^{-1} \\ \cdot [B^2 \beta^2 (\operatorname{Cosh} \beta (\bar{r} - \bar{r}_0))^{-4}] d\bar{r} \dots(3.12)$$

where, the first term in the first square bracket is due to the kinetic energy and the second term is due to the exchange and correlation energy. The parameter, λ , in the kinetic energy contribution has been taken as $1/9$ which is appropriate for perturbation calculations involving large wave lengths in comparison to Fermi wave length as suggested by Jones and Young [8] . The $C(r_s)$ is a gradient coefficient dependent on electron density through the radius of a volume containing one electron, r_s , as suggested by Rasolt et.al., [9] . In the equation (3.12) the value of $C(r_s)$ has been taken as 2×10^{-3} , an average of the values calculated in the metallic range of electron densities.

The integration involved in the equations (3.4) and (3.8) to (3.12) have been worked out numerically using 15-point Gaussian quadrature formula. Combining the equations from (3.8) to (3.12) one gets the total energy per atom, E_n , as

$$E_n = E_{PE} + E_{ee} + T + E_{xc} + E_{grad} \quad \dots(3.13)$$

which is a function of cell radius, R_a the gradient parameter, β , the radius of inflection, r_o . The optimum energy is obtained by a parametric variational calculation with respect to these parameters.

3.3 Results and discussion

The variation of the ground state energy with the core radius, r_c , in the continuous density model obtained through optimization as explained in the previous section, is plotted in figure 3.1. For a particular valency, the total energy is more negative for lower core radius i.e., stronger pseudopotential. With an increase in valency the pseudopotential again becomes stronger resulting in a higher total negative energy and the cohesive energy. The arrow mark in figure 3.1 separates the region between inhomogeneous electron gas as observed in the continuous density model and the uniform electron gas. At lower core radii the stronger potential favours an inhomogeneous distribution of electrons in the atomic cell but at the cross over core radius, r_c^* , indicated by the arrow, the energy of the inhomogeneous model smoothly joins with that of the uniform electron gas model. But the cross over core radius, r_c^* , shifts to higher values for an increase in valency due to the resulting stronger potential.

Figure 3.2 shows typical electron density distribution in continuous density model compared with those obtained in the step and the uniform gas model for the same valency and the core radius. It is observed that the inclusion of the gradient energy term as it has been done in continuous

density model reduces the extent of inhomogeneity as compared to that in the step model. It is evident from these figures that the step model exaggerates the inhomogeneity by taking advantage of the favourable ionic pseudopotential just outside the core region. The gradient energy in the continuous density model reduces the electron density in the inner region and enhances it in the outer region as compared to those in the step model. Thus, the gradient in the electron density in the continuous density model is kept low. But the uniform electron gas model maintains an average density as it is required in this model. The atomic radius in the uniform gas model and the continuous density model are similar but the step model yields a larger atomic radius. Because, the electron density in the outer region of the step model is determined by the balance of potential, kinetic and repulsion energies, but in the continuous density model gradient energy shifts the balance to a higher electron density. Thus, one observes that uniform electron gas model is a better model yielding a more reasonable estimate of atomic radius, energy and electron density as compared to the step model.

When one compares the figure 3.3 for valency, $Z = 4$, one observes that the extent of inhomogeneity reduces as the core radius increases. This trend is common to both the continuous density model and the step model. It has been

further demonstrated in figure 3.4 where the ratio of electron densities in the inner to that in the outer region has been plotted against the core radius, r_c , for different valencies. When the potential is strong by reasons of either lower core radii or increase in valency, the extent of inhomogeneity increases. But for every valency, there is a core radius at which the inhomogeneity vanishes.

Figure 3.5 shows the change in the cross-over core radius at which the inhomogeneity vanishes with the valency. The cross-over core radius, r_c^* , increases with an increase in the valency but saturates beyond a valency, $Z = 3$. It is interesting to note that both the step and the continuous density model yields the same cross-over core radii, r_c^* , although the extent of inhomogeneity differs significantly in both these models. When this cross-over core radii, r_c^* , are compared to the limit of stability of the uniform gas model as it has been analysed in the section 2.2.3, it is observed that the stability has been overestimated because it does not consider the additional energy factors in the outer region favouring the inhomogeneous distribution of electrons.

In table 3.1, the typical values of various energy terms involved in the continuous density model has been presented for the valency, $Z = 2.0$, and for the core

radii, $r_c = 0.6$ and 2.0 a.u. The various corresponding energy terms of the uniform electron gas model and the step model are also tabulated for comparison. The energy values in the continuous density model and the uniform gas model are comparable whereas the step model has energies quite different from these two models. Thus the positive gradient energy term is pushing the electron distribution and the energies away from the step model to ones akin to those obtained in the uniform gas model. This explains the success of the uniform gas model in explaining the cohesive energies and the observed atomic radii of the metals although the uniform gas model appears quite unrealistic. At higher core radii when the gradient energy term becomes small due to a reduction in the extent of inhomogeneity the step model, the uniform gas model and the continuous density model result into similar energy terms and electron densities.

The difference in the total energy obtained from the continuous density model and the uniform gas model, ΔE^{CD-U} , has been presented in figure 3.6 for various core radii. At low core radius the difference in total energy is observed to be more and it reduces steadily as the core radius increases for a particular valency. The difference in total energy also increases as the valency increases. It is expected because the inhomogeneity decreases as the potential

becomes weak and so the difference in energies in the uniform electron gas model and the continuous density model should become small.

The total energy of various metals obtained from the continuous density model has been presented in table 3.2 and the corresponding values obtained from the uniform gas model and the experiment have been shown for comparison. It is observed that the values calculated from the continuous density model for elements with valency, $Z = 1$ and 2 of lower core radii like Lithium, Sodium, Beryllium, Magnesium and Calcium have lower in total energy in comparison to those obtained from the uniform gas model. Whereas all the elements with higher valencies, $Z = 3$ and 4 , the calculations of the continuous density model show a lower total energy compared with the corresponding results from the uniform gas model. The energy values obtained from the continuous density model lies within a limit of 5% from those calculated using the uniform gas model.

The total energy of various elements obtained from continuous density model has also been compared in table 3.2 with the corresponding experimental values. It is observed that for elements with valency, $Z = 1$, the total energy for element Lithium is lower than the observed value, but for other elements with the same valency the

calculated total energies are nearer to and a little lower than the values observed experimentally. For valency, $Z = 2.0$, the elements show higher negative values compared to the observed ones but for elements with valencies, $Z = 3$ and 4 , the observed total energies are lower (higher negative values) than the calculated values. The calculated total energy of the continuous density model matches with the experimental total energy to within $\pm 10\%$.

3.4 Gradient correction to the step model

The total energy obtained from the step and the continuous models show a difference, ΔE^{S-CD} , which has been attributed primarily to the gradient correction and has been shown in figure 3.7 along with the difference in the electron densities, Δn , in the two segments of the atomic cell in the step model. This figure shows an approximately linear behaviour which can be represented as,

$$\Delta E^{S-CD} = X + Y \Delta n \quad \dots(3.13)$$

where, ΔE^{S-CD} is the energy correction. X and Y are the coefficients which are dependent on valency. The coefficients X and Y are evaluated by least square fit. The values of X and Y are calculated for various valencies and are shown in figure 3.8. X and Y are also observed to

vary linearly with the valency. Thus, the correction to the energy obtained from the step model has been obtained for the entire range of core radii and valencies under investigation.

3.5 Summary

In the continuous density model, the inhomogeneity in electron density within the atomic cell has been incorporated as a continuous tangent hyperbolic function to avoid the physical improbable discontinuity as in the step model. By using this density and Ashcroft's empty core pseudopotential the Hohenberg-Kohn density functional equation has been constructed along with the gradient term. Now the equation is a function of for parameters namely, the density in the inner region and the position at discontinuity, the density gradient parameter and the atomic radius.

The electron density distribution has been compared with the uniform gas and step model and found that, by including the gradient energy term in the continuous density model, the electron density in the inner region comes down considerably as compared to that in the step model. The charge neutrality is maintained by an increase in the electron density in the outer region and by an adjustment of atomic radius. The total energies obtained from the

continuous density model and the step model are found to merge with the uniform gas model at the same energy smoothly at a high core radius termed the cross-over core radius. This cross-over core radius has been compared with the limits of stability of the uniform gas model and it has been observed that the uniform gas model is less stable compared to that indicated by the limited analysis already performed.

The ground state total energies are calculated for various simple metals and compared with uniform gas model values and experimental values. The total energies of lower valency, $Z = 1$ and 2 , elements with lower core radii have lower values in comparison to the calculations of these elements on the basis of the uniform gas model. In higher valency elements with $Z = 3$ and 4 , all the elements show lower values of total energy in comparison to that obtained in the uniform gas model. The total energy of various elements calculated using the continuous density model has been within $\pm 10\%$ of the experimental values.

The difference in total energy obtained from this model and the step model shows a linear variation with the electron density difference within the atomic cell in the step model. The total energy in the step model has been corrected for the gradient contribution in the entire range of core radii and valencies under investigation.

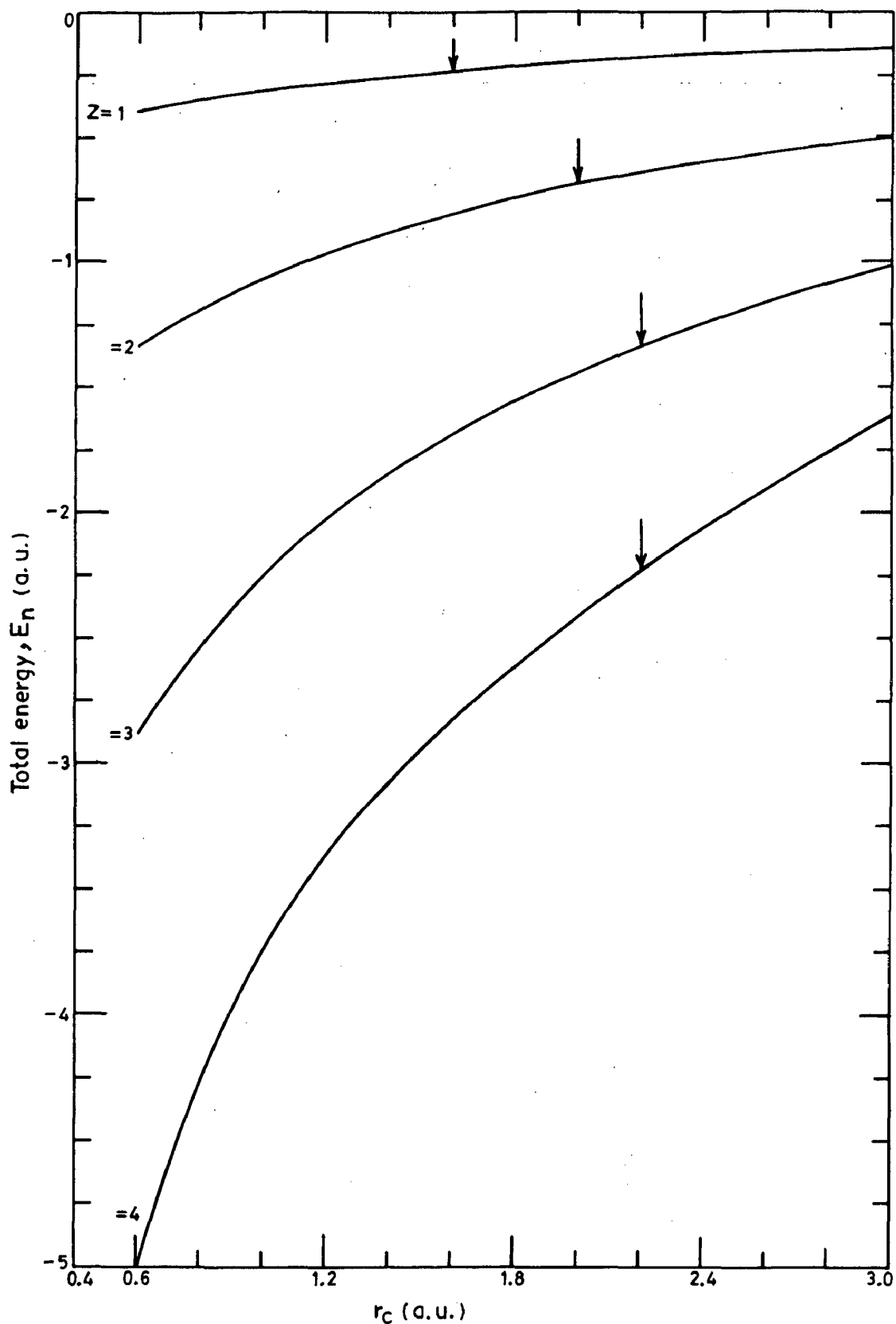


Fig. 3.1: THE VARIATION OF TOTAL ENERGY, E_n in a.u. WITH CORE RADIUS, r_c in a.u. IN CONTINUOUS DENSITY MODEL FOR VALENCIES, $Z=1$ TO 4. THE ARROW MARK INDICATES THE BOUNDARY WITH THE UNIFORM GAS MODEL.

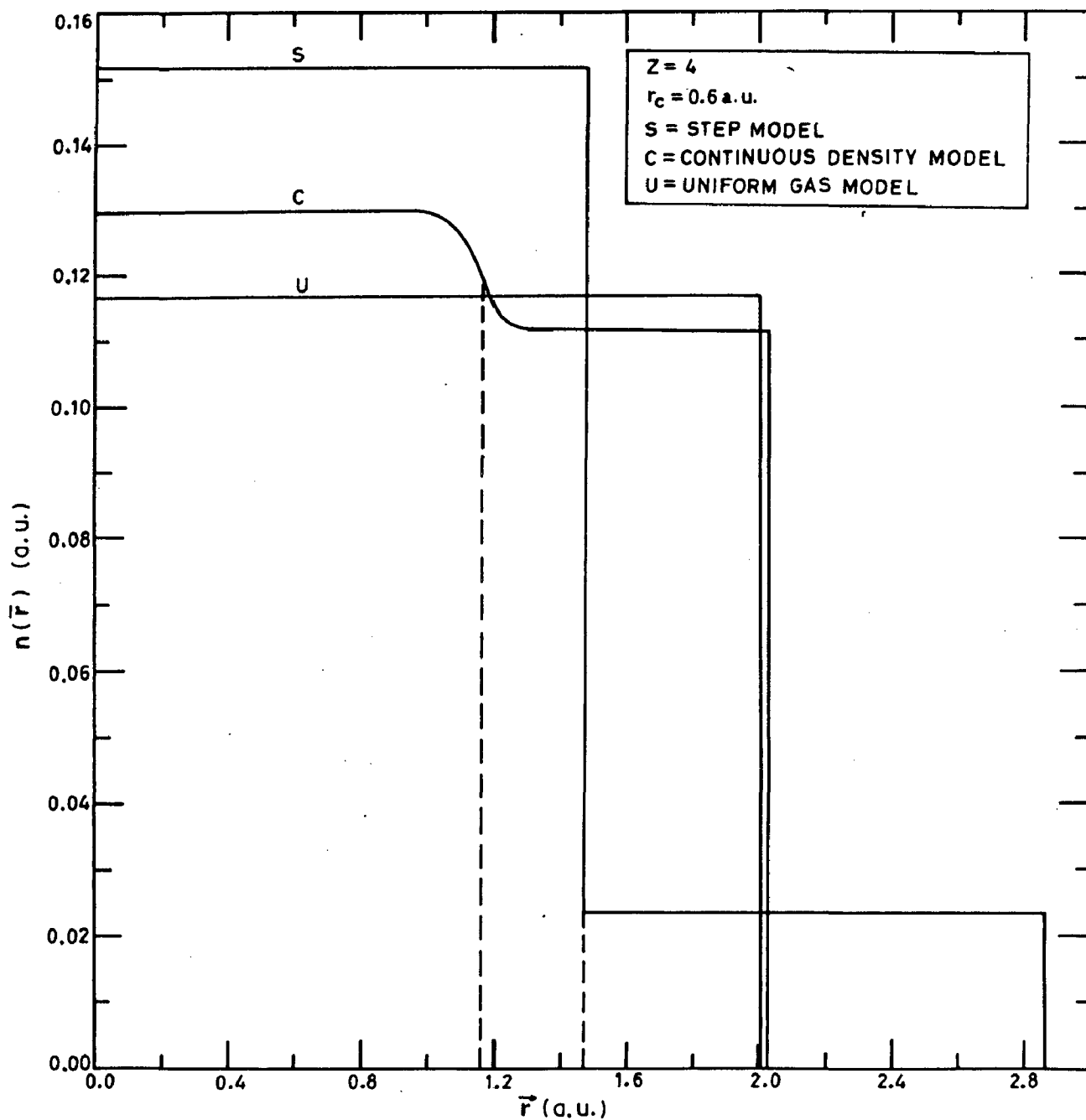


Fig. 3.2: THE ELECTRON DENSITY DISTRIBUTION, $n(\bar{r})$ IN THE STEP MODEL - S, THE CONTINUOUS DENSITY MODEL - C AND THE UNIFORM GAS MODEL - U FOR THE CORE RADIUS, $r_c = 0.6$ in a.u. AND VALENCY, $Z = 4$.

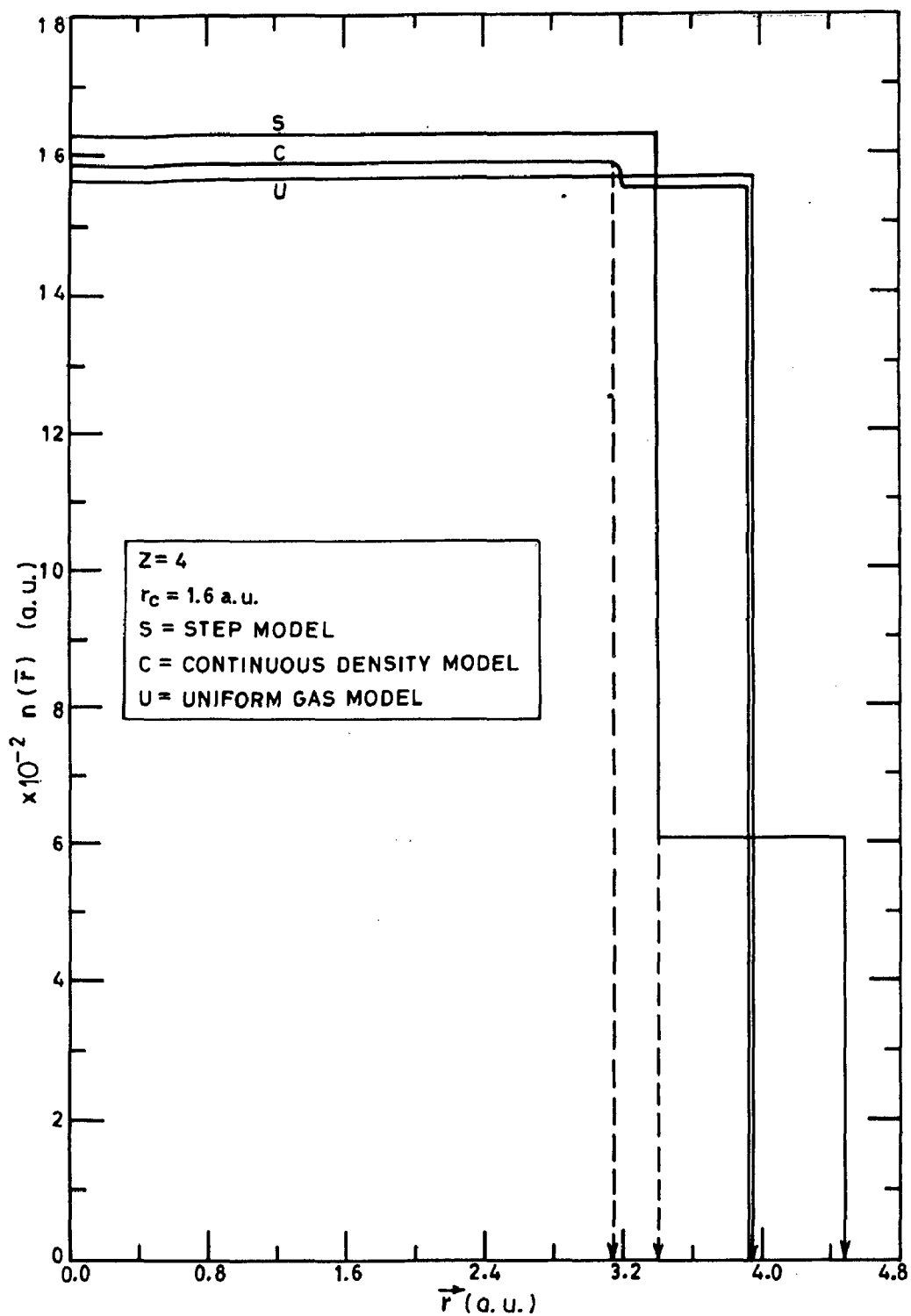


Fig.3.3: THE ELECTRON DENSITY DISTRIBUTION, $n(\vec{r})$ IN THE STEP MODEL -S, THE CONTINUOUS DENSITY MODEL -C AND THE UNIFORM GAS MODEL -U, FOR THE CORE RADIUS, $r_c = 1.6$ a.u. AND THE VALENCY, $Z=4$.

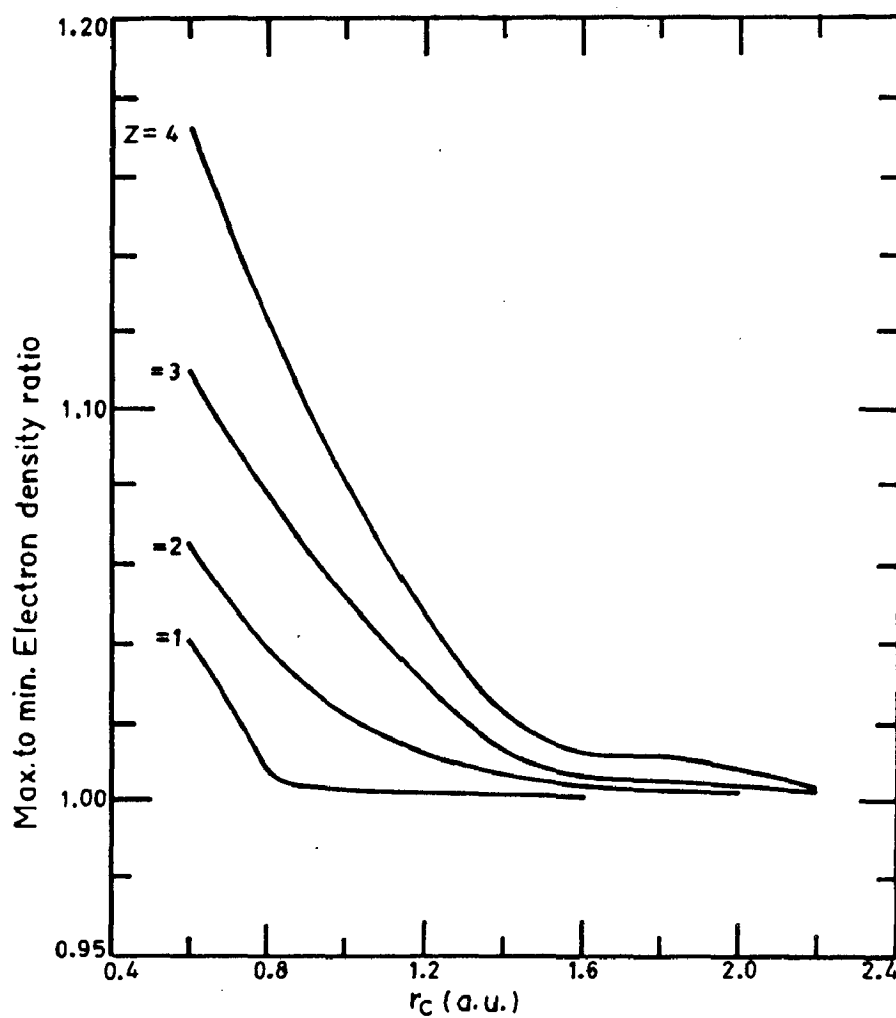


Fig.3.4: THE VARIATION OF MAXIMUM TO MINIMUM RATIO OF ELECTRON DENSITIES WITH THE CORE RADIUS, r_c in a.u. FOR THE VALENCIES, $Z=1$ to 4.

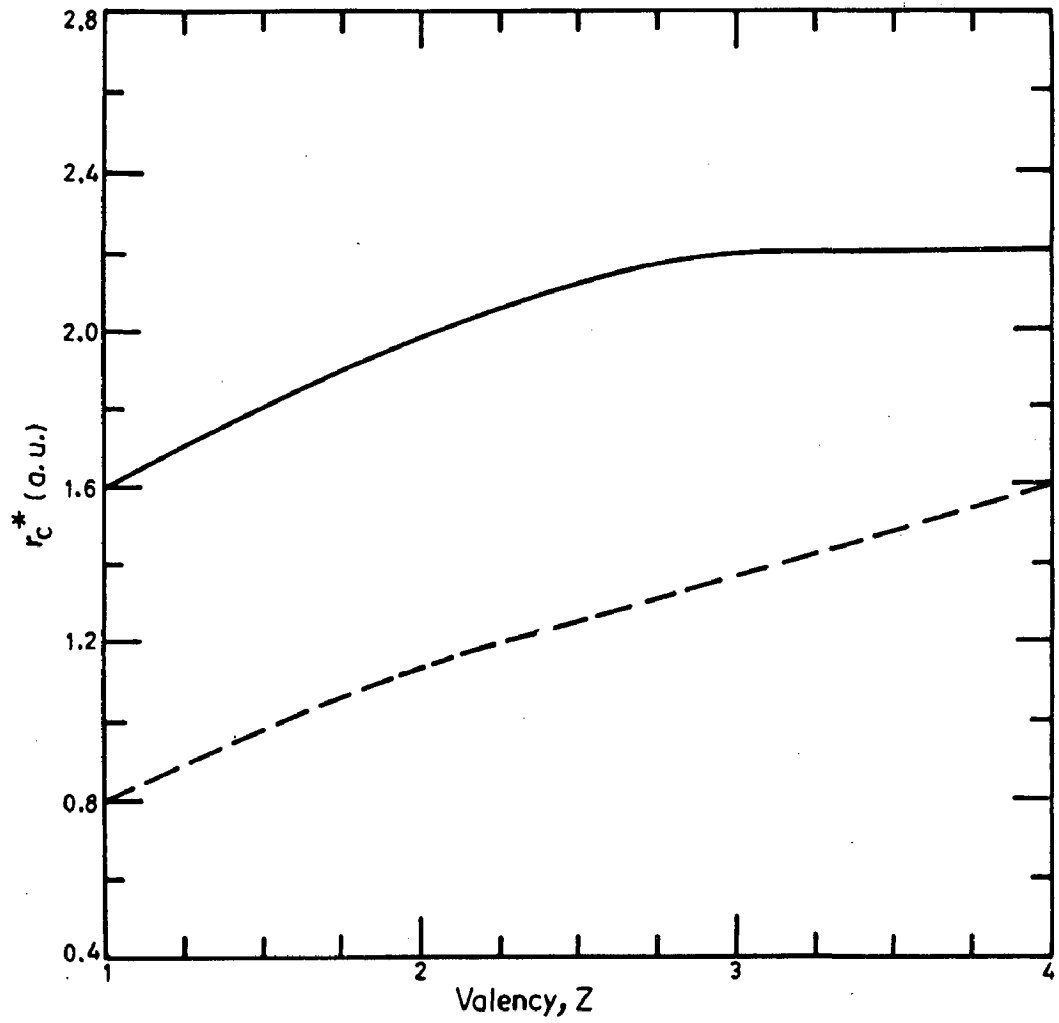


Fig. 3.5 : THE CHANGE IN CROSS-OVER CORE RADIUS, r_c^* in a.u. WITH VALENCY, Z. (—) LINE FOR STEP AND CONTINUOUS DENSITY MODELS AND (---) LINE INDICATES THE LIMITS OF STABILITY OF THE UNIFORM GAS MODEL.

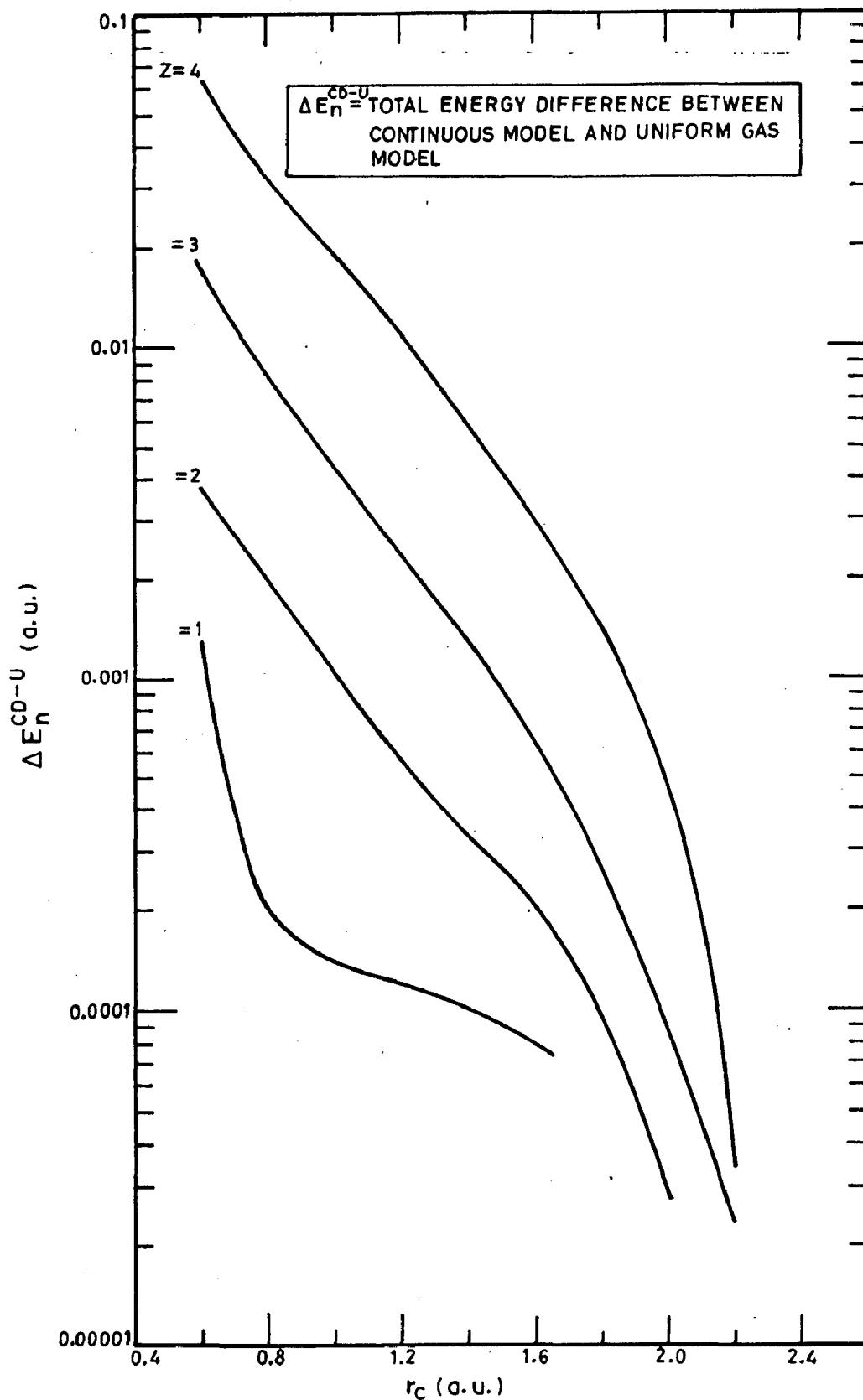


Fig.3.6: THE VARIATION IN THE DIFFERENCE IN TOTAL ENERGY, ΔE_n^{CD-U} AS OBTAINED FROM THE CONTINUOUS DENSITY MODEL AND THE UNIFORM GAS MODEL FOR VALENCIES, $Z = 1$ TO 4.

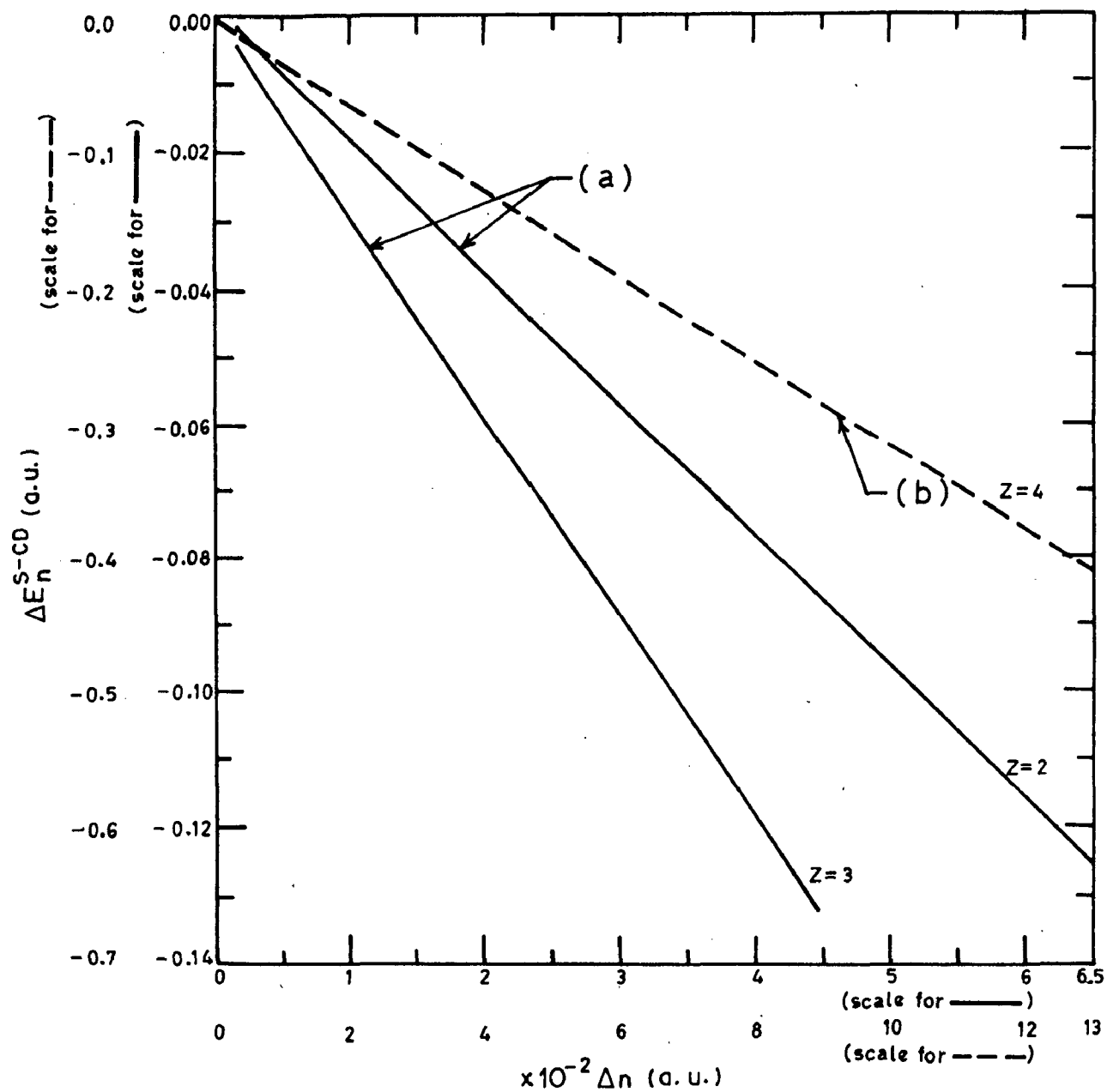


Fig.3.7: THE DIFFERENCE IN TOTAL ENERGY, ΔE_n^{S-CD} BETWEEN THE STEP MODEL AND THE CONTINUOUS DENSITY MODEL WITH THE DIFFERENCE IN ELECTRON DENSITY Δn IN THE ATOMIC CELL OF THE STEP MODEL FOR THE VALENCIES, (a) $Z=1$ & 3 AND (b) $Z=4$.

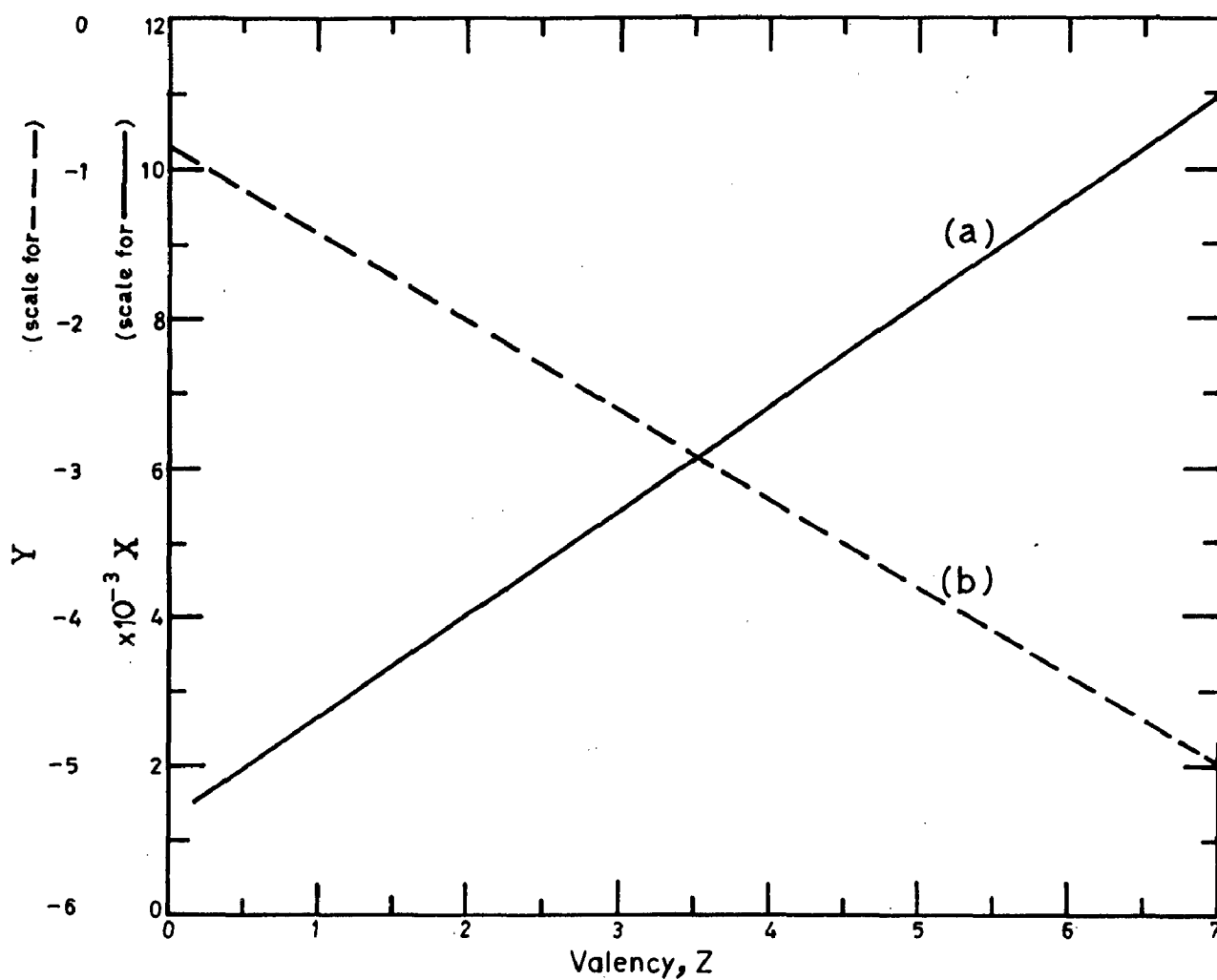


Fig.3.8 : THE VARIATION OF THE PARAMETERS [(a) X AND (b) Y] OF THE LINEAR LEAST SQUARE FIT OF TOTAL ENERGY WITH VALENCY.

Table- 3.1
The various energy terms involved in uniform gas, step and continuous density model, for the valency, $Z = 2.$, at $r_c = 0.6$ and 2.0 a.u.

	$r_c = 0.6$ (a.u.)			$r_c = 2.0$ (a.u.)		
	U	S	C	U	S	C
PE	-2.6256509	-2.1515214	-2.69844166	-1.0555085	-0.91513237	-1.051355687
E-E	1.1437813	0.60665167	+1.181618931	0.51965185	0.3790953	0.515886718
KE	0.79678738	0.67298347	0.83250833	0.164468	0.16283426	0.16238351
Exc	-0.649197491	-0.581257862	-0.66423459	-0.324615428	-0.323094215	-0.32290908
Grad.	-1.3342796	-1.4531442	-1.3380556	-0.69600409	-0.69638281	0.12200069 x 10 ⁻⁵
Total	-1.3342796	-1.4531442	-1.3380556	-0.69600409	-0.69638281	-0.69603348

U = uniform gas model
S = step model
C = continuous density model
all the energies are in a.u.

Table- 3.2 The total energies of different elements calculated in the continuous model and compared with the experimental values and uniform gas model

Elements	Valen- cy	Total Energy (a.u.)		
		Experi- mental[69]	Continuous density	Uniform gas
1. Li	1	-0.2581	-0.279	-0.2785
2. Na	1	-0.2299	-0.238	-0.2372
3. K	1	-0.1939	-0.1966	-0.1966
4. Rb	1	-0.185	-0.1852	-0.1852
5. Cs	1	-0.1726	-0.1724	-0.1724
6. Be	2	-1.1342	-1.2750	-1.2288
7. Mg	2	-0.8893	-1.0	-0.9224
8. Ca	2	-0.7287	-0.780	-0.7661
9. Sr	2	-0.6779	-0.7090	-0.7090
10. Ba	2	-0.629	-0.6860	-0.686
11. Al	3	-2.0824	-2.15	-2.129
12. Ga	3	-2.2088	-2.05	-2.0299
13. In	3	-2.0294	-1.875	-1.8663
14. Tl	3	-2.1401	-1.825	-1.8177
15. Si	4	-3.9607	-3.65	-3.475
16. Ge	4	-3.9173	-3.50	-3.35
17. Sn	4	-3.541	-3.225	-3.1525
18. Pb	4	-3.6275	-3.20	-3.047

CHAPTER 4

**MODEL FOR
COVALENT
BONDING**

4.1 Introduction

A study of the stability of the uniform gas model has shown that, for $r_s > 2.4127$ a.u., the uniform electron gas model works, but a large number of pure elemental solids with covalent and metallic bonding have the atomic radii corresponding to r_s less than 2.4127 a.u., (see figure 2.1) where the uniform gas model cannot be used justifiably. For these elements there is a lowering of energy when some amount of charge, ΔZ_e , is put away from the uniform gas atomic cells, thereby resulting in an inhomogeneous electron distribution.

The charge staying out of the uniform gas atomic cell can distribute itself in two different modes -

i) the electrons can form a shell around the former cell and result in a non directional metallic bonding as it has been discussed in chapter-2, or,

ii) these electrons can form electron cells in the bond directions and result in a directional covalent bonding.

In the present model for covalent bonding, the simplicity of the uniform electron gas model has been retained to the extent possible. The entire crystal space has been accounted by assuming that, it consists of the electron gas cells around the ions and purely electron cells

outside. Both these cells have uniform electron gas of different densities. The number of bonds per atom has been found out by the octet rule and the charge outside the uniform gas cell around the ion has been distributed in these many number of electron cells.

The electron distribution assumed in this model is quite crude and does not take into account the gradient energy contribution. But rigour has been sacrificed to maintain simplicity. Also, this crude picture makes it possible to conceive a mixed covalent-ionic bonding when a part of the purely electron cell charge shifts into the uniform gas cell of another atom. Pure ionic bonding can also be explained as an extreme case of electron gas cell merging entirely with the uniform electron gas cell of another atom to create the anion uniform gas cell.

The density functional formalism allows a better estimate of energy for the different segments of uniform gas compared to second or third order perturbation theory. However, the electron distribution obtained in the latter approach is superior.

The electron distribution in this model can be improved by dividing the uniform gas cells into smaller segments and thus, increasing the number of optimization parameters. When the size of the segments are small, the

gradient energy contribution can also be included. The present investigation is limited to the crude model of electron distribution, but the possibilities of refining the model has also been recognised.

4.2 Formulation

The electron density in the covalent solid is assumed as a superposition of the electron density of the uniform electron gas cell around the ion core with a density, n_o , and the remaining charge of the neutral atom, forming electron cells in the bond directions with a density of n_e

$$n(\bar{r}) = \begin{cases} n_o & 0 \leq r \leq R_o \\ n_e & 0 \leq (r-2R_o) \leq R_e \end{cases} \quad \dots(4.1)$$

where, the charged cell around the ion core has a radius R_o and the electron cell has the radius of R_e . Since, the electron distribution in the cell around the ion core is uniform, one can write the expression for energy for the charged cell, E_{n_o} , directly following equations (2.11), (2.12) and (2.17).

The remaining charge, ΔZ_e , which stays out of the cell around the ion core, can now be distributed outside as separate electron cells with a different charge density. The number of cells with radius R_e are the number of bonds

per atom, $\beta^*/2$, which can be calculated from the valency, Z , of the atom in question with,

$$\beta^* = Z \text{ for } Z \leq 4$$

and

$$\beta^* = (8-Z) \text{ for } Z > 4 \quad \dots(4.2)$$

The charge neutrality of the system imposes a condition that

$$\left(\beta^*/2 \right) \int_0^R n_e d\bar{r} = \Delta Z_e$$

or

$$n_e = 3 \Delta Z_e \left(\beta^*/2 \right)^{-1} / 4 \pi R_e^3 \quad \dots(4.3)$$

The constant β^* , for a structure also decides the magnitude of the Madelung energy between the electron cells and the cells around the ions as given below,

$$E_{es} = - \alpha_m \Delta Z_e^2 \left(\beta^*/2 \right)^{-1} / R_i \quad \dots(4.4)$$

where R_i is the distance between the positively charged cell and the negatively charged electron cell and is equal to the sum of the radii of these two cells and α_m is the Madelung constant which has values from 1.38 (for linear chain structure) to 1.76 (for bcc structure) in the range of observed crystal structures.

The energy of the negatively charged electron cell, E_{n_e} , can be written with the help of Hohenberg-Kohn

equation as

$$\begin{aligned}
 E_{n_e} = & \frac{1}{2} \int_0^{R_e} \int_0^{R_e} \frac{n_e n_e}{|\vec{r}-\vec{r}'|} \cdot d\vec{r} \cdot d\vec{r}' \\
 & + \int_0^{R_e} \left(t(n_e) n_e d\vec{r} + \int_0^{R_e} \epsilon_{xc}(n_e) n_e d\vec{r} \right) \\
 & \dots(4.5)
 \end{aligned}$$

In this equation, the first term is the electron-electron repulsion term in the electron cell, the second term is the kinetic energy and the third one is the exchange and the correlation energy. Now the energy as expressed in equation (4.5) is a function of the electron cell radius, R_e , and the number of electrons in the negatively charged cell, ΔZ_e . Replacing n_e with ΔZ_e in equation (4.5) from equation (4.3) and integrating one gets the resulting equation for energy as

$$\begin{aligned}
 E_n = & 0.6 \Delta Z_e^2 (\beta^*/2)^{-2} / R_e \\
 & + 1.105 \Delta Z_e^{5/3} (\beta^*/2)^{-5/3} / R_e^2 \\
 & - 0.458 \Delta Z_e^{4/3} (\beta^*/2)^{-4/3} / R_e \\
 & + \Delta Z_e (\beta^*/2)^{-1} [- 0.0575 \\
 & + 0.0155 \{ \ln R_e - \frac{1}{3} (\ln R_e - \ln (\beta^*/2)) \}] \\
 & \dots(4.6)
 \end{aligned}$$

The expression for total energy per atom of the covalent material, E_n , may now be written by combining the energies of the positively charged cell around the ion core, the electron cells and the electrostatic energy given respectively by equations, (2.17), (4.6) and (4.4) as

$$E_n = E_{n_0} + (\beta^*/2) E_{n_e} + E_{es} \quad \dots(4.7)$$

The energy per atom of the covalent material given by equation (4.7) has been optimized with respect to the floating parameters - R_0 , R_e and ΔZ_e to obtain the minimum energy per atom. At the minimum of energy, one can get the corresponding values of R_0 and R_e at equilibrium. The bond length for the covalent solid can also be calculated from these values of R_0 and R_e .

4.3 Results and discussion

The variation of energies of the cell around the ion core and the electron cells per atom for an increasing ΔZ_e have been shown for a given valency, $Z = 4$, with the core radius, $r_c = 0.6, 1.0, 1.6$ a.u., as shown in figure 4.1. From this figure, it is observed that the energy of the cell around the ion core is increasing from a highly negative value to zero, as the charge in this cell reduces. On the contrary, the energy of the electron cell is reducing from zero to a negative value with an increase in ΔZ_e as it has

also been shown in figure 4.1. However, the configuration of electron gas with two different densities as proposed in this model will be stable only when there is a minimum in the total energy for a specific value of ΔZ_e and this electron configuration will become energetically favourable when its energy will be lower than the energy of the atomic cell in the uniform electron gas or continuous electron density model.

The impact of core radius on the variation of the total energy with ΔZ_e for low and high core radius, r_c , have been shown in figure 4.2, for $r_c = 0.6, 1.0$ and 1.6 a.u. One observes that the total energy decreases as the charge in the electron cell increases. However, beyond an optimum, the total energy starts increasing. The depth of the energy minimum reduces as ionic pseudopotential becomes weak and its position shifts to lower ΔZ_e . Finally, beyond a particular core radius, the minima disappears. The details of different energy terms of the charged cell around the ion core and those of the electrons outside constituting the total energy are shown with respect to a variation in ΔZ_e in the figure 4.3. At low ΔZ_e values the positive energy terms like kinetic energy and electron-electron repulsion energy of the cell around the ion core reduces with an increase in the charge staying out in the electron cell. Similarly, the magnitude of the negative energy terms like

the potential, the exchange and the correlation energies of the electron gas around the ion core also reduces. The energy of the electron cell is negative, but small because the exchange and the correlation energy more than balances the kinetic and electron-electron repulsion energy in this cell.

As the number of electrons in the electron cell increases outside for the elements with valency, $Z = 4.0$ and core radii, $r_c = 0.6, 1.0, 1.6$ a.u., the corresponding changes in the density of the electrons in the cell with the ion core, n_o , and that in the electron cell, n_e , have been shown in figure 4.4. For an element with core radius, $r_c = 0.6$ a.u. the electron density in the cell around the ion core, n_o , has first increased upto an electron cell charge $\Delta Z_e = 2.0$ then the electron density, n_o , decreases beyond $\Delta Z_e = 2.0$, but the electron density, n_e , in the electron cell increases monotonically with the flow of charge to it. The increase in the electron density of the inner cell around the ion core with the flow of charge from it initially is driven primarily by an attempt to recover some potential energy by an appropriate redistribution of electrons where the cost in the kinetic and the electron - electron repulsion energies are less. The Madelung energy, although small initially, strengthens the tendency to increase electron density because of a consequent reduction of its size. But, as the charge transfer to electron cell increases, it is no longer possible

to gain any advantage in potential energy by increasing the density, because the cost in the kinetic and the electron-electron repulsion energy becomes prohibitive. Rather, it is possible to reduce energy by reducing the electron density because of larger reduction in the positive energy terms and thus, the electron density in the ion core cell reduces. In the electron cells, the electron density increases continuously, although it causes an increase in kinetic energy and the electron-electron repulsion energy. The electrostatic energy term tries in general to reduce the size of both the ion core and the electron cell. This term could not influence the size of the ion core cell because of high energy cost, but it has been effective in controlling the size of the electron cell to cause a continuous rise in the electron density, n_e . As the core radius, r_c , increases from 0.6 to 1.6 for elements with valency, $Z = 4$, the rate of increase in density as well as its magnitude in the ion core cell reduces and the maximum in density shifts to lower values of electron transfer to the electron cell, ΔZ_e . In the electron cell, the density is lower for an element with higher core radius, r_c , i.e., weaker ionic pseudopotential because the large size of the cell around the ion core makes the Madelung energy weak and so, it is less effective in controlling the size of the electron cell outside. The variation in radius of the ion core cell, R_0 , and the radius of the electron cell,

R_e , with the flow of charge to the electron cell, ΔZ_e , has been shown in figure 4.5. The size of the cell around the ion core decreases continuously, but the radius of the electron cell increases with an increase in the charge, ΔZ_e , in it, initially but subsequently the electron cell size reduces when the Madelung energy starts dominating. When the flow of charge to the electron cell, ΔZ_e , is small the Madelung energy is not strong enough to force a reduction in the size of these cells even under most favourable Madelung constant. But the charge flow is still accompanied by a lowering of energy. The cell around the ion core has a lower energy compared to the neutral atomic cell. This is due to a large reduction in the kinetic and the electron-electron repulsion energy compared to the increase in the potential, the exchange and the correlation energies. In addition, this trend is further helped by the negative energy of electron cell and the Madelung energy helps a continued increase in the charge inside the electron cell outside.

When ΔZ_e is large the electrons outside the cell containing the ion core increases the energy of this cell but the Madelung energy becomes the dominating term to such an extent that it compresses the electron cell to a density where its energy becomes positive. Thus, the only energy term favouring the charge transfer is the Madelung energy.

The minimum in energy with charge transfer is observed at a level of charge transfer when the Madelung energy is not strong enough to dictate the energy of the electron cell around the ion core. But the energy of the electron gas cell at this stage may be either positive or negative depending on the extent of influence of the Madelung energy.

The figures 4.6 and 4.7 show the total energy of the covalent bonded elements in the present model optimized with respect of R_o , ΔZ_e and R_e for a given valency, $Z = 2$ to 7 , and core radius, r_c . The structural constant, α_m , has been taken as 1.76 for all the elements. It has been observed from these figures that for a particular valency, Z , at lower core radii the total energy is large and more negative compared to those observed at a higher core radii. As valency increases the total energy becomes more negative. The arrow marks in these figures indicate the core radii at which the covalent model evolves to the limit of uniform electron gas model as the charge outside the atomic cell becomes zero. This core radius termed as crossover core radius, r_c^* , and its variation for different valencies has been presented in figure 4.8. For valency, $Z = 1$, the elements under investigation do not show any covalency because the charge transfer is always zero in the range of core radii of 0.6 to 3.0 a.u. But for

valencies $Z = 2$ onwards, the crossover core radius, r_c^* , increases from 2.0 a.u. and increases further upto $Z = 5$ and saturates. This trend is in conformity with the observation that covalency becomes more and more prevalent at higher valencies. In the figure 4.9, the total energy at the crossover core radius has been plotted against valency. The energy at the crossover is more negative with an increase in the valency but the observed total energies in the elements becomes far more negative thereby increasing the possibility to become covalent.

The variation of the charge in the electron cell for different elements characterised by valency and core radius of the ionic pseudopotential are shown in figure 4.10. For a given valency it is observed that at low core radii i.e., for stronger pseudopotential the ΔZ_e is high and it reduces with an increase in core radii. As the core radius reaches the crossover point the charge in the electron cell becomes zero as it has been pointed out earlier and the contribution from electron cell energies and the Madelung energy vanishes. When the valency increases the electron cell charge, ΔZ_e , increases for the same core radii.

The variations in the electron densities of the charged ion core, n_o , and the electron cell, n_e , are also plotted with the core radii, in figures 4.11 and 4.12 for

various valencies. These figures show that the electron density in the ion core cell reduces smoothly and steadily as core radius increases, whereas the electron density in the electron cell reduces upto a certain core radius because the Madelung energy favouring an increase in density becomes weak as core radii increases resulting in a lower electron cell charge.

The variation in the total energy for elements with valency, $Z = 4$ has been reported earlier with the most favourable observed Madelung constant $\alpha_m = 1.76$. The calculation of the exact Madelung constant has been avoided as it will depend on the number of electron cells and its precise arrangement which may vary from element to element. However the impact of α_m on the total energy has been investigated for the lowest observed α_m of 1.386 and the highest observed α_m of 1.76. The figure 4.13 shows the energy difference between the highest observed $\alpha_m = 1.76$ and lowest observed $\alpha_m = 1.386$ scaled with respect to the total energy obtained with $\alpha_m = 1.76$ for different core radii, r_c . The contribution of an error in α_m is highest for small core radius because electron cell charge and Madelung energy is higher at lower core radii. As the core radius increases the impact of α_m reduces steadily till the crossover core radius, $r_c^* = 2.4$ a.u.

The difference in atomic radii, R_a , obtained from the two extreme values of α_m , has also been scaled with the atomic radius obtained with $\alpha_m = 1.76$ and presented in the figure 4.14. At the core radius of, $r_c = 0.6$ a.u., the fractional deviation is negative and high (-8%) but with the increase in core radius it comes down leading finally to a positive deviation with a maximum of + 2.6% then the deviation falls to zero.

The total energies obtained from the calculations of the model for covalent bonding for various elements have been compared with the experimental total energies of those elements to determine the corresponding core radii, r_c . The observed atomic radii of the elements from the unit cell dimension show large deviations from those calculated on the basis of total energies. Since the model yields an energy expression quite insensitive to a variation in the atomic radius the calculations have given poor results for atomic size. The reported values of the core radii of various elements are taken from Harrison [78] who has obtained these values using the model potential due to Animalu and Heine [49], except for Oxygen, Sulphur and Chlorine which are obtained from fitted pseudopotentials by Cohen and Heine [31] .

In the case of Carbon with valency, $Z = 4$, the core radius, r_c , obtained here is 0.4 a.u. whereas the reported

value of 0.6994 a.u. is much higher. The core radius, r_c , obtained for Silicon is 0.96 a.u. and the reported value is 1.0586 a.u. Similarly, for elements with higher valency of $Z = 5$ and above Phosphorous, Oxygen, Sulphur and Chlorine show a comparatively lower core radii than those reported. As the core radii increases i.e., the elements with a large diameter like Antimony, Selenium the core radii are quite similar to but lower than the reported values with very small differences except for Bismuth and Tellurium where the obtained values of core radii are slightly more than the reported values. This indicates that the variation in energy with the core radii is more accurate at higher core radii.

4.4 Summary

The inhomogeneity in the electron distribution under covalent bonding has been created by removal of electrons from the atomic cell and by allowing a separate electron cell to form in the bond directions where it is possible to take into account directionality of the covalent solids. The electrons around the ion core termed as ion core cell and the cell of electrons are allowed to have different densities. With the help of octet rule, the number of bonds are calculated and it is assumed that the number of electron cells are equal to the number of **bonds**. The gradient energy contribution has been neglected here for

simplicity. The total energy has been calculated with the optimizing parameters as the radius of the ion core cell, the electron cell and the amount of charge present in the electron cell. The Madelung energy term has been included but it requires the structural orientation of electron cells around the ion core cell for each individual element. This problem has been avoided by assuming the maximum Madelung constant observed uniformly for all elements. The impact of this assumption has been assessed by examining the situation with the most unfavourable Madelung constant.

The total energy calculated from this model shows that for valency, $Z = 1$, the charge transfer is always zero and so, there is no possibility of co-valency. For valency, $Z = 2$, and above the total energy of this model is lower than that of the uniform gas model but evolves to it at higher core radius. But there are no elements in the range of core radius where the energy obtained from model for covalent bonding is lower than that in the uniform gas model. The cross-over core radius, r_c^* , increases to higher values at higher valencies and comes within the range of occurrence of various elements. This trend is in conformity with the observations from the periodic table as the co-valency becomes more prevalent at valencies higher than four.

The comparison of the calculated energies with the observed ones yields the values of core radii for different

elements like Carbon, Silicon, Oxygen, Phosphorous etc. It has been observed that the difference between the core radii so obtained the ones reported earlier reduces for higher core radii.

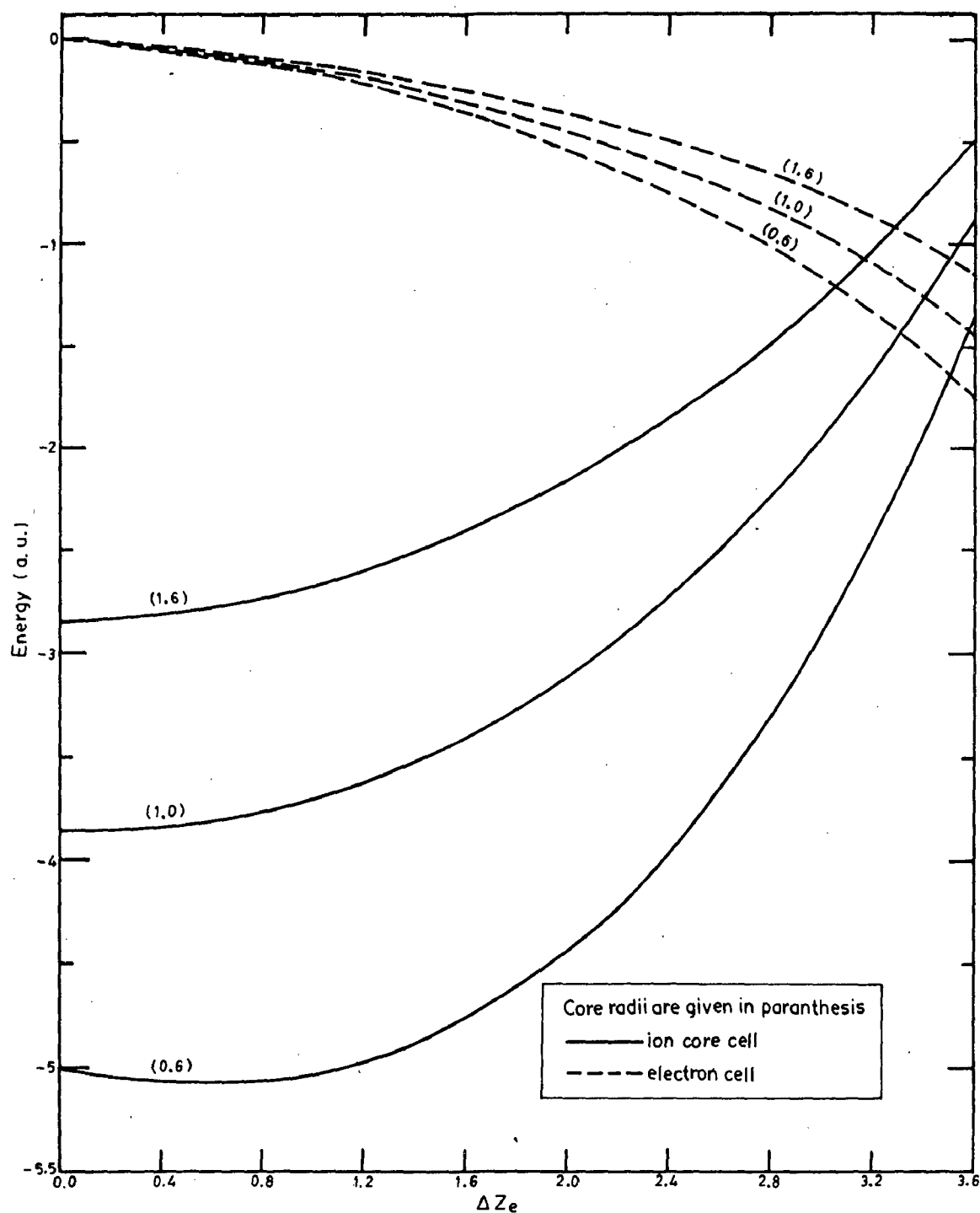


Fig.4.1: THE VARIATION OF ENERGIES in a.u. OF THE ION CORE CELL AND ELECTRON CELL WITH FLOW OF CHARGE, ΔZ_e FOR VALENCY, $Z=4$ AND CORE RADII, $r_c = 0.6, 1.0, 1.6$ a.u. .

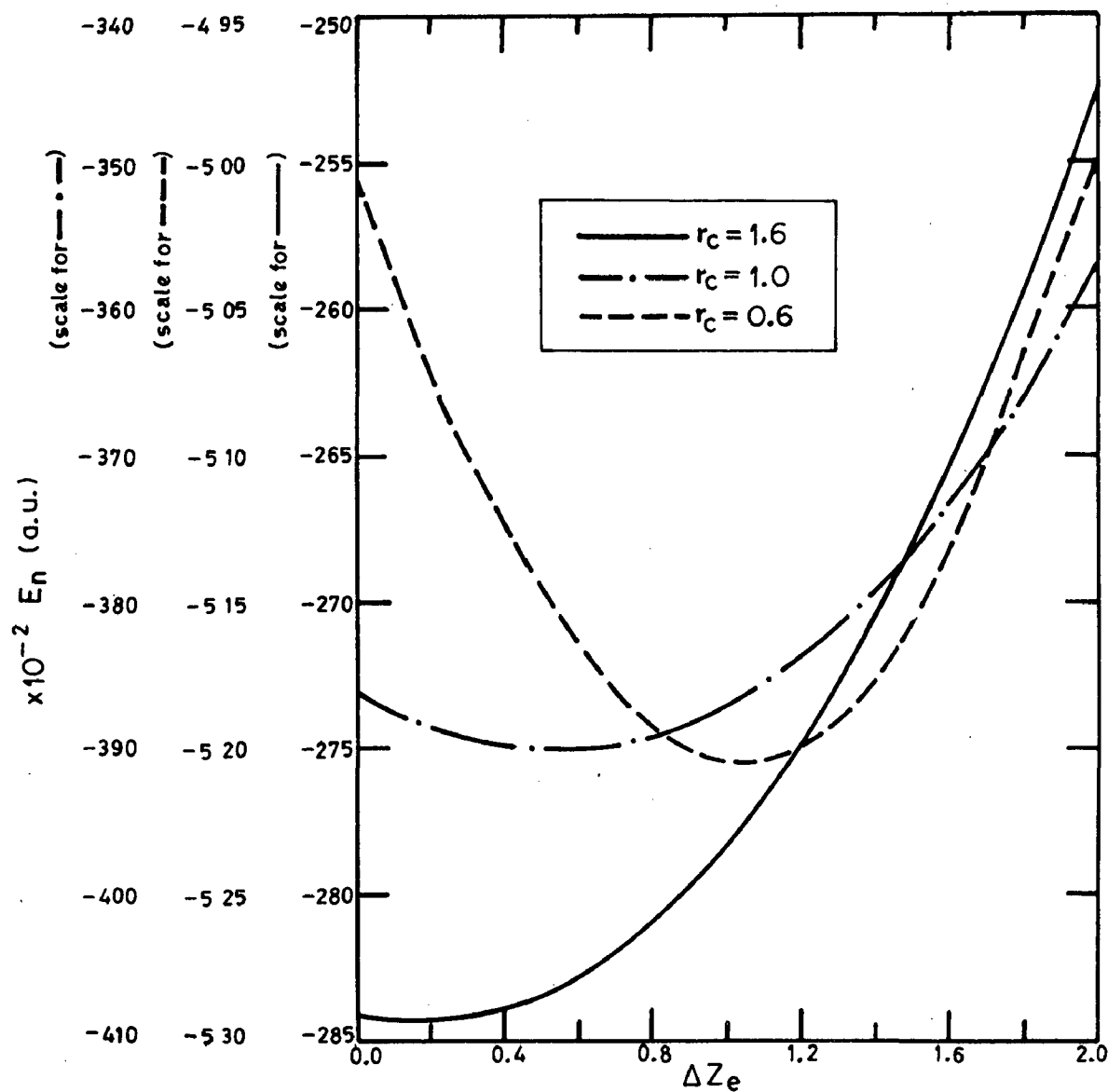


Fig. 4.2 : THE VARIATION OF THE TOTAL ENERGY, E_n in a.u. WITH CHARGE FLOW, ΔZ_e FOR THE VALENCY, $Z=4$ AND CORE RADII, $r_c = 0.6, 1.0, 1.6$ a.u. .

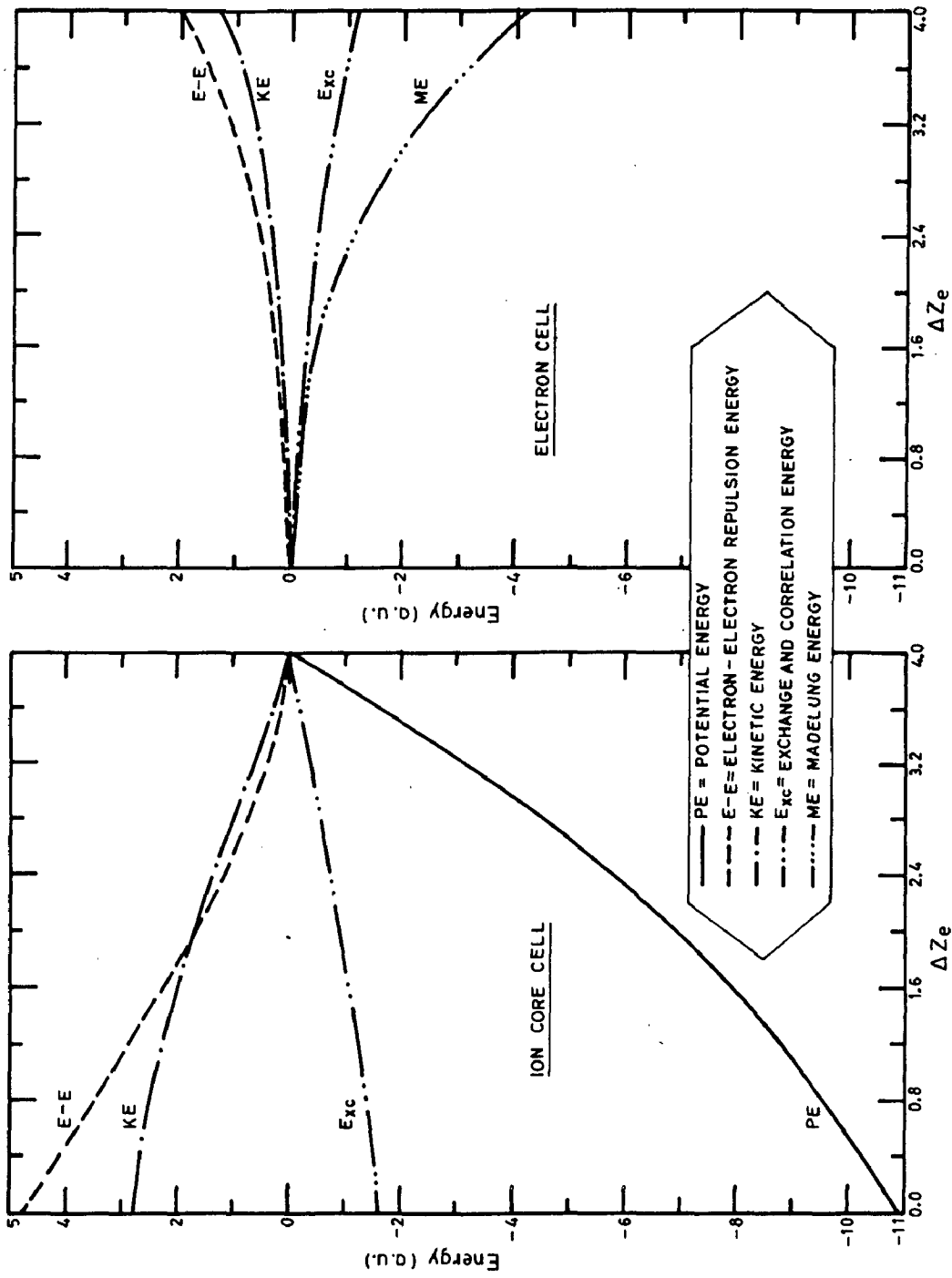


Fig.4.3: THE CHANGE IN THE DIFFERENT ENERGY TERMS WITH THE FLOW OF CHARGE, ΔZ_e RELATING TO THE ION CORE CELL AND THE ELECTRON CELL FOR THE VALENCY, $Z=4$ AND CORE RADIUS, $r_c=0.6$ a.u. .

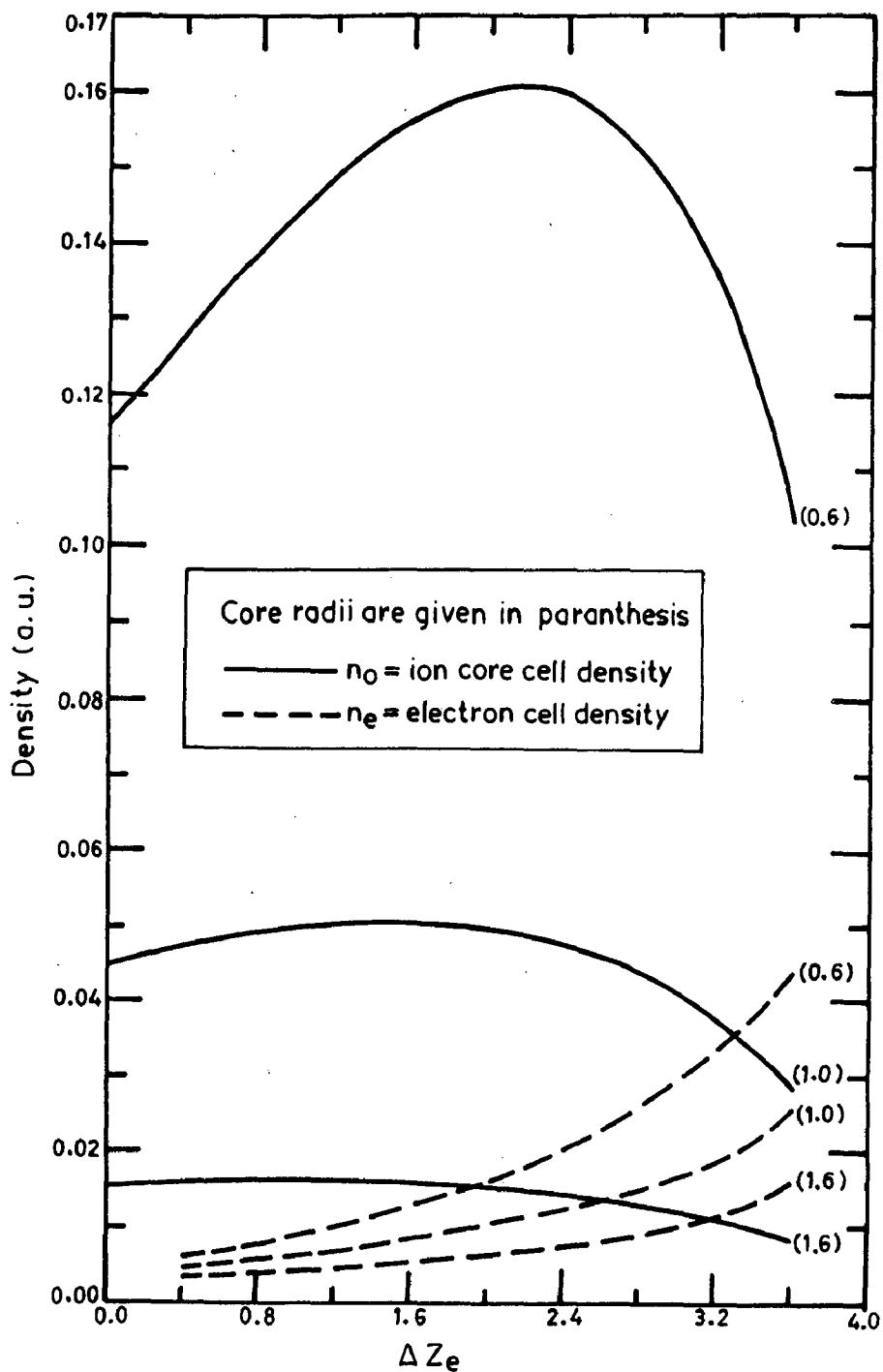


Fig.4.4: THE CHANGE OF DENSITY OF ELECTRONS IN THE ION CORE CELL, n_0 in a.u. AND THE ELECTRON CELL, n_e in a.u. WITH THE FLOW OF CHARGE, ΔZ_e FOR VALENCY, $Z=4$ AND CORE RADII, $r_c=0.6, 1.0, 1.6$ a.u. .

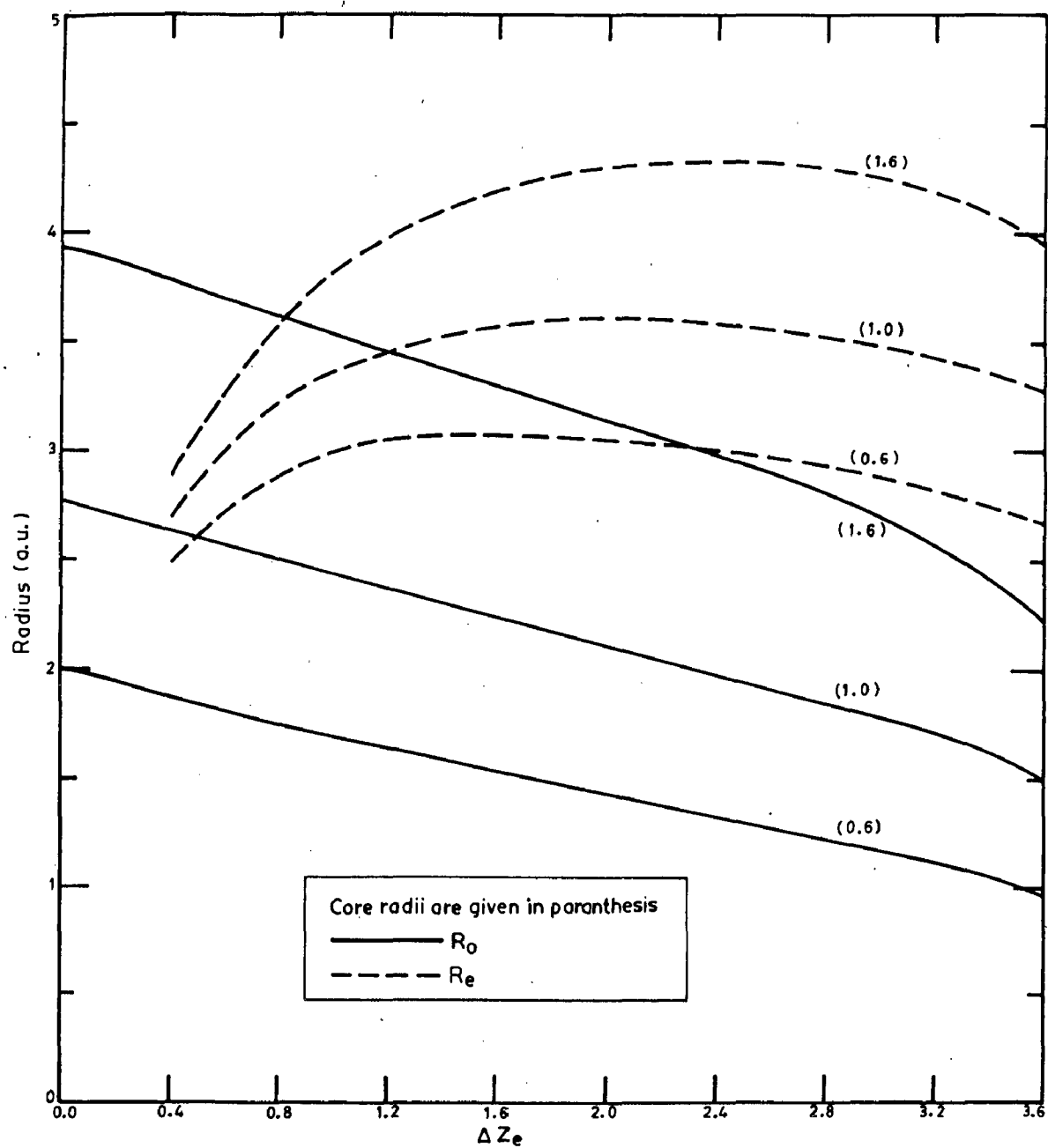


Fig.4.5: THE VARIATION IN THE RADIUS OF THE ION CORE CELL, R_0 in a.u. AND THE RADIUS OF THE ELECTRON CELL, R_e in a.u. WITH THE FLOW OF CHARGE, ΔZ_e FOR VALENCY, $Z=4$ AND CORE RADII, $r_c=0.6, 1.0, 1.6$ a.u. .

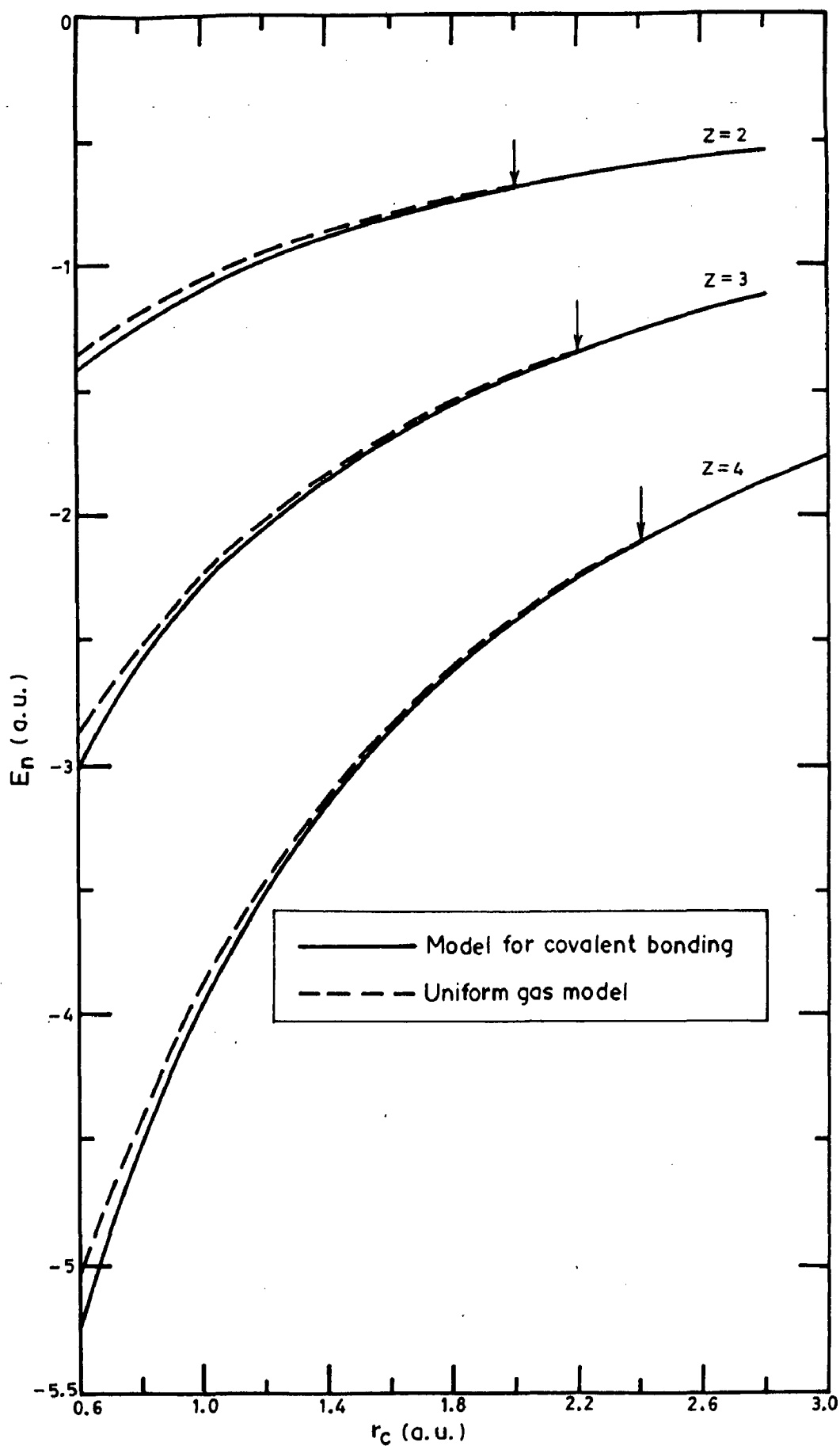


Fig.4.6: THE VARIATION OF TOTAL ENERGIES, E_n in a.u. WITH CORE RADII, r_c in a.u. FOR VALENCIES, $Z = 2$ to 4 .

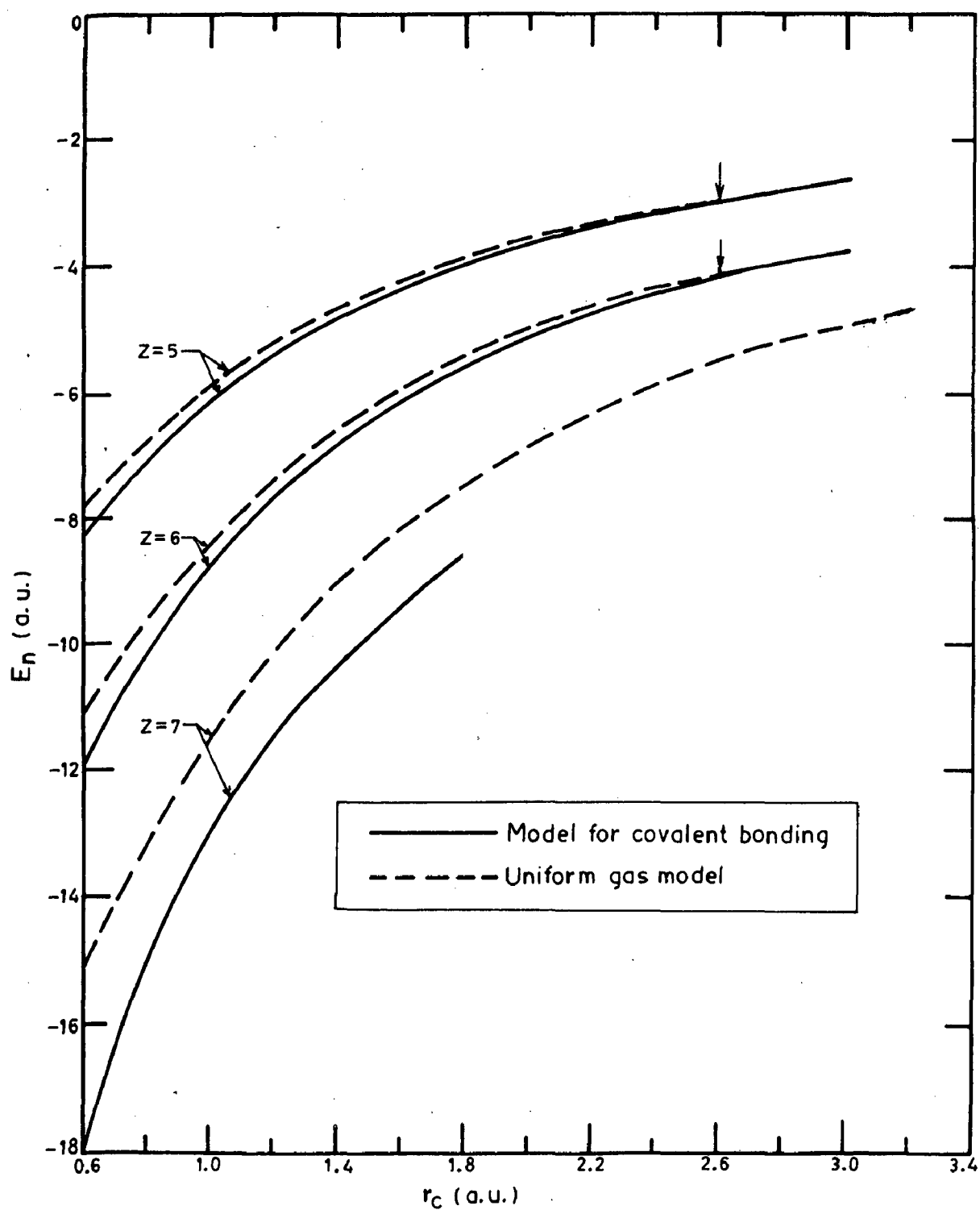


Fig.4.7: THE VARIATION OF TOTAL ENERGIES, E_n in a.u. WITH CORE RADII, r_c in a.u. FOR VALENCIES, $Z = 5$ TO 7.

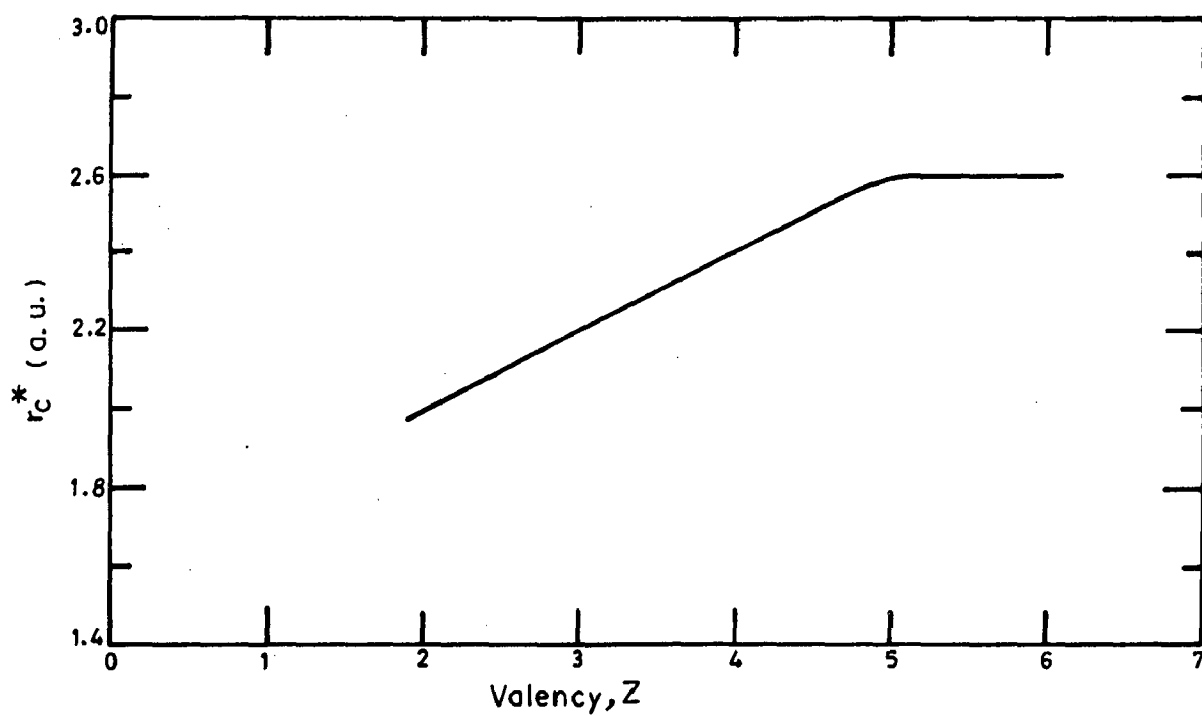


Fig.4.8 : THE CHANGE IN THE CROSS-OVER CORE RADII, r_C in a.u. WITH THE UNIFORM GAS MODEL FOR DIFFERENT VALENCIES.

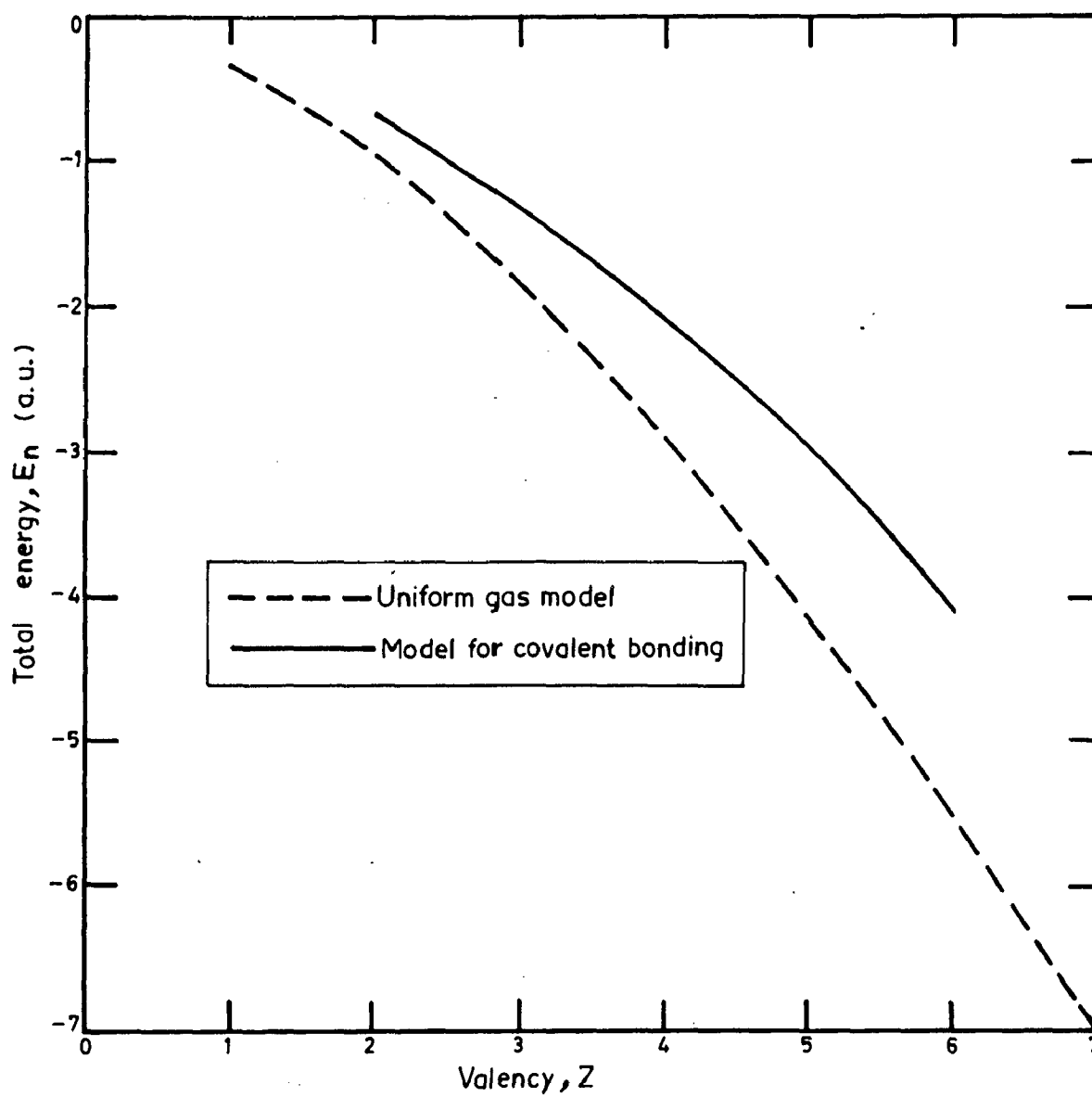


Fig.4.9 : THE VARIATION OF TOTAL ENERGIES, E_n in a.u. AT THE CROSS-OVER CORE RADII, r_c^* in a.u. FOR DIFFERENT VALENCIES.

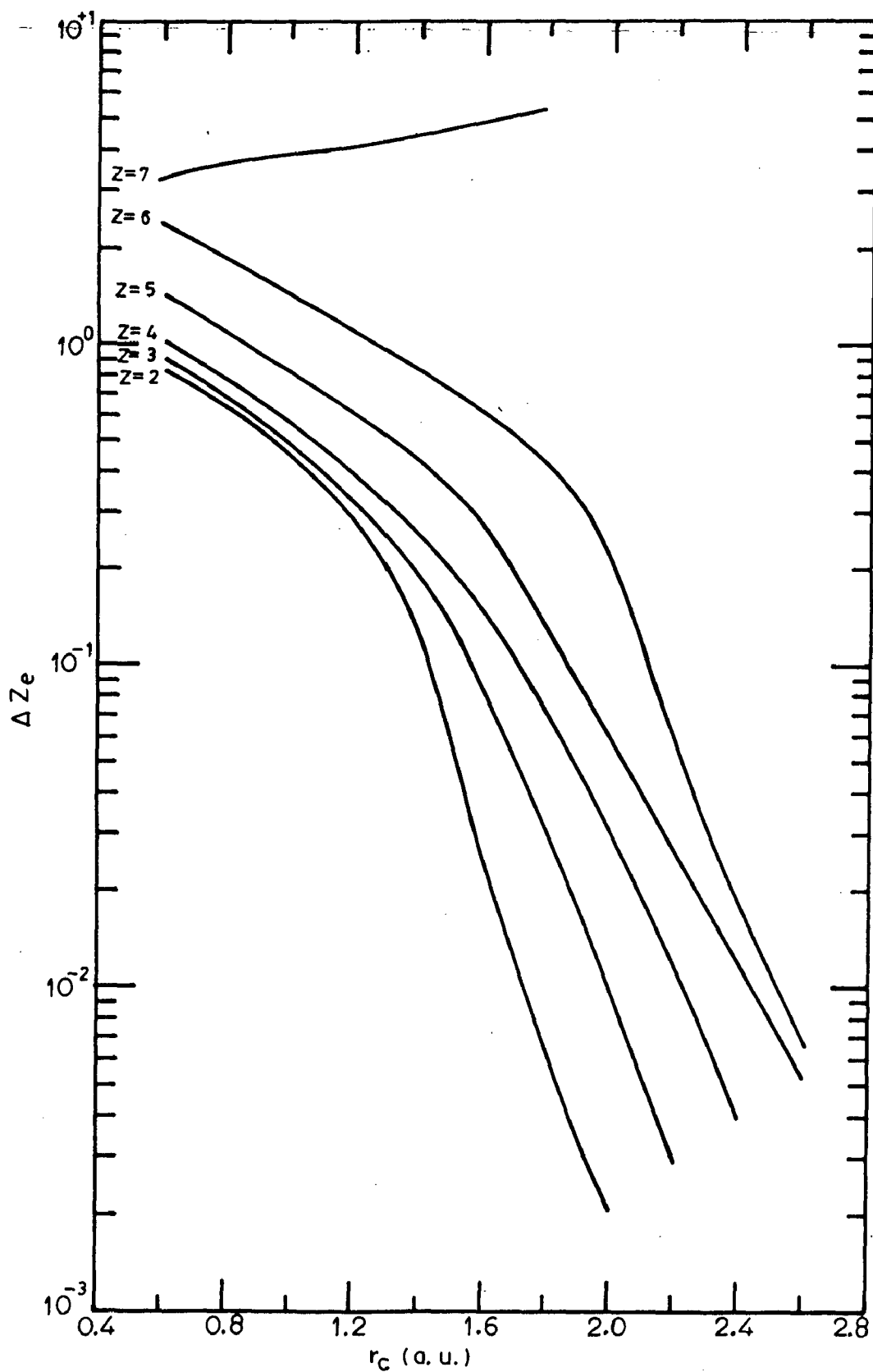


Fig.4.10: THE VARIATION OF CHARGE FLOW, ΔZ_e WITH CORE RADII, r_c in a.u. FOR THE VALENCIES, $Z=2$ TO 7 .

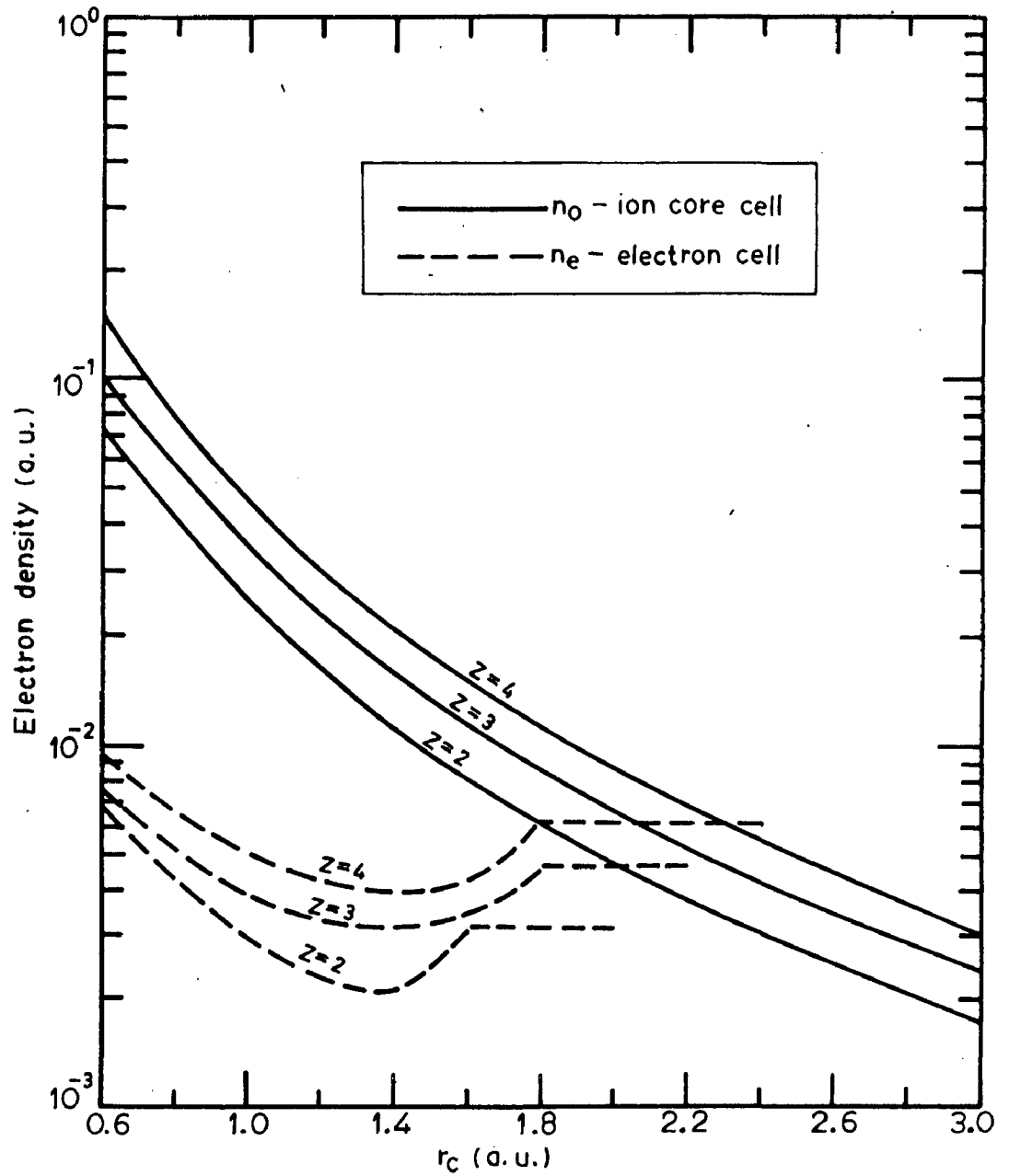


Fig.4.11: THE VARIATION OF ELECTRON DENSITIES IN THE ION CORE CELL, n_0 in a.u. AND THE ELECTRON CELL, n_e in a.u. WITH CORE RADII, r_c in a.u. FOR THE VALENCIES, $Z = 2$ TO 4.

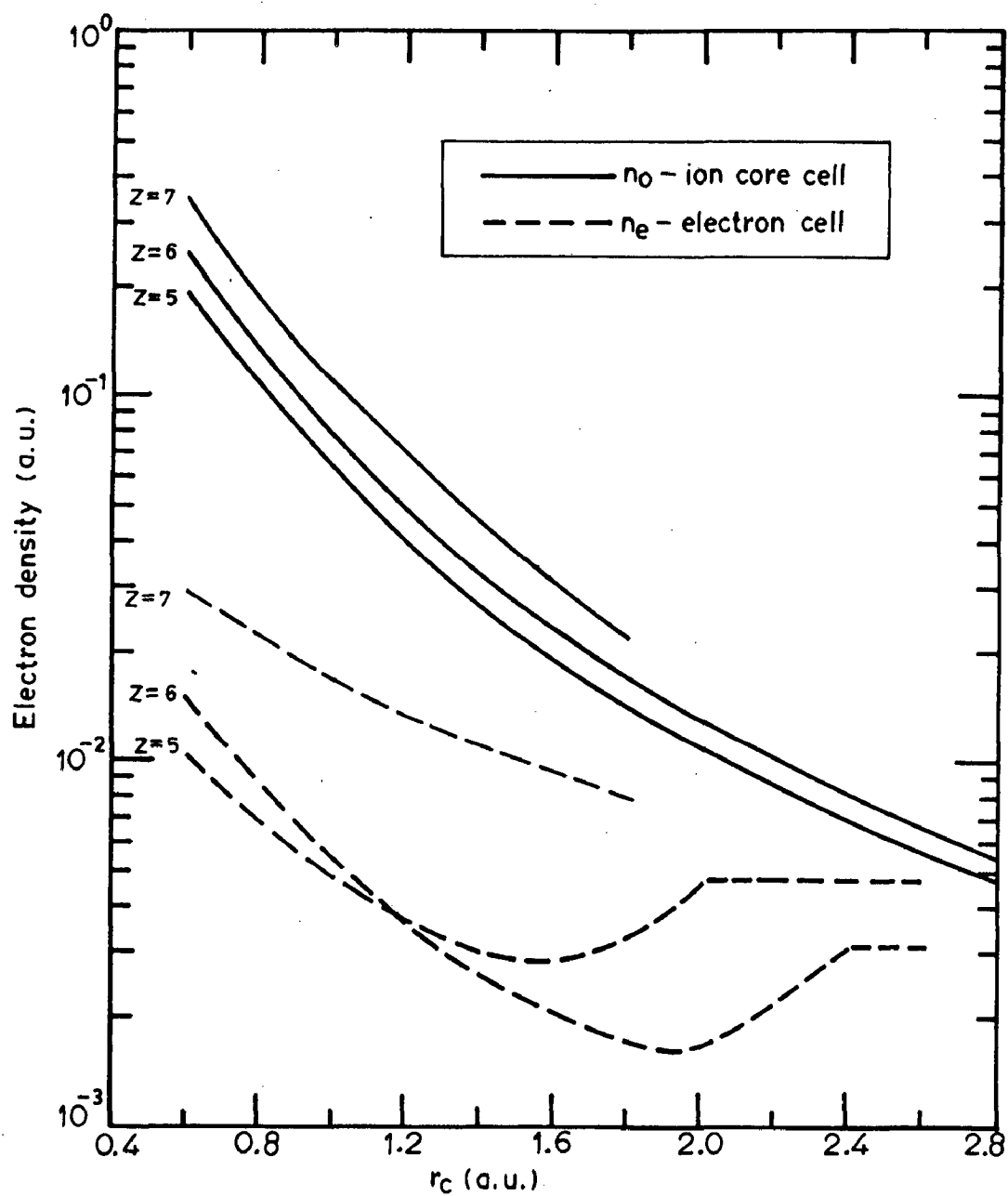


Fig.4.12: THE VARIATION OF ELECTRON DENSITIES IN THE ION CORE CELL, n_0 in a.u. AND THE ELECTRON CELL, n_e in a.u. WITH CORE RADII, r_c in a.u. FOR THE VALENCIES, $Z = 5$ to 7.

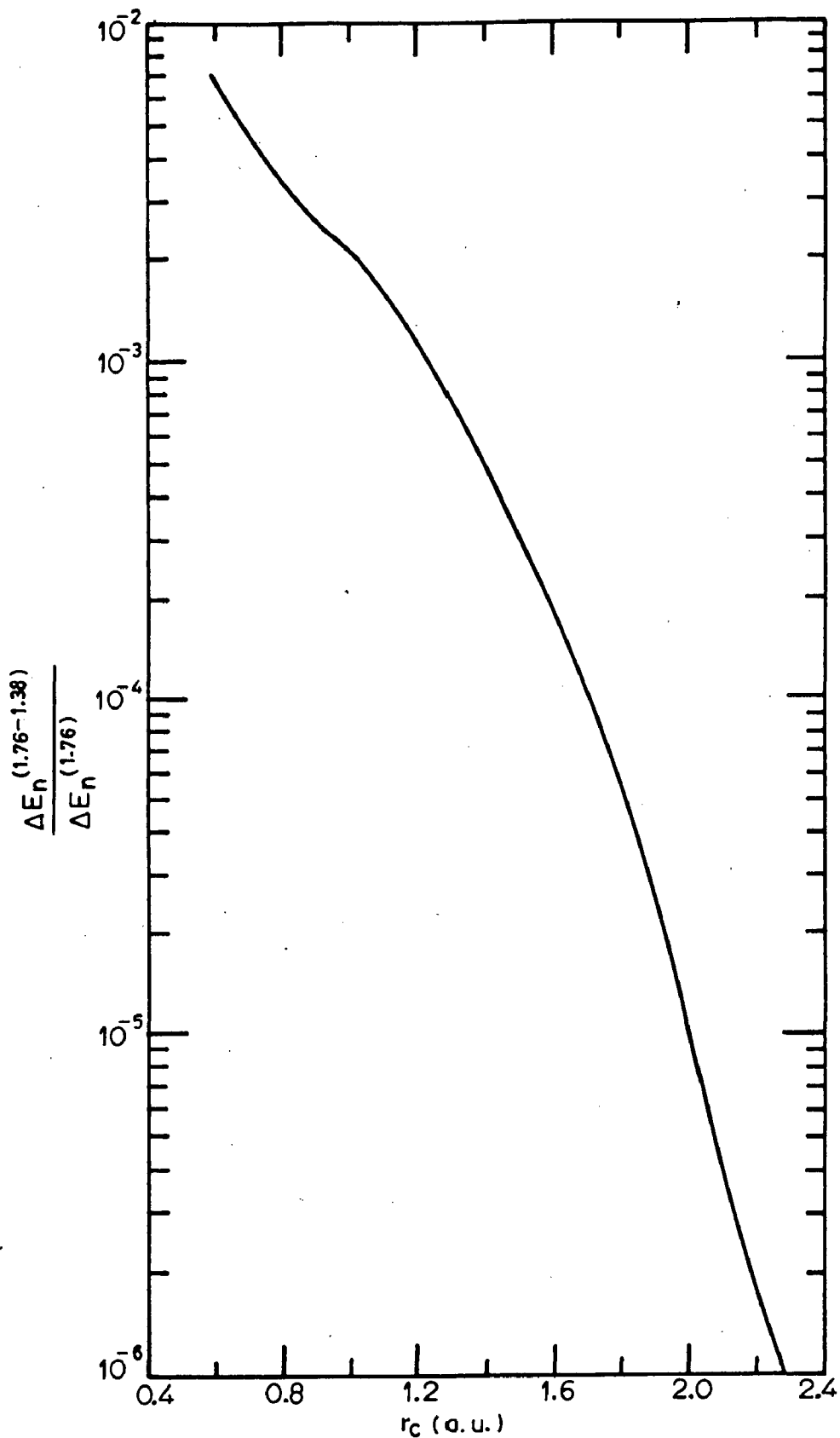


Fig.4.13 : THE DIFFERENCE IN TOTAL ENERGY in a.u. WITH MADELUNG CONSTANT, $\alpha_m = 1.76$ AND 1.386 SCALED WITH TOTAL ENERGY OBTAINED WITH $\alpha_m = 1.76$ FOR VALENCY, $Z = 4$.

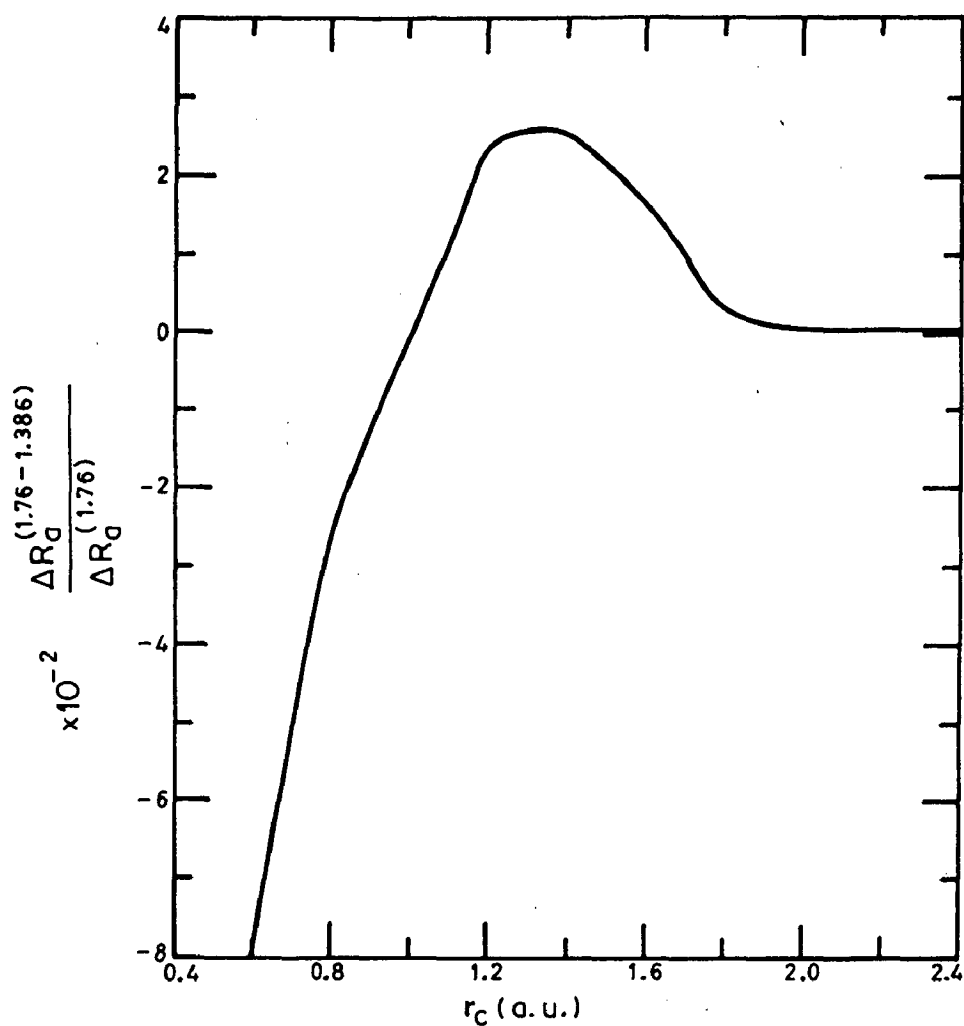


Fig.4.14: THE DIFFERENCE IN THE ATOMIC RADIUS in .
 OBTAINED FROM $\alpha_{\bar{m}} 1.76$ AND 1.386, SCALED WI
 ATOMIC RADIUS OBTAINED FROM $\alpha_{\bar{m}} 1.76$ FOR
 VALENCY, $Z = 4$.

CHAPTER **5**

CONCLUSION

The total energy for various elements are analysed with the assumption of the electrons in the atomic cell are uniform in density. The ground state energy has been achieved with the help of Hohenberg-Kohn[2] density functional equation for the known valency of an element and the core radius of the element has been expressed as a function of atomic radius. The observed values of the total energies of various elements are found to be lower than the values obtained in the uniform gas model for the corresponding atomic radii. It has been realised that by introducing an inhomogeneity in electron density should improve the ground state energy with the shift in atomic radius as it has been observed while applying second order perturbation theory. A study of the stability of uniform gas model has demonstrated the range of atomic radii corresponding to $r_s < 2.4217$ a.u , where the inhomogeneous electron gas will be more stable.

The inhomogeneity in electron gas has been introduced in the step model by splitting the atomic cell into inner cell and outer shell by maintaining two different uniform electron densities respectively. The total energy calculated from the step model for various elements are found to be lower as compared to the corresponding values obtained experimentally. This is attributed to ignoring

the gradient energy term.

The continuous electron density model has been introduced to account for the gradient energy contribution and the electron density in this model varies continuously within the atomic cell. A parametric tangent hyperbolic function has been chosen to model the electron density as it closely retains the feature of step model. The total energies of various elements are observed to be in good agreement with the experimental values. Further, the total energy obtained from the continuous density model and the step model slowly evolves to a uniform density model at higher core radius and the energy is a continuous function of core-radius. The core radius at which the uniform gas model becomes stable is termed as the crossover core radius. The difference in total energy obtained from continuous model and step model shows a linear variation with the difference in electron density between the inner and the outer segment of the atomic cell in the step model. Thus the gradient contribution to the total energy in the step model has been corrected for the entire range of elements under investigation in order to utilize the results of the step model.

In covalent solids the inhomogeneity in electron density has been constructed by removal of electrons from the atomic cell and allowing a separate electron cell to

form in covalent bond directions, so as to achieve directionality in covalent bonding. With the help of octet rule the number of bonds are calculated and the number of electron cells are thereby fixed. In the total energy calculation the Madelung energy term has been incorporated for the structural orientation in the electron cells around the ion core cell. The highest observed value of Madelung constant has been assumed for all the elements which gives an over estimate of the stability of covalent bonding. To assess the impact of Madelung constant calculations have also performed with the lowest observed Madelung constant.

The results of the model for covalent bonding are compared with the gradient corrected step model and here the gradient corrected step model also has been compared with the uniform gas model to bring out the regions of relative stability of each model in the entire range of core radii and valencies investigated. Already it has been pointed out that the model for covalent bonding evolves to uniform gas model beyond a certain core radius for a given valency. But the inhomogeneous electron gas model like the step model is not built in the model for covalent bonding presented here. So, the energies of each model have been compared for the given values of valencies and core radii in order to identify the most stable model.

For valency $Z=1$, it has been observed that the covalent model has always a higher energy compared to the uniform gas and gradient corrected step model. Also, the gradient corrected step model yields a higher energy for lower core radii when compared to those in the uniform gas model and merges with it at a core radius of $r_c = 1.6$ a.u. Thus, the uniform gas model is excellently suited for simple metals with valency, $Z = 1$.

For elements with valency, $Z \geq 5$., it has been observed that the model for covalent bonding gives the lowest energy within the range of experimentally observed energies for different elements as compared to the energies observed in the other two models. However, the corrected step model and uniform electron gas model becomes stable at a very high core radius where no elements occur in the periodic table.

Fig. 5.1 shows the region of stability of the uniform, corrected step and the model for covalent bonding for valencies, $Z=2,3$ and 4 . It is observed that upto $r_c = 1.8, 1.8$ and 2.0 a.u. the model for covalent bonding remains the most stable for valencies $Z=2,3$ and 4 respectively. These estimates are highly in favour of covalent model because the most favourable value of $\alpha = 1.76$ has been taken for the calculations. If these energy values are adjusted with the observed deviation factor for $Z = 4.0$ the model

for covalent bonding becomes less favourable and it remains stable upto $r_c = 1.2, 1.0,$ and (1.2) respectively for valencies, $Z = 2, 3$ and 4 . Beyond the range of stability of the model for covalent bonding, the corrected step model representing inhomogeneous electron gas distribution becomes energetically more favourable upto $r_c = 2.0, 2.2$ and 2.2 a.u. for valencies $Z = 2, 3$ and 4 respectively. When the core radii is above these values of $2.0, 2.2$ and 2.2 a.u. the uniform gas model gives the lowest energy.

The figure 5.2 shows the region of stability of the uniform, corrected step models and model for covalent bonding for valencies, $Z = 2, 3$ and 4 , in terms of energy. It is observed that at lower ranges of negative energy the uniform gas model is more stable but the corrected step model becomes more stable at a higher range of negative energies. Subsequently, model for covalent bonding becomes more stable in comparison to even corrected step model at still higher ranges of negative energies. As valency increases the range of stability of each model shifts to higher energies. Since the model for covalent bonding is calculated with most favourable Madelung constant, $\alpha_m = 1.76$, its stability may have been unduly enhanced but when the calculations are carried out with the most unfavourable, $\alpha_m = 1.386$, corresponding to linear chain the model for covalent bonding becomes stable only at higher energies as

indicated by the dotted lines. Thus, the stability ranges of the corrected step model becomes extended in energy scale.

The table 5.1 gives the values of the core radius obtained from the corrected step model for simple metals and from the model for the covalent bonding in cases of covalent solids. These values are compared with the core radius obtained by earlier workers. It is observed from the table 5.1 that the core radius obtained by comparing the energies of different elements with the calculated curves for the corresponding model are quite comparable to those used by the earlier workers. The core radii obtained here are generally lower than the reported values. The total energies have been compared to find core radii because the atomic radii has been observed to become a relatively insensitive variable for the variation of energy in the model for covalent bonding and corrected step model. It is evident from the large mismatch between the observed size of the atoms and the calculated atomic radii for different elements.

The present investigation has shown that it is possible to study the phenomenon of bonding within the frame work of Density Functional Formalism. The systematic results are in conformity with the general trends in bonding

as observed in the elements of the periodic table. The quantitative matching of results are not always very satisfactory due to sacrifice of rigour in order to maintain simplicity.

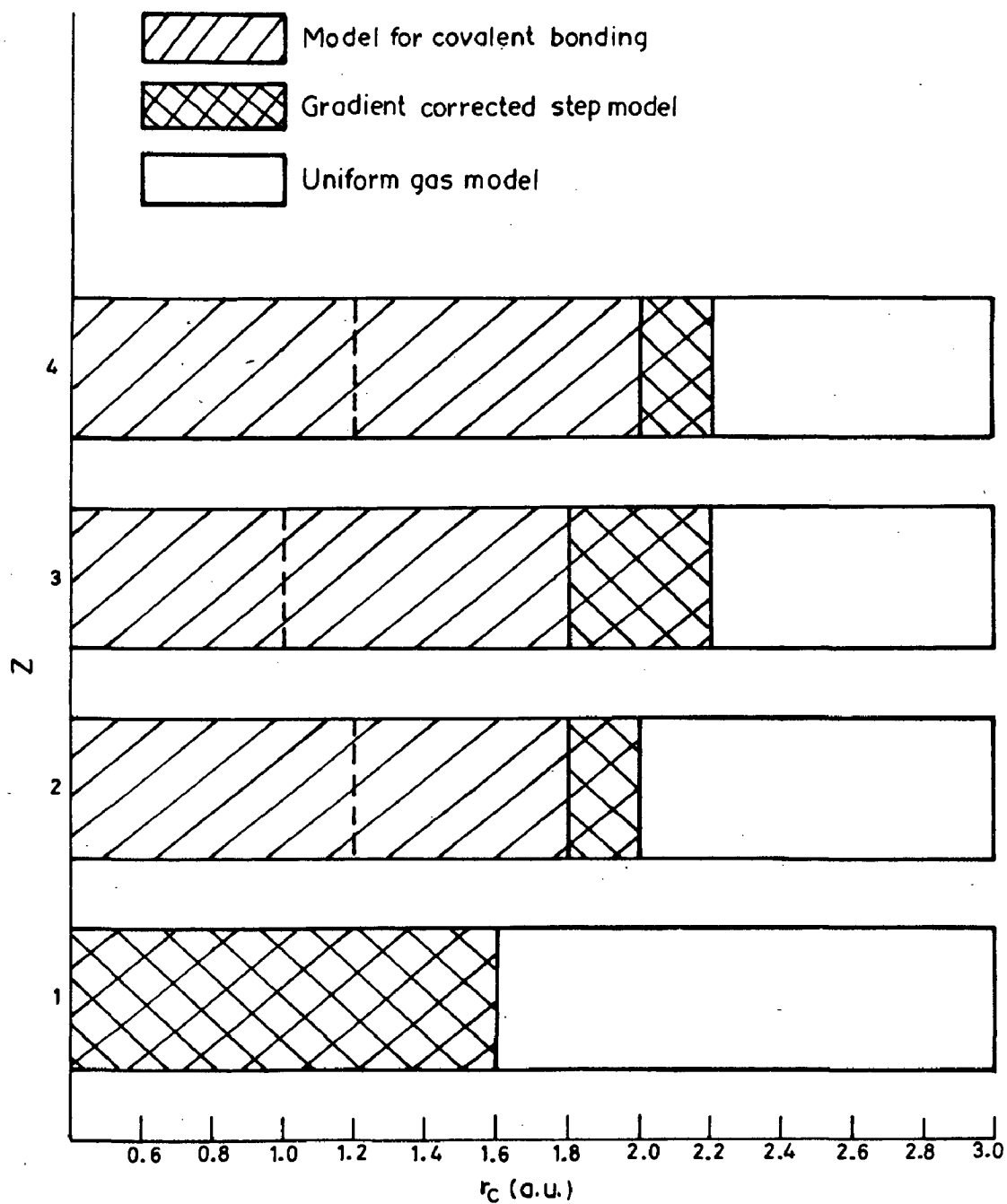


Fig.5.1: THE RANGE OF STABILITY OF VARIOUS MODELS IN TERMS OF CORE RADIUS, r_c in a.u. FOR VALENCIES, $Z=1, 2, 3$ & 4 .

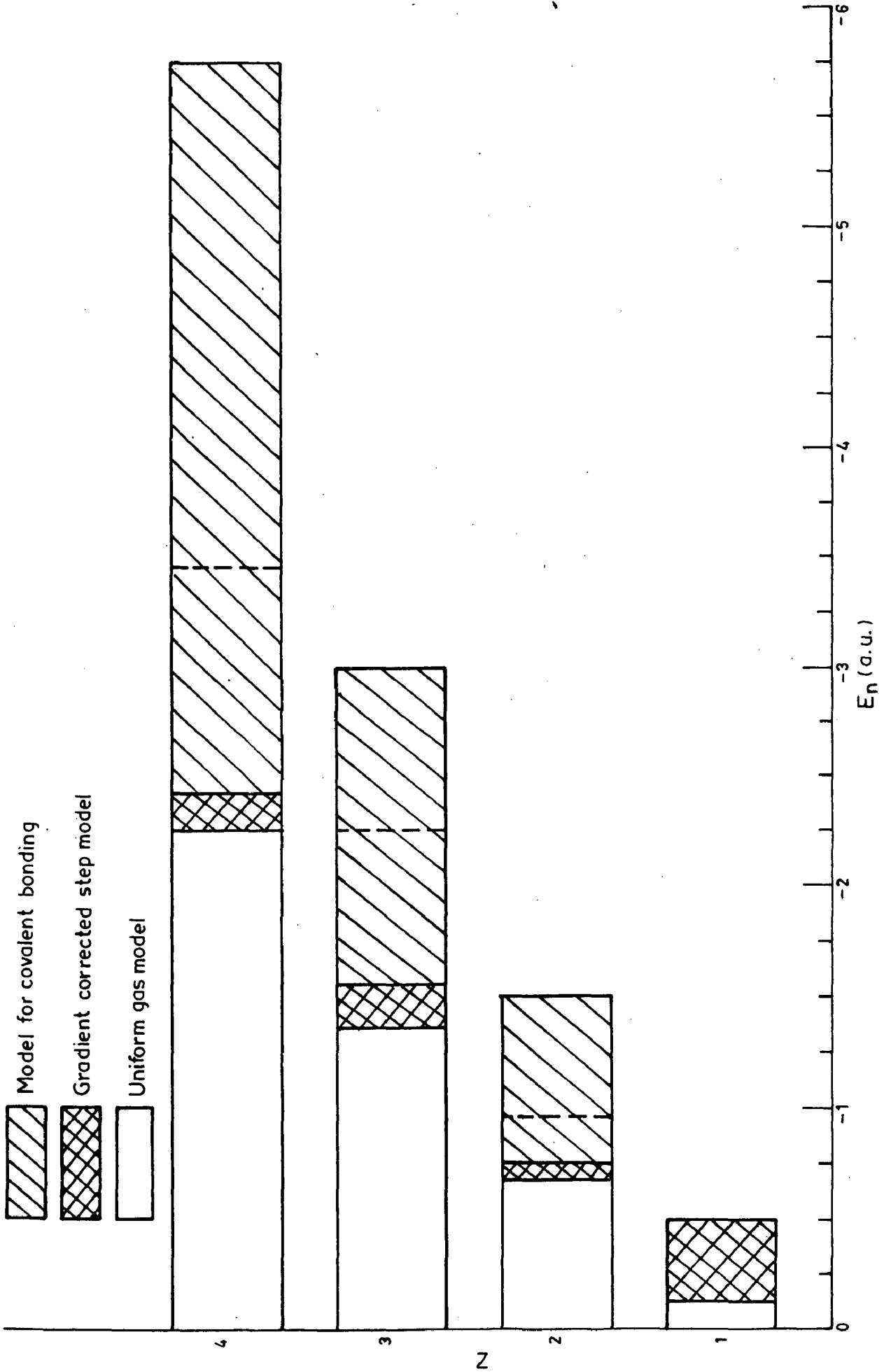


Fig.5.2: THE RANGE OF STABILITY OF VARIOUS MODELS IN TERMS OF TOTAL ENERGY, E_n in a.u. FOR VALENCIES $Z = 1, 2, 3$ and 4 .

Table- 5.1 The values of core radius, r_c , for various elements obtained by matching the experimental total energy

METALS

Element	Val- ency	Experimental values		Gradient corr cted step model		Reported values	
		E_n [69]	R_a	R_a	r_c	r_c [78]	r_c [72]
Z		(a.u.)	(a.u.)	(a.u.)	(a.u.)	(a.u.)	(a.u.)
1	2	3	4	5	6	7	8
Li	1	-0.2581	3.258	3.70	1.50	1.739	1.06
Na	1	-0.2299	3.931	4.08	1.80	1.815	1.67
K	1	-0.1939	4.862	4.88	2.30	2.268	2.13
Rb	1	-0.1850	5.197	5.04	2.42		2.61
Cs	1	-0.1726	5.625	5.30	2.60		2.93
Be	2	-1.1342	2.351	3.15	0.91	1.096	
Mg	2	-0.8893	3.339	3.84	1.38	1.399	1.39
Ca	2	-0.7287	4.123	4.64	1.88	1.701	

Table-5.1 Contd....

1	2	3	4	5	6	7	8
Sr	2	-0.6779	4.494	4.84	2.08	2.155	
Ba	2	-0.6290	4.661	5.00	2.21	3.025	
B	3	-2.8357	2.273	2.90	0.64	0.832	
Al	3	-2.0824	2.984	3.72	1.16	1.153	1.12
Ga	3	-2.2088	3.154	3.48	1.06	1.115	
In	3	-2.0294	3.472	3.84	1.21	1.190	1.32
Tl	3	-2.1401	3.577	3.63	1.10	1.134	
Si	4	-3.9607	3.184	3.38	0.98	1.059	(0.976)*
Ge	4	-3.9173	3.309	3.48	1.0	1.021	(0.96)*
Sn	4	-3.5410	3.512	3.84	1.17	1.115	1.3 (1.072)* α Sn
Pb	4	-3.6275	3.648	3.76	1.14	1.078	1.12

* Cohen and Bergstresser's pseudopotential [68] interpolation procedure [67]

Table-5.1 Contd....

COVALENT SOLIDS

Element	Valency	Experimental values		Model for covalent bonding		Reported values
		E_n [69] (a.u.)	R_a (a.u.)	R_a (a.u.)	r_c (a.u.)	
C	4	-5.7121	2.091	3.36	0.40	0.699
P	5	-6.6255	2.991	4.025	0.86	0.964
As	5	-6.3424	3.263	4.25	0.92	0.964
Sb	5	-5.6405	3.652	4.40	1.10	1.059
Bi	5	-5.6257	3.852	4.375	1.12	1.078
O	6	-12.9599	-	3.12	0.52	0.794 ⁺
S	6	-10.270	3.453	3.84	0.78	0.888 ⁺
Se	6	-9.448	3.529	4.05	0.88	0.945
Te	6	-8.2595	3.787	4.38	1.06	1.021
Cl	7	-15.0834	3.597	2.91	0.80	0.945 ⁺
Br	7	-13.582	3.745	3.115	0.94	-

⁺ Values from Cohen and Heine fitted pseudopotentials [42]

REFERENCES

REFERENCES

1. Lewis, G.N., The Atom and the Molecule, J. Am. Chem. Soc. 38, 762 (1916).
2. Hohenberg, P., Kohn, W., Inhomogeneous electron gas, Phys. Rev., 136, pp. B864-B871, (1964).
3. Kohn, W. and Sham, L.J., Self consistent equations including exchange and correlation effects, Phys. Rev., 140, pp. A1130-A1138, (1965).
4. Wigner, E., On the interaction of electrons in metals, Phys. Rev. 46, pp. 1002-1011, (1934).
5. Gunnarson, O., Lundqvist, B.I. and Lundqvist, S., Screening in a spin-polarized electron liquid., Sol. Stat. Commun., 10, pp. 149-152, (1972).
6. Nozieres, P. and Pines, D., Correlation energy of a free electron gas, Phys. Rev. 111, pp. 442-454, (1958).
7. Weizsacker, V., Z. Physik., 96, 431, (1935).
8. Jones, W. and Young, W.H., Density functional theory and the von Weizsacker method, J. Phys. C 4, pp. 1322-1330, (1971).
9. Rasolt, M. and Geldart, D.J.W., Gradient corrections in the exchange and correlation energy of an inhomogeneous electron gas, Phys. Rev. Letts., 35, pp. 1234-1237, (1975); Geldart, D.J.W. and Rasolt, M., Phys. Rev., B 13, 1477, (1976).

10. Theophilou, A.K., The energy density functional formalism for excited states, J.Phys., C 12 , pp. 5419-5430, (1979).
11. Wang, W.P., Parr, R.A., Murphy, D.R. and Henderson, G.A., Chem. Phys. Letts., 43, 409, (1976).
12. Alonso, J.A. and Girifalco, L.A., Nonlocal approximation to the exchange potential and kinetic energy of an inhomogeneous electron gas., Phy. Rev., B 17 , pp. 3735-3743, (1978).
13. Feenberg, E., Theory of quantum fluids, Academic, New York, (1969).
14. Clark, J.W. and Westhaus, P., Method of correlated basis functions., Phys. Rev. 141, pp. 833-857, (1966); Ristig, M.L. and Clark, J.W., Nucl. Phys., A 199 , 351, (1973).
15. Ceperley, D., Chester, G.V. and Kalos, M.H., Monte-carlo simulation of a many-fermion study, Phys. Rev., B 16 , pp. 3081-3099, (1977).
16. Rajan, V.T., and Woo, C.W., Variational approach to inhomogeneous electron liquids: Application to metallic hydrogen, Phys. Rev., B 18 , pp. 4048-4063, (1978).
17. Frost, A.A. and Braunstein, J., Hydrogen molecule energy calculation by correlated molecular orbitals, J.Chem. Phys., 19 , pp. 1133-1138, (1951).
18. Laurent, D.G., Wang, C.S. and Callaway, J., Energy bands, Compton profile, and optical Conductivity of Vanadium., Phys. Rev., B 17 , pp. 455-461, (1978).

19. Cohen, M.L., Schlutter, M., Chelikowsky, J.R. and Lcuie, S.G., Self-consistent pseudopotential method for localized configurations: Molecules, Phys. Rev. B 12, pp. 5575-5579, (1975).
20. Pratt, Jr, G.W., Wave functions and energy levels for Cu^+ as found by the slater approximation to the Hartree- Fock equations, Phys. Rev., 88 , pp. 1217-1224, (1952).
21. Ferriera, L.G., J.Comput. Phys. 36 , 198, (1980).
22. Kerker, G.P., Efficient iteration scheme for self-consistent pseudopotential calculations, Phys. Rev. B 23, pp. 3082-3084, (1981).
23. Rose, J.H. and Shore, H.B., Solid State Commun , 17 , 327, (1975).
24. Rose, J.H. and Shore, H.B., Self-consistent calculation of surface properties of electron-hole droplets, Phys. Rev. B. 17 , pp. 1884-1892, (1978).
25. Garvy, R.H. Jackman, C.H. and Green, A.E.S., Independent- particle- model potentials for atoms and ions with $36 \leq Z \leq 54$ and a modified Thomas- Fermi atomic energy formula, Phys. Rev. A 12 , pp. 1144-1152, (1975).
26. Aashamar, A., Luke, T.M. and Talman, J.C., Properties of single-term atomic states calculated in a variationally optimized-local-central-potential model, Phys. Rev. A 19, pp. 6-16, (1979).
27. Hartree, D.R., The calculation of atomic structure, Wiley, New York, (1957).

28. Herring, C., Phys. Rev. 57, 1169, (1940).
29. Phillips, J.C. and Kleinman, L., New method for calculating wave functions in crystals and molecules, Phys. Rev. 116, pp. 287-294, (1959).
30. Harrison, W.A., Pseudopotentials in the theory of metals, Benjamin, New York, (1966).
31. Heine, V., Solid state Physics, edited by Ehrenreich, H., Seitz F. and Turnbull, D., Vol. 24, Academic Press, New York, (1970).
32. Austin, B.J., Heine, V. and Sham, L.T., General theory of pseudopotentials, Phys. Rev., 127, pp. 276-282, (1962).
33. Pick, R. and Sarma, G., Orthogonalized plane wave method and total energy of a metal, Phys. Rev., 135, pp. A1363-A1370, (1964).
34. Schiff, L.I., Quantum mechanics, 3rd Edition, McGraw-Hill, New York, (1968).
35. Hafner, J., Structural, thermochemical and thermo-mechanical properties of binary alloys, J.Phys. F 6, pp. 1243-1257, (1976).
36. Shaw, Jr, R.W., Optimum form of a modified Heine-Abarenkov model potential for theory of simple metals, Phys. Rev. 174, pp. 769-781, (1968).
37. Appapillai, M. and Williams, A.R., The optimized model potential for thirty-three elements, J.Phys., F. 3, pp. 759-771, (1973).

38. Williams, A.R. and Appapillai, M., Applications of the optimized model potential, J.Phys., F 3, pp.772-780, (1973).
39. Zunger, A. and Cohen, M.L., First principles nonlocal-pseudopotential approach in the density-functional formalism: Development and application to atoms, Phys. Rev. B., 18, pp. 5449-5472, (1978).
40. Hamann, D.R., Schluter, M. and Chiang, C., Norm-conserving pseudopotentials, Phys. Rev. Lett., 43, pp. 1494-1497, (1979).
41. Bachelet, G.B. and Schluter, M., Relativistic norm-conserving pseudopotentials, Phys.Rev., B 25, pp.2103-2108, (1982).
42. Cohen, M.L. and Heine, V., Solid State Physics, eds. by Seitz, F., Turnbull, D. and Ehrenreich, Vol.24, Academic Press, New York, (1970).
43. Ashcroft, N.W., Electron-ion pseudopotentials in metals, Phys. Letts., 23, pp. 48-49, (1966).
44. Abarenkov, I.V. and Heine, V., The model potential for positive ions, Phil. Mag., 12, pp. 529-537, (1965).
45. Simons, G. and Bloch, A.N., Pauli-Force model potential for solids, Phys. Rev. B., 7, pp. 2754-2761, (1973).
46. Simons, G., J.Chem. Phys, 55, pp. 756-761, (1971) also Chem. Phys. Letts. 12, 404, (1971).
St. John, J. and Bloch, A.N., Quantum-defect electro-negativity scale for nontransition elements, Phys. Rev. Letts., 33, pp. 1095-1098, (1974).

47. Pauling, L., The nature of the chemical bond., Cornell Univ. Press, Ithaca, New York, (1960).
48. Cohen, M.H., J.Phys. Radium 23, 643, (1962) Reprinted in Metallic Solid Solutions., J. Friedal and A.Guinier Eds. Benjamin, New York, (1963).
49. Animalu, A.O.E. and Heine, V., The screened model potential for 25 elements, Phil. Mag., 12 , pp.1249-1270, (1965).
50. Heine, V. and Weaire, D., Solid State Physics, eds. by Seitz, F., Turnbull, D. and Ehrenreich, Vol.24, Academic Press, New York, (1970).
51. Ziman, J.M., The method of neutral pseudo-atoms in the theory of metals, Advan. Phys. 13, pp. 89-138, (1964).
52. Ziman, J.M., Principles of theory of solids, Cambridge Univ. Press, London and New York, (1964).
53. Heine, V. and Abarenkov, I., A new method for the electronic structure of metals, Phil. Mag., 9, pp.451-465, (1963).
54. Sham, Jr. R.W. and Harrison, W.A., Reformulation of the screened Heine-Abarenkov model potential, Phys. Rev., 163 , pp. 604-611, (1967).
55. Blandin, A., Phase stability in metals and alloys, P.S. Rudman et.al. eds, , McGraw-Hill, New York, (1966).
56. Hellmann, H., Quantenchemie Deuticke (1937) and R.E.Peierls, Quantum theory of solids, Clarendon, Oxford, (1955).

57. Phillips, J.C., Chicago Lectures in Physics series: Covalent bonding in crystals, molecules and polymers, Univ. of Chicago Press, Chicago and London, (1969).
58. Mott, N.F. and Jones, H., The theory and properties of metals and alloys, Oxford Univ. Press (Clarendon), London and New York, (1936).
59. Coulson, C.A., Physical chemistry an advanced Treatise, Vol.5. Eyring, H, Henderson, D. and Jost, W., eds., Academic Press, New York, (1970).
60. Pantelides, S.T., and Harrison, W.A., Structure of the valence bands of Zinc-blende-type semiconductors, Phys. Rev. B 11, pp. 3006-3021, (1975).
61. Harrison, W.A. and Sokel, R., Extension of the Gorden-Kim overlap interaction to open shell systems, J. Chem. Phys., 65 , 379, (1976).
62. Harrison, W.A., Pseudopotential theory of covalent bonding, Phys. Rev., B 14 , pp. 702-711, (1976).
63. Goroff, I. and Kleinmann, L., First-principles calculation of the bulk modulus of diamond, Phys. Rev. B 1, pp. 2574-2581, (1970).
64. Schmid, L.A., Calculating of the cohesive energy of Diamond, Phys. Rev. 92, pp. 1373-1379, (1953).
65. Asano, S. and Tomishima, Y., Calculation of the cohesive energy of Zinc blende, J. Phys. Soc. Japan, 11 , pp. 644-653, (1956).
66. Goto, F., Cohesive energy of diamond, J. Phys. Soc. Japan, 21, pp. 895-906, (1966).

67. Morita, A., Soma, T. and Takeda, T., Perturbation theory of covalent crystals. I. Calculation of cohesive energy and compressibility, *J. Phys. Soc. Japan*, 32, pp. 29-45, (1972).
68. Cohen, M.L. and Bergstresser, T.K., Band structures and pseudopotential form factors for fourteen semiconductors of the Diamond and Zinc-blende structures, *Phys. Rev.*, 141, pp. 789-796, (1966).
69. The experimental total energy has been calculated by the addition of cohesive energy of the element and ionization energy of all the valence electrons. The values are represented in atomic units (a.u.) throughout ($\hbar = m = e = 1$). The cohesive energy values for various elements obtained from: Kittel, C., *Introduction to solid state physics*, 5th ed. Wiley, New York, (1976). The ionization energy of all the valence electrons of various elements obtained from: *CRC Hand book of Chemistry and Physics*, 63rd ed., CRC Press, Boca Raton, Florida, pp. E64-E65, (1983).
70. Heine, V. and Jones, R.O., Electronic band structure and covalency in diamond-type semiconductors, *J Phys. C* 2, pp. 719-732, (1969).
71. Heine, V., *Theory of metals, Vol. I, Electrons* (J.M. Ziman, ed.) Cambridge Univ. Press, London and New York, (1968).
72. Ashcroft, N.W. and Langreth, D.C., Compressibility and binding energy of the simple metals, *Phys. Rev.*, 155, pp. 682-684, (1967).

73. Janak, J.F., Moruzzi, V.L. and Williams, A.R., Ground-state thermomechanical properties of some cubic elements in the local-density formalism, Phys. Rev., B 12, pp. 1257-1261, (1975).
74. Moriarty, J.A., Simplified local-density theory of the cohesive energy of metals, Phys. Rev., B 19, pp.609-619, (1979).
75. Rao, S.S., Optimization : theory and applications, 2nd ed., Wiley Eastern Ltd., New Delhi, (1982).
76. Smith, J.R., Self-consistent many electron theory of electron work functions and surface potential characteristics for selected metals, Phys. Rev. 181 , pp.522-529, (1969).
77. Lang, N.D. and Kohn, W., Theory of metal surfaces: Charge density and surface energy, Phys. Rev., B 1 , pp. 4555-4568, (1970)
78. Harrison, W.A., Electronic structure and the properties of solids - The physics of the chemical bond, Freeman and Company, San Francisco, (1979).